Manuscript Details

Manuscript number	PRECAM_2018_526_R1
Title	A Palaeoproterozoic dolomite (Vempalle Formation, Cuddapah Basin, India) showing Phanerozoic-type dolomitisation
Article type	Research Paper

Abstract

The Palaeoproterozoic Vempalle Formation of the Cuddapah Basin, India, significantly adds to our understanding of the evolution of Precambrian marine carbonate systems and the redox state of the Earth's early oceans. A facies-microfacies-diagenetic-geochemical examination of samples from a 900-m long exposure in a freshly-cut canal section shows that 10 to 15 % of precursor limestone is still preserved in the Vempalle Formation in the form of remnant patches of calcimicrite and ooids with calcite spar cement. The ooids, preserving primary radial and concentric fabrics and radial fractures, are considered to have been originally precipitated as calcite, which may have been low-Mg. In places the preserved calcite spar, that is partially replaced by fabric-destructive dolomite, shows Type I calcite twin lamellae. Petrographic observations demonstrate that Vempalle Formation dolomite formed through very early precipitation, which in stromatolites preserved microbial filaments, as well as through fabric-destructive dolomitization during shallow to moderate burial. Vempalle Formation dolomite is characterized by micritic dolomite crystals which suggest rapid early dolomitization of lime mud and micritic calcite from a supersaturated Mg-Ca-rich solution, probably near-surface or during shallow burial. Depletion of Na and Sr contents of Vempalle Formation dolomite along with negative $\delta^{18}O$ values indicate dolomite recrystallisation during burial and further replacement. Dolomite $\delta^{13}C$ values of -0.5 to 2 ‰ are likely inherited original marine values. Geochemical proxies (trace elements and rare earths) imply that Cuddapah Basin seawater and dolomitizing fluids were anoxic and ferruginous but not euxinic. Geochemical analyses also indicate that the burial diagenetic fluids evolved from Eu-enriched seawater that probably resulted from continental rifting around 1.9 – 2.0 Ga. This probable ocean chemistry is in contrast with the anoxic, ferruginous and extremely high Mg/Ca "dolomite oceans" that prevailed during Proterozoic time. The Vempalle dolomite shows more similarities with dolomitised Phanerozoic platform carbonates than typical Precambrian dolomite with its well-preserved textures and burial dolospar cements.

Keywords	Dolomitization, Proterozoic carbonate rocks, redox, fluid chemistry

Corresponding Author	Amlan Banerjee
Corresponding Author's Institution	Indian Statistical Institute
Order of Authors	Amlan Banerjee, Miroslaw Slowakiewicz, tuasha majumder, Sayani Khan, Sarbani Patranabis Deb, Maurice Tucker, Dilip Saha

Suggested reviewers	Alan Collins, Nic Beukes, Santanu Banerjee, Ian Somerville, Abhijit Basu

Submission Files Included in this PDF

File Name [File Type]

Cover_letter_27-3-19.doc [Cover Letter]

Reply to Reviewers_comments_27-3-19.doc [Response to Reviewers]

Revised_Manuscript_27-3-19.doc [Revised Manuscript with Changes Marked]

Highlights.doc [Highlights]

Revised_Manuscript_27-3-19-unmarked.doc [Manuscript File]

Revised Manuscript Figures_27-3-19.doc [Figure]

Revised Manuscript Tables_27-3-19.doc [Table]

Revied_Supplementary Materials_27-3-19.doc [Table]

To view all the submission files, including those not included in the PDF, click on the manuscript title on your EVISE Homepage, then click 'Download zip file'.

Research Data Related to this Submission

There are no linked research data sets for this submission. The following reason is given:
all the data are given in Tables and Supplementary files

Dear Prof. Pease
Editor, Precambrian Research

Thank you and the reviewers for their thoughtful comments and suggestions. Here in the revised draft we have taken into account all the suggestions and comments and modified the manuscript accordingly. All the modifications are highlighted in yellow in the revised draft, figure, table and supplementary files and outline every change made by us with line numbers. Please note that Section 4 is rewritten and abridged and Figs. 2 and 3 are added. The revised manuscript was checked by all the coauthors and they agreed about its content.

Also note that we have taken out the name of Marcin D. Syczewski from the author list. He helped one of the co-authors (MS) with SEM and according to MS it is not enough for a co-authorship.

Sincerely

Amlan Banerjee
Geological Science Unit
Indian Statistical Institute

Dear Dr. Banerjee,

Re: A Palaeoproterozoic dolomite (Vempalle Formation, Cuddapah Basin, India) showing Phanerozoic-type dolomitisation

Thank you for submitting your manuscript to Precambrian Research. I have received comments from two reviewers on your manuscript and they both enjoyed reading your manuscript. Nonetheless, some improvements can be made and your paper should become acceptable for publication after moderate revisions. In particular, please address the following points:

1. Better integrate the classical sedimentology (facies, facies associations, depositional environments) and dolomite geochemistry in the paper by discussing as a function of the facies/depositional environments. This may in fact work well with converting Table 1 into a facies-graphic.

Section 4 is rewritten and abridged (line number 194 – 267). New Table 1 and Figs. 2 and 3 are also added.

2. Clarify why the positive Eu anomaly and the relatively high Fe and Mn contents indicate dolomitization of Phanerozoic type rather than Precambrian type?

The argument that the VF dolomitization is more of Phanerozoic type rather than Precambrian type is based more on petrographic rather than geochemical analysis. Precambrian dolomites are generally characterised by very well-preserved fabrics of the original carbonate grains and early cements likely a reflection of seawater chemistry higher Mg/Ca ratio, higher partial pressure CO2 (pCO2), higher temperature, and lower SO42- (Tucker 1982, Hood and Wallace 2018), in addition, many Precambrian dolomites have drusy dolospar cements, precipitated during shallow to moderate burial (e.g. Tewari and Tucker, 2011), a feature rarely seen in Phanerozoic dolomites.

Petrographic analysis suggests that the VF carbonates originally precipitated as lime mud and calcimicrite and 10 to 15 % of precursor limestone is still preserved in the Vempalle Formation in the form of remnant patches of calcimicrite and ooids with calcite spar cement. The ooids preserve primary radial and concentric fabrics and radial fractures, and are considered to have been originally precipitated as calcite. In places the preserved calcite spar, that is partially replaced by fabric destructive dolomite, shows Type I calcite twin lamellae. Petrographic observations suggest fabric destructive dolomitization in VF carbonate rocks (Tucker et al., 2002), and the mimetic to obliterated mosaic texture indicate progressive dolomite replacement (Braithwaite, 1991). It is likely that this was a time of calcite precipitation (a “calcite sea”), with anoxic, Eu anomaly and ferruginous conditions, and an elevated Mg/Ca ratio but not so high that either dolomite precipitation or very early fabric-retentive dolomitization of ooids and cements could take place, like those of the Beck Spring Dolomite (Tucker, 1983). On the other hand the occurrence of dolomitic micritic facies in the VF suggests that the dolomite crystals rapidly precipitated from a dolomite supersaturated fluid having high Mg/Ca ratio and low SO4-2 concentration as primary precipitates due to evaporation or due to microbial activity and as would be expected in the Proterozoic environments.

3. There is a notable lack of references to other Paleoproterozoic carbonate successions (e.g., Grotzinger on the Canadian shield and late Archean carbonate platform successions in South Africa and Australia with positive Eu anomalies of Kamber and Webb, 2001, Geochim Cosmochim Acta; Schier et al 2018, Precam Research; Eroglu et al., Precam Research, 2017).

We have added several references (six in numbers) of J.P Grotzinger and the references recording positive Eu anomalies from carbonate platform successions as suggested by the reviewer.

1.Grotzinger, J.P., 1989. Facies and evolution of Precambrian carbonate depositional systems: emergence of the modern platform archetype, in, SEPM Special Publication 44, p. 79-106 (line number 52; and 748-749)

2. Grotzinger, J. P., Read, J. F., 1983. Evidence for primary aragonite precipitation, lower Proterozoic (1.9 Ga) dolo- mite, Wopmay orogen, northwest Canada: Geology, v. 11, p. 710-713 (line number 52; and 750-751)

3. Grotzinger, J.P., Kasting, J. 1993. New constraints on Precambrian ocean composition. Journal of Geology, v. 101, p. 235-243 (line number 52; and 752-753)

4. Pope, M. C., Grotzinger, J. P., 2003. Paleoproterozoic Stark Formation, Athapuscow basin, northwest Canada: Record of cratonic-scale salinity crisis. Journal of Sedimentary Research, v. 73, p. 280-295. (77) (line number 49; and 901-903)

5. Saylor, B. Z., Grotzinger, J. P., Germs, J. B. 1995. Sequence stratigraphy and sedimentology of the Neoproterozoic Kuibis and Schwarzrand Subgroups (Nama Group), southwestern Namibia. Precambrian Research, v. 73, p. 153-171. (line number 48; and 935-937)

6. Kamber B. S., Webb, G. E., 2001. The geochemistry of late Archaean microbial carbonate: implications for ocean chemis- try and continental erosion history. Geochim. Cosmochim. Acta 65, 2509–2525. (line number 457; and 801-803)

7. Schier, K., Bau, M., Münker, C., Beukes, N., Viehmann, S., 2018. Trace element and Nd isotope composition of shallow seawater prior to the Great Oxidation Event: Evidence from stromatolitic bioherms in the Paleoproterozoic Rooinekke and Nelani Formations, South Africa. Precambrian Research 315, 92-102 (line number 472; and 939-942)

8. Eroglu, S., van Zuilen, M.A., Taubald, H., Drost, K., Wille, M., Swanner, E.D., Beukes, N.J., Schoenberg, R., 2017, Depth-dependent δ13C trends in platform and slope settings of the Campbellrand-Malmani carbonate platform and possible implications for Early Earth oxygenation. Precambrian Research 302, 122-139. (line number 471; and 712-715)

4. Convert data Table 1 into a schematic strat column or a stylized facies cartoon/graphic.

See Fig. 2 and Fig. 3

5. Move data tables 2-6 into supplementary material.

See Supplementary section where Tables 1S to 5S are presented showing all the data (XRD; Ca excess and ordering; Major and Trace element concentrations in wt% and ppm; PAAS normalized REE values; and oxygen and carbon isotope values).

6. Add scale bars on all images in Figs 3 & 4.

Done

When resubmitting your manuscript, please carefully consider my comments above and the reviewers' comments, outline every change made by line number, and provide suitable rebuttals for any comments not addressed.

Reviewer 1

- This is a very well written manuscript.

Thank you

I have only two major concerns:

1. I do not follow the argument that the dolomitization is of Phanerozoic type rather than Precambrian type if you refer to the positive Eu anomaly and the relatively high Fe and Mn contents.

The argument that the VF dolomitization is more of Phanerozoic type rather than Precambrian type is based more on petrographic rather than geochemical analysis. Precambrian dolomites are generally characterised by very well-preserved fabrics of the original carbonate grains and early cements likely a reflection of seawater chemistry higher Mg/Ca ratio, higher partial pressure CO_2 (pCO_2), higher temperature, and lower SO_4^{2-} (Tucker 1982, Hood and Wallace 2018), in addition, many Precambrian dolomites have drusy dolospar cements, precipitated during shallow to moderate burial (e.g. Tewari and Tucker, 2011), a feature rarely seen in Phanerozoic dolomites.

Petrographic analysis suggests that the VF carbonates originally precipitated as lime mud and calcimicrite and 10 to 15 % of precursor limestone is still preserved in the Vempalle Formation in the form of remnant patches of calcimicrite and ooids with calcite spar cement. The ooids preserve primary radial and concentric fabrics and radial fractures, and are considered to have been originally precipitated as calcite. In places the preserved calcite spar, that is partially

replaced by fabric destructive dolomite, shows Type I calcite twin lamellae. Petrographic observations suggest fabric destructive dolomitization in VF carbonate rocks (Tucker et al., 2002), and the mimetic to obliterated mosaic texture indicate progressive dolomite replacement (Braithwaite, 1991). It is likely that this was a time of calcite precipitation (a "calcite sea"), with anoxic, Eu anomaly and ferruginous conditions, and an elevated Mg/Ca ratio but not so high that either dolomite precipitation or very early fabric-retentive dolomitization of ooids and cements could take place, like those of the Beck Spring Dolomite (Tucker, 1983). On the other hand the occurrence of dolomitic micritic facies in the VF suggests that the dolomite crystals rapidly precipitated from a dolomite supersaturated fluid having high Mg/Ca ratio and low SO4-2 concentration as primary precipitates due to evaporation or due to microbial activity and as would be expected in the Proterozoic environments.

2. I miss references to other Paleoproterozoic carbonate successions for example as described by Grotzinger from the Canadian shield and late Archean carbonate platform successions in South Africa and Australia with positive Eu anomalies (refer for example to Kamber and Webb, 2001, Geochim Cosmochim Acta; Schier et al 2018, Precam Research; Eroglu et al., Precam Research, 2017).

We have added several references (six in numbers) of J.P Grotzinger and the references recording positive Eu anomalies from carbonate platform successions as suggested by the reviewer.

1. Grotzinger, J.P., 1989. Facies and evolution of Precambrian carbonate depositional systems: emergence of the modern platform archetype, in, SEPM Special Publication 44, p. 79-106 (Line number 52; and 748-749)

2. Grotzinger, J. P., Read, J. F., 1983. Evidence for primary aragonite precipitation, lower Proterozoic (1.9 Ga) dolo- mite, Wopmay orogen, northwest Canada: Geology, v. 11, p. 710-713 (Line number 52; and 750-751)

3. Grotzinger, J.P. and Kasting, J. 1993. New constraints on Precambrian ocean composition. Journal of Geology, v. 101, p. 235-243 (Line number 52; and 752-753)

4. Pope, M. C., and Grotzinger, J. P., 2003. Paleoproterozoic Stark Formation, Athapuscow basin, northwest Canada: Record of cratonic-scale salinity crisis. Journal of Sedimentary Research, v. 73, p. 280-295. (77) (Line number 49; and 901-903)

5. Saylor, B. Z., Grotzinger, J. P., and Germs, J. B. 1995. Sequence stratigraphy and sedimentology of the Neoproterozoic Kuibis and Schwarzrand Subgroups (Nama Group), southwestern Namibia. Precambrian Research 73, 153-171. (Line number 48; and 935-937)

6. Kamber B. S., Webb, G. E., 2001. The geochemistry of late Archaean microbial carbonate: implications for ocean chemis- try and continental erosion history. Geochim. Cosmochim. Acta 65, 2509–2525. (Line number 457; and 801-803)

7. Schier, K., Bau, M., Münker, C., Beukes, N., Viehmann, S., 2018. Trace element and Nd isotope composition of shallow seawater prior to the Great Oxidation Event: Evidence from stromatolitic bioherms in the Paleoproterozoic Rooinekke and Nelani Formations, South Africa. Precambrian Research 315, 92-102 (Line number 472; and 939-942)

8. Eroglu, S., van Zuilen, M.A., Taubald, H., Drost, K., Wille, M., Swanner, E.D., Beukes, N.J., Schoenberg, R., 2017, Depth-dependent δ13C trends in platform and slope settings of the Campbellrand-Malmani carbonate platform and possible implications for Early Earth oxygenation. Precambrian Research 302, 122-139. (Line number 471; and 712-715)

Reviewer 2

The manuscript submitted to Precambrian Research by Banerjee and co-authors is an interesting work contributing to a better knowledge of the evolution of ocean geochemistry in deep time, essentially to what concerns carbonate sediments. It is therefore a paper that adds new knowledge for Earth's history.

Thank you Prof. Pittet.

The manuscript is separated into 2 parts, one devoted to classical sedimentology (facies, facies associations, depositional environments) and one to dolomite geochemistry. The problem in the manuscript is that these 2 parts are not clearly linked together as dolomite geochemistry is not analysed as a function of the facies, or of the environments. It seems that dolomite sampling was done rather randomly, at a more or less constant step (15m). I wonder if these 2 parts should not be published separately. Alternatively, it is necessary to better relate these 2 parts to write a more integrative/homogenous paper. Another alternative possibility is to drastically reduce the facies analysis in the present manuscript to focus on dolomite geochemistry. I however think that the data presented are of importance, and should be published. I have made comments and corrections all along the pdf file -both for the text and the figures- that I will not repeat here

Thank you Prof. Pittet for the comments. Changes made based on your comments and suggestions in the text (including figures) are described below.

1. Corrected in line 76 and 77 deleted "a short" and "short"

2. Line 82 corrected "^{18}O depleted"

3. Line 107, 109, change gradational in to "transitional"

4. The Facies section is re-written and abridged. Table 1 is added along with Fig. 3. Table 2 is modified. All the other tables are shifted to Supplementary section. See Supplementary section where Tables 1S to 5S are presented showing all the data (XRD; Ca excess and ordering; Major and Trace element concentrations in wt% and ppm; PAAS normalized REE values; and oxygen and carbon isotope values).

5. Line number 196 Fig 1a, b, c are now marked.

6. Line no. 244 the environment is “quiescent” is interpreted from the presence of stromatolite with low synoptic relief and parallel lamination. Probable interpretation is deposition in a relatively quiet-water protected area between two bars or in a relatively deeper-water environment.

7. Line number 285 reference added. Dolomite petrology of the formation is described depending on the dolomite classification system by Sibley and Gregg (1987, 1984) where they have designated mainly three types of dolomite depending on crystal size distribution and crystal boundary shape (preserved crystal face junction). Planar-e dolomites are described as euhedral crystals with intercrystalline boundaries filled by other minerals. Planar-s dolomites are subhedral to anhedral crystals with straight compromise boundaries and many crystal face junctions with low intercrystalline matrix. Nonplanar dolomites are defined by closely packed anhedral crystals with irregular intercrystalline boundaries and fewer (<30%) preserved crystal face junction.

8. Line 340-341, Figure 7 is modified and Fig. 7 d) and 7 e) added.

9. Line 347 (Table 3Sa, see Supplementary section) added.

10. Line 399 Tucker (1982) reference added.

11. Line 445 Fig. 7c corrected.

12. Fig. 1 the three figures are labeled a) b) and c); Fig. 2 is modified and New Fig 3 is added; in Figure 4 Planer-s explained in the text (see line no. 285); in Figure 5 captions heading e) and f) corrected.

A Palaeoproterozoic dolomite (Vempalle Formation, Cuddapah Basin, India) showing Phanerozoic-type dolomitisation

Amlan Banerjee[1*], Mirosław Słowakiewicz[2,3], Tuasha Majumder[1], Sayani Khan[1], Sarbani Patranabis-Deb[1], Maurice E. Tucker[4,5], Dilip Saha[1]

[1]Indian Statistical Institute, Geological Studies Unit, Kolkata 700108, India
[2]Faculty of Geology, University of Warsaw, ul. Żwirki i Wigury 93, 02-089 Warszawa, Poland
[3]Kazan Federal University, Kremlovskaya St. 18, 420008 Kazan, Russia
[4]Cabot Institute, University of Bristol, Cantock's Close, Bristol, BS8 1UJ, UK
[5]School of Earth Sciences, University of Bristol, Bristol BS8 1RJ, UK
[*]corresponding author: amlan@isical.ac.in

Abstract: The Palaeoproterozoic Vempalle Formation of the Cuddapah Basin, India, significantly adds to our understanding of the evolution of Precambrian marine carbonate systems and the redox state of the Earth's early oceans. A facies-microfacies-diagenetic-geochemical examination of samples from a 900-m long exposure in a freshly-cut canal section shows that 10 to 15 % of precursor limestone is still preserved in the Vempalle Formation in the form of remnant patches of calcimicrite and ooids with calcite spar cement. The ooids, preserving primary radial and concentric fabrics and radial fractures, are considered to have been originally precipitated as calcite, which may have been low-Mg. In places the preserved calcite spar, that is partially replaced by fabric-destructive dolomite, shows Type I calcite twin lamellae. Petrographic observations demonstrate that Vempalle Formation dolomite formed through very early precipitation, which in stromatolites preserved microbial filaments, as well as through fabric-destructive dolomitization during shallow to moderate burial. Vempalle Formation dolomite is characterized by micritic dolomite crystals which suggest rapid early dolomitization of lime mud and micritic calcite from a supersaturated Mg-Ca-rich solution, probably near-surface or during shallow burial. Depletion of Na and Sr contents of Vempalle Formation dolomite along with negative $\delta^{18}O$ values indicate dolomite recrystallisation during burial and further replacement. Dolomite $\delta^{13}C$ values of -0.5 to 2 ‰ are likely inherited original marine values. Geochemical proxies (trace elements and rare earths) imply that Cuddapah Basin seawater and dolomitizing fluids were anoxic and ferruginous but not euxinic. Geochemical analyses also indicate that the burial diagenetic fluids evolved from Eu-enriched seawater that probably resulted from continental rifting around 1.9 – 2.0 Ga. This probable ocean chemistry is in contrast with the anoxic, ferruginous and extremely high Mg/Ca "dolomite oceans" that prevailed during Proterozoic time. The Vempalle dolomite shows more similarities with dolomitised Phanerozoic platform carbonates than typical Precambrian dolomite with its well-preserved textures and burial dolospar cements.

Keywords: Dolomitization, Proterozoic carbonate rocks, redox, fluid chemistry

1. INTRODUCTION

Carbonate ramps and rimmed platforms are a distinctive feature of Neoarchean to Neoproterozoic deposition and in many cases the dolomite content of these ancient carbonate platforms is high in comparison with those of the Mesozoic and Cenozoic (Saylor et al., 1995; Holland and Zimmermann, 2000; Pope and Grotzinger, 2003). The processes of formation of these ancient dolomites are still the subject of much debate. The Precambrian sedimentary record to about 3.5 Ga includes dolomites and limestones that likely precipitated as primary aragonite and calcite (Grotzinger and Read, 1983; Grotzinger, 1989; Grotzinger and Kasting, 1993). Palaeoproterozoic carbonate sedimentation was marked by less spectacular occurrences of massively-precipitated aragonite and calcite (Grotzinger and Kasting, 1993). Precambrian dolomites may have also formed by precipitation directly from seawater or by dolomitization during very early diagenesis from fluids comparable with seawater (e.g., Veizer and Hoefs, 1976; Tucker, 1982, 1983; Hood and Wallace, 2018). Precambrian dolomites are generally characterised by very well-preserved fabrics of the original carbonate grains and early cements, leading to arguments over primary versus replacement dolomite (Tucker 1982, Hood and Wallace 2018). In addition, many Precambrian dolomites have drusy dolospar cements, precipitated during shallow to moderate burial (e.g. Tucker, 1983; Tewari and Tucker, 2011), a feature rarely seen in Phanerozoic dolomites. In India, several Precambrian sedimentary basins are reported to host dolomite successions several kilometres thick. The Palaeoproterozoic Vempalle Formation (VF), located in the crescent-shaped intracratonic Cuddapah Basin (CB), Eastern Dharwar craton, and a part of the Papaghni Group (Fig. 1), is characterized by the presence of a ~1.9 km-thick stromatolitic dolomite. The VF carbonate platform can be traced for more than 1000 km without any significant physical break from the SE to the NW part of the basin.

Zachariah et al. (1999) obtained a Pb-Pb age of 1756 ± 29 Ma for the VF dolomite. Taking into consideration the age of intruded sills (1817±24 Ma; Bhaskar Rao et al., 1995) within VF carbonate rocks/Pulivendla quartzites and the age of VF dolomite (1756 ± 29 Ma), Zachariah et al. (1999) proposed 1756 ± 29 Ma as the time of dolomitization of the precursor VF limestone. Rai et al. (2015), based on a Pb–Pb (PbSL) age of VF dolomite and of the intruded sills of 1885 Ma (U-Pb and Ar-Ar methods; French et al., 2008; Anand et al., 2003), proposed that

dolomitization of VF limestone might have taken place within 100 My duration of time (from 1900-2000 Ma). This time duration of sedimentation and dolomitization is also reported from the Wittenoom Formation and Carawine Dolomite of the Hamersley Group, Western Australia, where the time between deposition, diagenesis and dolomitization is thought to be within 100-150 My (Jahn and Cuvellier, 1994; Jahn and Simson, 1995). On the other hand, Chakrabarti et al. (2011, 2014), using isotopic ($\delta^{13}C$ and $\delta^{18}O$) and elemental (Mg, Ca, Fe, Mn, Sr and SO_4^{-2}) data, concluded that VF dolomite is primary in nature and precipitated either from ^{18}O depleted marine water or from a geochemically distinct mixed fluid source. Based on collective geochemical signatures, $\delta^{13}C$ and $\delta^{18}O$ isotopic values, flat REE patterns along with Ce, Eu and Gd anomalies, and chondritic to superchondritic Y/Ho ratios, Khelen et al. (2017) have recently proposed that VF dolomite was precipitated from marine water having a hydrothermal signature. These discrepancies in the plumbing mechanism(s) of VF dolomite warrant the need to revisit the question about the origin of VF dolomite and related dolomite-precipitating fluids.

In this project we have used field and petrographic observations and various geochemical proxies to understand the mechanism(s) of formation of the shallow-marine VF dolomite and to assess the redox heterogeneity existing during its time of formation. Geochemical data, integrated with petrology and tectonic history of the CB, help not only to infer the source of Mg-rich fluids but also to contribute to a better understanding of the redox conditions of this Proterozoic shallow-water carbonate. In addition, as will be shown, this Palaeoproterozoic dolomite has more features in common with dolomitised Phanerozoic platform carbonates, than the typical Precambrian dolomite with well-preserved fabrics, likely a reflection of seawater chemistry, redox and microbes.

2. GEOLOGICAL BACKGROUND

The Papaghni Group (~2110 m thick) represents the first sedimentary cycle of the Cuddapah Supergroup (Patranabis-Deb et al., 2012) in the CB. The succession unconformably overlies the basement granite, gneiss and greenstone complex of the Eastern Dharwar craton, which in turn is unconformably overlain by the Chitravati Group (4975 m). The VF (~1900 m) of the Papaghni Group constitutes the lowermost carbonate-dominated unit of the Cuddapah Supergroup and overlies a basal siliciclastic unit, the Gulcheru Quartzite (~210 m), with a

transitional contact (Nagaraja Rao et al., 1987). The Gulcheru Quartzite constitutes a basal conglomerate and immature sandstone unit, deposited in a fan-delta to prodelta setting, which transitionally passes up into a mature quartz arenite unit, deposited in a shallow-shelf environment (Majumder et al., 2015). The VF is represented mostly by thick stromatolitic dolomite and minor limestone (10 to 15%). Near the transition zone to the Gulcheru Quartzite, thin beds of splintery red mudstone alternate with siliciclastic and carbonate beds to form a mixed siliciclastic-carbonate unit (Fig. 2). Tidal and storm currents played a major role in sculpturing the sandstone bodies at this transition.

Tepee structures, desiccation cracks filled with lime mud and sand and halite casts, are common in the lower VF (Fig. 2). The upper part is dominated by bedded dolomite deposited in a range of environments, starting from shallow shelf with intermittent exposure to fairly deep-water conditions below normal wave base. Stromatolite morphologies reflect environments varying from intertidal to subtidal and facies cycles are the result of multiple rhythms of sea-level change (Patranabis-Deb et al., 2018). Demise of the carbonate platform is marked by the deposition of thick brown shale with laterally persistent beds of chert. The common occurrence of sills up to a metre or more thick and thinner dykes of basalt and/or dolerite in the upper part of the VF succession indicates tectonic-magmatic activity (Anand et al., 2003). Conglomerate and pebbly sandstone of the basal Chitravati Group, upon a sharp unconformity, mark the beginning of the second sedimentary cycle. Clasts of chert with stromatolite, oolite, vein quartz, jasper and volcanics, derived from the Papaghni Group, reflect subaerial exposure and erosion during the formation of the unconformity between the two groups.

Rifting of the Eastern Dharwar craton and passive-margin sedimentation deposited the Gulcheru fan-delta succession (Majumder et al., 2015) followed by deposition of the extensive VF carbonate platform (Tripathy and Saha, 2008; Patranabis-Deb et al., 2018). Rai et al. (2015) inferred a minimum age of 2000 Ma for the onset of sedimentation in the Cuddapah Supergroup and this coincides with the onset of rifting of the supercontinent Columbia, as evidenced by widespread emplacement of mafic dykes in and around the CB during this period. The intermittent occurrence of mafic flows, ash-fall tuffs and associated shallow-crustal intrusives in the upper part of the VF (~1.88 Ga; Ravikant, 2010) is related to the second cycle of rifting that

possibly represents the initial phase of fragmentation and separation of the south Indian craton from the North China craton (Ravikant, 2010). With continued passive subsidence, the CB evolved into a large epicontinental sea with a near-complete cessation of coarse clastic influx and deposition of the extensive shale–carbonate succession of the Chitravati Group. Tectonically, the CB is punctuated by multiple unconformities, major tectonic contacts, faults and various basic sills (Saha and Tripathy, 2012; Saha and Mazumder, 2012; Patranabis-Deb et al., 2012; Collins et al., 2015), which affected and shaped its sedimentary succession.

3. METHODS

3.1. *Sample collection for petrological analysis*

Samples were collected at 5-15 m intervals up-section (Table 1) along a freshly cut canal section, nearly 4 km long (hereafter referred as the 'canal section') that exposed the dolomite beds of the VF (~1000 m thick dolomite unit, Fig. 2) near Parnapalle village (N14º32'58.3", E77º58'09.9") in the Cuddapah district, Rayalaseema. Samples collected from the dolomite beds covered eight facies namely F1, F2, F4, F5, F7, F8, F9 and F10 (Table 1; Fig. 2). F3 and F11 are intentionally avoided as they are mostly composed of shale, siltstone and dolomite (Table 2). Thin-sections were made from twenty-nine selected dolomite samples for petrographic analysis. Carbonate components (calcite, dolomite) were determined by staining the thin-sections with Alizarin Red S.

3.2. *X-Ray diffraction*

Twenty-nine selected dolomite samples were powdered for X-ray diffraction analysis on a Panalytical X'Pert Pro diffractometer, equipped with a Cu Kα X-ray source and an X'Celerator detector, operating at the following conditions: 40 kV and 40 mA; range 5 – 80 deg 2θ; step size 0.017 deg 2θ; time per step 50.2 sec; fixed divergence slit, angle 0.5º; sample rotation 1 rev sec^{-1}. The quantities of the mineral phases were determined using the Rietveld method.

3.3. *Major and trace elements*

Forty-two selected dolomite samples were powdered for bulk major, trace and REE analyses, undertaken at the Wadia Institute of Himalayan Geology. The elemental analysis was

performed using an ICP-MS PerkinElmer SCIEX ELAN DRC-e. Concentrations of REE + Y (n = 42) were normalized to the Post-Archaean Australian Shale (PAAS) representing an estimate for the composition of average terrigenous input to the oceanic environment. Specifically, REE fractionation was calculated as Pr_{SN} / Yb_{SN} (SN, shale normalized) to avoid problems in case of anomalous La and Ce concentrations. To avoid any anomalous behaviour of La, Ce, Eu and Gd, the anomalies were calculated using the geometric equations of Lawrence and Kamber (2006) and are given as Ce/Ce^*, Eu/Eu^*, Gd/Gd^* and La/La^*.

3.4. Scanning electron microscopy with energy-dispersive spectroscopy

Thin-sections were examined under a scanning electron microscope (SEM) FE-SIGMA VP (Carl Zeiss Microscopy GmbH) with energy-dispersive (EDS) detector (Quantax XFlash 3|10, Bruker Nano GmbH). Thin-sections were placed on the mount with carbon conductive tape. Then, samples were coated with a 20 nm layer of carbon by vacuum coater (Quorum 150T ES). Furthermore, carbon tape bridges were made for each sample to avoid excessive accumulation of charge. Analyses were done with 120 µm aperture and 15 keV accelerationvoltage. Beam intensity was 2.5 nA and working distance was 7.5 mm.

3.5. *Oxygen and carbon stable isotope analysis*

Thirty-five selected dolomite samples were analysed for bulk carbon and oxygen stable isotopes at the Activation Laboratories Ltd., Canada. Samples were run on a DELTAPlus XL stable isotope ratio mass spectrometer (IRMS) coupled with ConFlo III Interface and EA1110 elemental analyser. Standards NBS-19 ($\delta^{13}C$ = 1.95 ‰ and $\delta^{18}O$ = -2.20 ‰) and NBS-18 ($\delta^{13}C$ = -5.05 ‰ and $\delta^{18}O$ = -23.1 ‰) were used for comparison. The results are expressed relative to the Vienna Peedee Belemnite (VPDB).

4. Sedimentation Pattern and Depositional Environment

The VF is well exposed along the south-western margin of the CB outcrop (Fig. 1a, b and c), represented by a ~1000-m thick succession of stromatolitic dolomite, dolomitic limestone and limestone (~70%), with minor calcimicrite (~20%), and ~10% siliciclastic sandstone and mudstone. Facies analysis reveals that the succession can be sub-divided into 11 distinct lithofacies (Table 1) which may be grouped into inner, mid and outer – ramp associations,

stacked in different orders as part of a major ramp-type carbonate platform (Fig. 3). The platform maintained a shallow depth throughout its life, thus indicating a keep-up mode of deposition, that is where the carbonate succession built up to sea level and kept pace with subsequent sea-level changes, such that a balance was maintained with the generation of accommodation space. Occasional storms and regular tides were important, distributing clastic sediments at particular times, which hampered the growth of the platform in time and space. The depth-controlled growth patterns of the stromatolites give clues to their depositional environment (Patranabis-Deb et al., 2018), which in the canal section reflects a gradient from shallow-water with exposure to shallow to moderate depths.

The VF succession in the canal section (Fig. 2) starts with a basal mixed unit, representing the transition between the basal siliciclastic unit of the Gulcheru Formation and carbonate rocks of the VF. It comprises mixed siliciclastic-dolomite (F1), bedded dolomite with crinkled laminites (F2) and intraformational conglomerate (F9). The mixed siliciclastic-dolomite beds are characterized by flaser bedding and lenticular bedding with preservation of desiccation cracks filled with lime mud and sand and halite casts within shale intervals, tepee structures and fluid-escape structures. The presence of these sedimentary features, suggests intermittent exposure in a supratidal to upper intertidal flat, in an inner ramp setting. Palaeocurrent directions measured from trough cross-stratification from the sandy units indicate east-north-easterly flow.

The mixed siliciclastic unit passes upward to a thick succession of bedded dolomite with crinkled laminites (F2), black dolomite with or without stromatolite (F4), dolomite-micrite rhythmite (F5) and brown shale (F3), without any break. Steel grey to black coloured massive to stromatolitic dolomite beds (F4) with isolated to laterally-linked mutually-aligned stromatolites are observed, alternating with dolomite-micrite rhythmite (F5). Isolated occurrences of stromatolite with low synoptic relief and parallel lamination in black dolomite (F4) indicate a quiescent water environment. The close association of F4 and F5 also suggests their deposition in a low-energy protected environment. Thick occurrences of F2 alternating with F5, with signatures of intermittent exposure at different stratigraphic levels, suggest that they have possibly formed a barrier, which imposed a rimmed-shelf profile to the platform, creating lagoons on the shoreward side with an open shelf to seaward.

The mid-ramp association consists of oolite (F6), with intercalations of dolomite mud rhythmite (F5), columnar stromatolite (F7), conical stromatolite (F8) and thickly – bedded dolomite (F10). The association starts with the occurrence of oolite (F6), as shoaling-up bars. The oolites comprise well-rounded, well-sorted medium- to coarse-grained ooids, usually preserving a concentric fabric with a clastic grain as the nucleus. Medium-to-fine-grained ooids with a radial fabric (with or without a clastic grain in the centre) and superficial ooids are also observed. Oolite beds are generally trough cross-stratified, showing NE and SW palaeocurrent directions with bidirectional pattern. The abundance of siliciclastic grains as nuclei to ooids indicates a ready source of clastics on the landward side. The oolite bank may have further acted as a barrier with the seaward side being cut off from the coastal sediments so that ooids formed without sand nuclei and a radial fabric. F6 is interbedded with small columnar stromatolites (4-14 cm in height). F7 suggests spatial and temporal variations in the intensity and fluctuations of wave action (Swett and Knoll, 1989; Holland and Patzkowsky, 1998) in a lower intertidal to upper subtidal environment. The rhythmite facies (F5) may have been deposited as interbars in a relatively quiet-water protected area between two bars or in a relatively deeper-water environment. Up-section the columns increase in number and size and coalesce to form a continuous biostromal structure (F7), many metres thick, commonly intercalating with parallel-stratified dolomite (F10).

Planar-parallel to wavy-parallel stratified and trough cross-stratified dolomite beds of F10 strongly suggest that this facies was deposited by traction currents. Gutter casts (Fig. 3d) and pillow and ball structures within the dolomite beds suggest storm waves on a shallow shelf. Changes of stromatolite type from shallow intertidal columnar to columnar biostromes, and a conical type, indicate deposition on a low-gradient ramp where the distribution of microbialite facies is distinctly depth-partitioned (Patrabanis-Deb et al., 2018). The gradual change in the shape, size and synoptic relief of stromatolites also suggests balanced sedimentation, deposition and accommodation space generation.

The top part of the VF is mainly characterized by F10 and F11, interpreted to be deposited in an outer ramp environment, below fair-weather wave base. The association comprises a rhythmic occurrence of plane-parallel laminated dolomite (F10) with interbedded

green shale/siltstone and dolomite (F11), commonly interrupted by igneous intrusions. This depozone predominantly involved deposition from background suspension rarely interrupted by strong storm surges. Isolated gutter casts within the dolomite beds are thought to have been produced by storm-generated return flows (Fairchild and Herrington, 1989; Myrow, 1992). Chert and steatite nodules of various shapes and sizes (Fig. 3f) are common with iso-volumetric metasomatic alteration of dolomite to talc observed in the upper part of the VF.

5. RESULTS

5.1. *Petrography*

Petrographic analysis of the VF dolomite led to the identification of four microfacies: i) dolo-micrite with few quartz and feldspar grains, ii) stromatolitic dolomite bindstone, iii) oolitic grainstone (limestone and dolomite), and iv) calcimicrite with local limestone clasts. Micritic dolomite is plane-parallel laminated, where laminae are defined by alternating light (micrite) and dark (clay-rich) layers (Fig. 4a). Dolomicrite is commonly mixed with fine sand or silt-sized grains of well-rounded to sub-rounded quartz and feldspar (Fig. 4b). Dolomicrite shows grain enlargement due to recrystallization (Fig. 4c). Stromatolitic dolomite preserves crinkly to smooth lamination defined by alternating dolomicrite and microbial filaments (Fig. 4d). Preservation of the primary microbial texture suggests that this VF dolomite is either a very early mimetic replacement of $CaCO_3$, preserving the original microbial filaments, or it is a primary microbial dolomite precipitating directly from ancient seawater (Tucker, 1983, Corsetti et al., 2006, van Smeerdijk Hood and Wallace, 2012). Good preservation of microbial structures also indicates little or no recrystallization during diagenesis. The stromatolitic dolomite is characterized by polymodal planar–e and subhedral to anhedral planar–s or non–planar micritic dolomite crystals (see dolomite classification by Sibley and Gregg, 1984, Gregg and Sibley, 1987), with sharp intercrystalline boundaries (Fig. 4e, f). Moreover, the SEM-EDS analysis of thin-sections did not show any relics of calcite crystals.

The coarser carbonate facies include grainstone, mostly with spheroidal ooids, but also eye-shaped ooids. Stages of dolomitization are well-documented and recorded by the ooids (Fig. 5a-f). At one extreme, the ooids are composed entirely of calcite crystals having a radial fabric, such that a continuous sweep of the extinction is seen on stage rotation under crossed polars (Fig.

5a, b). Preserved calcite ooids show well-developed primary concentric, radial and radial–concentric fabrics; some have an outer silicified zone (cf. Tucker, 1984, 1985). Some of the ooids are radially fractured as a result of compaction (Fig. 5a). These radial fractures crudely coincide with the radial fabric which is probably a primary feature. Also the presence of primary radial – concentric fabrics as observed within the unreplaced calcite ooids suggest its growth in a mud-free environment whereas the radial fabric results from ooid growth in a relatively calm environment with the presence of lime mud (Tucker, 1984). The good fabric preservation of the ooids could suggest that they were originally composed of low-Mg calcite since this tends to resist dolomitization; however, they could originally have been high-Mg calcite, with the Mg leached out before dolomitisation (Tucker 1984, 1985). Some calcitic ooids have euhedral rhombic dolomite crystals in the nucleus of the ooid (Fig. 5c). At the other extreme, the ooid cortex is completely replaced by planar–e (euhedral) and subhedral to anhedral planar–s (subhedral) or non–planar micritic dolomite crystals, with sharp but slightly ragged intercrystalline boundaries, completely obliterating the internal fabric but still preserving the shape of the ooids (Fig. 5f). In between there are ooids that show incomplete replacement phenomena where the central part of the ooid is composed of coarse euhedral and mostly planar–e to planar–s dolomite crystals obliterating the internal fabrics, but the outer rim is composed of calcite crystals still preserving the original radial–concentric fabrics (Fig. 5d). The primary radial fabric of the ooid at the peripheral margin is commonly partially destroyed by replacement micritic dolomite (Fig. 5e). Within massive dolomite there are still patches and lenses of limestone that preserve the primary micritic calcite matrix and calcite spar (Fig. 6a); the latter shows Type I calcite twin lamellae and it is partially replaced by dolomicrite destroying the primary fabric (Fig. 6b). Thin-section evidence of fabric-destructive dolomite in VF carbonate rocks indicates a replacement origin (Tucker et al., 2002), and the mimetic to obliterated mosaic texture indicates progressive dolomite replacement (Braithwaite, 1991).

5.2. X-ray diffraction

XRD analysis shows that dolomite is the dominant mineral in the samples analysed, with subordinate quartz and minor K-feldspar (Table 1S, Supplementary section). Barring three samples, calcite is absent in VF dolomite samples analysed. Trace amounts of talc, barite, mica, chlorite and hematite were also detected. Calcium excess of VF dolomites is calculated using the

formula: $CaCO_3$ mol% = 333.33*d_{104} – 911.99 (Lumsden, 1979, where d_{104} is the peak position in angstrom units, Table 2S). VF dolomites have a nearly stoichiometric composition (mole % $CaCO_3$ = 49–51, mean 50) indicating an ideal composition of the dolomite (Mg:Ca = 1). Ordering of VF dolomite crystals ranges from 0.40 to 1.07 (average 0.56), according to the method described by Hardy and Tucker (1988). Only five samples had an ordering ratio <0.5 and >0.4.

5.3. *Geochemistry*

Total iron content of VF dolomite varies from 19,235 ppm to 2170 ppm (average 5240 ppm); Mn ranges from 2040 ppm to 125 ppm (average 320 ppm), whereas Al varies from 19,955 ppm to 160 ppm (average 5475 ppm) (Table 3Sa,b). Average Fe/Mn and Fe/Al ratios are 19.6 and 3.4, respectively. Sodium and Sr concentrations range from 60 ppm to 735 ppm (average 290 ppm) and from 40 ppm to 420 ppm (average 85 ppm), respectively (Table 3Sa,b). Fe and Mn concentrations show a positive correlation (Fig. 7a), whereas the Sr/Ca ratio versus Na_2O shows a poor correlation (Fig. 7b). Mn and Fe concentrations versus the Mg/Ca ratio can be used to explore modification of the carbonate chemistry during burial diagenesis (Gilleaudeau and Kah, 2013). Fe and Mn concentrations of VF dolomites are independent of the Mg/Ca ratio (Fig. 7d, e). The Fe/Sr and Mn/Sr ratios can also be regarded as sensitive indicators of diagenetic alteration as both of the elements Fe and Mn replace Sr during diagenesis (Veizer, 1983; Derry et al., 1992). The Mn/Sr ratio is typically >2 (average 5.1; only five samples have Mn/Sr <2) and the Fe/Sr versus Mn/Sr ratios show positive covariance (Fig. 7c).

V/(V+Ni) ratios vary from 0.6 to 0.9 (average 0.7), whereas the (Cu+Mo)/Zn ratios (Hallberg, 1976; 1982) vary from 5.9 to 0.4 (Table 3Sa). The enrichment factors of redox-sensitive trace elements such as Mo, V and Co ($EF_X = (X_T/Al_T)/(X_{SN}/Al_{SN})$) can be calculated to estimate their relative enrichment or depletion (Tribovillard et al., 2006). VF dolomite is significantly enriched in Mo, V and Co (enrichment factor > 1) relative to PAAS.

The ΣREEs (Table 4S) in dolomite samples range from 0.49 to 11.06 ppm (average 2.4 ppm; standard deviation, SD = 2.5 ppm). Dolomites have mostly homogeneous geochemical features (flat REE + Y patterns, Fig. 8; $(La/Sm)_{SN} \approx 1$, $(Gd/Yb)_{SN} \approx 1$, Fig. 9) with MREE

enrichment and a positive Eu anomaly (Eu/Eu* = 82.2 to 1.02, average Eu/Eu* = 8.25, SD = 15.6). The dolomite samples display a small negative Gd anomaly (0.8<Gd/Gd*<1.3, average Gd/Gd* = 0.99, SD = 0.09), a positive La anomaly (0.7<La/La*<2.08, average La/La* = 1.08, SD = 0.3) and a slightly positive Ce anomaly (0.7<Ce/Ce*<1.3, average Ce/Ce* = 1.03, SD = 0.16). The Y/Ho ratios range between 0.94 and 1.46 (average 1.15, SD = 0.14) and the Pr/Yb ratios range from 0.73 to 3.83 (average 1.32, SD = 0.59), respectively. Marine carbonate sediments in general have a ΣREE range of 0.04 to 14 ppm (Turekian and Wedepohl, 1961). The average ΣREE of typical marine carbonate is 28 ppm (Bellanca et al., 1997). The ΣREE of VF dolomite samples, normalized to PAAS ranges from 11.06 to 0.49 ppm (average 2.4 ppm) and does not show any positive correlation with the major elements (Fe, Mn, Al and Si).

5.4. *Oxygen and carbon isotopes*

The whole–rock $\delta^{18}O$ and $\delta^{13}C$ values of VF dolomite range from −8.1 to −5.2 ‰ (average –6.8 ‰) and −0.35 to 2.0 ‰ (average 0.5 ‰), respectively (Table 5S), and they show an inverse correlation (Fig. 10). Most of the $\delta^{13}C$ values are near 0 ‰ (average 0.5 ‰), with six samples showing slightly depleted values (-0.35 ‰ < $\delta^{13}C$ < 0 ‰), and the majority with slightly elevated $\delta^{13}C$, maximizing at 2‰.

6. Discussion

6.1. *XRD mineralogy and petrography*

The non-ferroan type dolomites ($FeCO_3$ <2 mol%; Tucker and Wright, 1990) are nearly stoichiometric (mol% $CaCO_3$ = 49 to 51, mean 50, Lumsden, 1979) and they are relatively well ordered (degree of order ranging from 0.4 to 1.0, mean 0.6, Hardy and Tucker, 1988). The near stoichiometric and relatively well-ordered nature of the dolomite crystals could reflect slow growth controlled by elevated temperature. This could be the result of dolomitization during burial or burial recrystallization of earlier, near-surface-formed dolomite. Lithospheric stretching and crustal sagging associated with volcanic activity during the interval 1.8 – 2.0 Ga in the CB (Anand et al., 2003; Ravikant et al., 2014) could have provided a higher than normal geothermal gradient during burial.

Petrographic analysis of VF dolomite shows patches of remnant calcimicrite (Fig. 6a) and calcite spar still preserving their primary fabrics like calcite twin-lamellae (Fig. 6b). The presence of twin-lamellae in the precursor calcite suggests a minimum temperature of 170°C is required for diagenetic deformation (Ferrill et al., 2004). Since the calcite ooids with original internal fabrics and textures are primary, and there is no evidence of calcitised aragonite (cf. Tucker, 1985), it is likely that the original lime mud (now calcimicrite) would have been calcitic and this was probably the precursor sediment of VF dolomite. Planar-s dolomite crystals (mostly 5-15 μm) show cloudy centres (due to the presence of minute inclusions) and clear rims; this could suggest either replacement of original limestone or recrystallization of an earlier dolomicrite at depth. Petrographic study has shown that VF dolomite is characterized by the presence of micritic dolomite crystals that commonly exhibit crystal enlargement (recrystallization). The widespread occurrence of dolomitic micritic facies in the VF suggests that the dolomite crystals precipitated rapidly from a dolomite-supersaturated fluid with a high Mg/Ca ratio and low SO_4^{-2} concentration, as would be expected in the Proterozoic compared to typical Phanerozoic environments (Tucker, 1982), because of rapid nucleation and crystallization in a supratidal/upper tidal-flat environment. Rapid dolomite precipitation/replacement might also have been facilitated by fine-grained precursor carbonate sediment that had a high reactive surface area to volume ratio and high density of nucleation sites (Sibley and Gregg, 1987). Microbial influences within the sediment inducing suitable conditions for dolomite precipitation may well have been involved as well (e.g. Bontognali et al., 2010; Petrash et al., 2017; Perri et al., 2018).

6.2. *Redox conditions*

MREE enrichment (Haley et al., 2004) (Fig. 8), strong Europium anomalies (Bau, 1991) (Fig. 8) and absence of negative Ce anomalies (Bau and Koschinsky, 2009) (Fig. 11) in VF dolomite are compelling evidence suggesting its formation from anoxic marine-derived waters. High Fe and Mn concentrations (>1000 ppm and >50 ppm, respectively) of dolomites indicate that the fluids responsible for dolomite formation were iron-rich (Fe^{2+}) and reducing in nature (Budd, 1997). The Fe/Mn ratio of VF dolomite, correlated with the Fe/Al ratio, implies insignificant sulphate reduction and pyrite precipitation during dolomite formation (Barnaby and Read, 1992), and this is consistent with the petrographic observations, where little pyrite was

detected. The Fe/Al ratio (Anderson and Raiswell, 2004; Lyons and Severmann, 2006) of VF dolomite also implies that the fluids responsible for dolomite formation were anoxic but not euxinic. Had the palaeo-fluids been euxinic, Fe^{2+} and other metal ions would have preferred to precipitate as sulphides (such as pyrite), and these were not observed. Hatch and Leventhal (1992) suggested a V/(V+Ni) ratio greater than 0.84 for euxinic, 0.54–0.82 for anoxic, and 0.46–0.60 for dysoxic conditions. The V/(V+Ni) values of VF dolomite vary from 0.6 to 0.88 (average 0.7) indicating chiefly anoxic waters of precipitation. The highest V/(V+Ni) ratio likely suggests euxinic depositional conditions. Hallberg (1976, 1982) proposed that the (Cu+Mo)/Zn ratio can also be used as a proxy to infer redox conditions. This ratio increases under reducing conditions and decreases when the environment is oxidising. VF dolomite samples show that the (Cu+Mo)/Zn ratio can be as high as 5.9 or as low as 0.37; this suggests dolomite formation mostly under reducing conditions. The V/(V+Ni) and (Cu+Mo)/Zn ratios also indicate anoxic depositional conditions. Molybdenum and vanadium are enriched in more reducing environments (Crusius et al., 1996; Algeo and Maynard, 2004; Breit and Wanty, 1991; Wanty and Goldhaber, 1992), whereas Co tends to be less soluble under reducing conditions (Algeo and Maynard, 2004). The enrichment factors ($EF_X = (X_T/Al_T)/(X_{SN}/Al_{SN})$; Tribovillard et al., 2006) of redox-sensitive trace elements (Mo, V and Co) show that dolomite samples are significantly enriched in redox-sensitive trace elements relative to PAAS, suggesting reducing conditions during dolomite precipitation.

6.3. *Post-depositional alteration*

The flat REE patterns of VF dolomite could indicate very limited siliciclastic input to the basin during carbonate deposition. The range of PAAS normalized ΣREE values (0.5 ppm-11.0 ppm) and average ΣREE value (2.4 ppm) of VF dolomite suggests that the precursor rock is probably of marine origin (Turekian and Wedepohl, 1961; Bellanca et al., 1997) and the REE contribution from non-carbonate fractions (Fe-Mn oxides and siliciclastic contamination) appears to be minor (Fig. 12, Piper, 1974; Palmer, 1985). In addition, the Mn and Fe concentrations are independent of the Mg/Ca ratio suggesting minimal post-depositional alteration of VF dolomite (Nordeng and Sibley, 1994; Malone et al., 1996; Machel, 2004). However, The Fe/Sr versus Mn/Sr plot (Fig. 7c) shows clustered data with moderate covariance, suggesting that diagenesis could have altered the parent sediment geochemical signal. However,

447 elevated Mn/Sr ratios of VF dolomite (average 4.9) could be interpreted as a signature of
448 diagenetic alteration (following, for example, Derry et al., 1992, 1994; Kaufman and Knoll,
449 1995; Montañez et al., 1996), although on the other hand, this may not necessarily always be the
450 case (for an alternative view see Knoll et al., 1995; Lindsay and Brasier, 2000); it could be
451 related to the fluid chemistry (Yoshioka et al., 2003; Shen et al., 2005; Font et al., 2006; Hurtgen
452 et al., 2006; Nédélec et al., 2007). Also, Archean and Palaeoproterozoic dolomites on average
453 contain more Fe and Mn than younger carbonate rocks (Veizer et al., 1990), thus complicating
454 the application of the Mn/Sr ratio as an index of alteration. The low Y/Ho ratio (0.94-1.46; mean
455 1.15, SD = 0.14) and the Y/Ho and Ce/Ce* cross-plot (Fig. 13) probably indicate a variable
456 degree of contamination of the precursor carbonate by clay material, reflecting the depositional
457 setting in a shoreline or lagoonal environment (Kamber and Webb, 2001).
458
459 **6.4. *Fluid source***
460 The PAAS-normalized REE profiles for VF dolomite show no LREE depletion, show
461 MREE enrichment (cf. Haley et al., 2004) and have positive Eu and Y/Ho anomalies with a
462 weakly positive Ce anomaly. These observed REE characteristics are consistent with the
463 chemistry of anoxic marine basins (Bau and Möller, 1993), ferruginous lakes, marine
464 hydrothermal plumes and anoxic diagenetic waters (Johannesson and Zhou 1999; Sherrell et al.,
465 1999; Haley et al., 2004; Wang et al., 2018). The weakly positive Gd anomaly present in VF
466 dolomite may reflect seawater precipitation (Bau, 1999). Eu is also normally enriched in
467 Archean seawater-precipitated carbonate too (Bolhar and Karnendonk, 2007), the source of
468 which can be either hydrothermal solutions derived from mid-ocean ridges and/or back-arc
469 spreading centres, or burial diagenetic fluids (Michard et al., 1983; Michard, 1989; Derry and
470 Jacobsen, 1990; German et al., 1990; Murray et al., 1991; Danielson et al., 1992; German et al.,
471 1993; German et al., 1999; Douville et al., 1999; Kamber and Webb, 2001; Eroglu et al., 2017;
472 Schier et al., 2018). In VF dolomite significant positive correlation is observed between Eu/Eu*
473 and Ba content (Fig. 14) and this clearly indicates the influence of hydrothermal activity on the
474 studied carbonates (Khelen et al., 2017). Extensive volcanic activity in the CB around 1.9 to 2.0
475 Ga in a continental rift setting (Anand et al., 2003; Ravikant et al., 2014) could be the source for
476 Eu. However, diagenetic alteration of the precursor carbonate sediments is suggested by the

Fe/Sr versus Mn/Sr plot (Fig. 8c), low Y/Ho ratio (0.94-1.46; mean 1.15, SD = 0.14) and the Y/Ho and Ce/Ce* plot (Fig. 13), and this could also have enhanced the Eu anomaly.

Sodium content of dolomites can be used as an indicator of salinity of the fluid from which the dolomites precipitated (Land and Hoops, 1973; Sass and Katz, 1982; Sass and Bein, 1988; Budd, 1997). The low Na concentrations (60-735 ppm, average 290 ppm) of VF dolomite along with the poor correlation of Sr/Ca vs. Na_2O (Fig. 8b) rules out their hypersaline fluid origin and probably suggests a diagenetic fluid source. Depletion in Na, however, can also be a consequence of burial (Sachan, 1993), as successive episodes of dolomitization of limestone and dolomite recrystallisation would reduce the levels of Na (Warren, 2000). Similarly, low strontium concentrations (40–420 ppm, average 85 ppm; average Sr value of lithospheric carbonate rocks is 610 ppm; Turekian and Wedepohl, 1961) of VF dolomite probably reflect a Sr-depleted water-buffered diagenetic system (Budd, 1997; Warren, 2000; Azmy et al., 2001), supporting a burial diagenetic effect (Sachan, 1993; Warren, 2000). Tucker (1983), from studies of the Precambrian Beck Spring Dolomite, suggested that low concentrations of Na and Sr in ancient dolomites excludes precipitation from marine fluids and warrants either fluid–mixing or wet–recrystallization of an initially precipitated poorly-ordered calcian dolomite that drives out Na and Sr.

The $\delta^{13}C$ values (− 0.4 ‰ to 2.0 ‰; average value 0.5 ‰) of dolomite samples probably reflect the carbon isotopic composition of the precursor carbonate precipitated from the Proterozoic seawater. Palaeoproterozoic carbonate successions are characterized by $\delta^{18}O$ values ranging from –6 to –12 ‰ (Tucker, 1982; Burdett et al., 1990; Veizer et al., 1992a; 1992b; Melezhik et al., 1997; Bekker et al., 2001; 2003a, b). The oxygen isotope range (–5.2 to –8.1 ‰) for VF dolomite is within this range and is consistent with precipitation (or recrystallization) during shallow to moderate burial (Sachan, 1993; Warren, 2000).

7. PROBABLE MECHANISM OF DOLOMITIZATION

The field observations and petrographic features of the dolomites within the Palaeoproterozoic VF can be interpreted in terms of early dolomitization of peritidal platform carbonate sediment consisting of lime mud and calcimicrite. Preservation of microbial fabric

elements of the stromatolitic dolomite suggests that either VF dolomite associated with microbial-laminites formed as primary precipitates due to microbial activity and minor evaporation (Hird et al., 1987) or that they are very early, replacement mimetic dolomites. During subsequent shallow sub-surface burial and diagenesis, fabric-destructive dolomitization of the undolomitized oolitic grainstones and calcimicrite, along with recrystallization of the early-formed peritidal dolomite happened as suggested by the petrographic textures. In terms of seawater chemistry in the Palaeoproterozoic CB, it is likely that this was a time of calcite precipitation (a "calcite sea"), with anoxic and ferruginous conditions, and an elevated Mg/Ca ratio but not so high that very early fabric-retentive dolomitization of ooids and cements could take place, like those of the Beck Spring Dolomite (Tucker, 1983). The lack of a very high seawater Mg/Ca ratio could be related to the onset of rifting of supercontinent Columbia around 2.0 Ga that coincides with the VF carbonate sedimentation. Grotzinger (1989) proposed that Precambrian seawater was oversaturated with respect to calcium carbonate that favoured abiotic carbonate precipitation that gradually decreased the carbonate saturation through the Proterozoic to Phanerozoic levels. This process, coupled with a fast rate of sea-floor spreading, would draw Mg^{2+} down producing a "calcite ocean" (Wilkinson and Algeo, 1989; Bots et al., 2011). This ocean chemistry is in contrast to the anoxic, ferruginous and extremely high Mg/Ca conditions that prevailed during Neoproterozoic time (Hood and Wallace, 2018). In addition, the coarse replacement VF dolomite crystallized from a burial fluid that evolved from the europium-enriched anoxic seawater with a lower SO_4 content (Hood and Wallace, 2018), as marine water or its derivative is the only known infinite source of Mg^{2+} and Ca^{2+}. The PAAS-normalized REE profiles for VF dolomite are consistent with the chemistry of anoxic diagenetic waters. Low Na and Sr concentrations of VF dolomite in and around Parnapalle also suggest their precipitation (or early recrystallisation) during burial diagenesis (Veizer, 1983; Vahrenkamp and Stewart, 1990; Tucker and Wright, 1990; Banner, 1995; Budd, 1997; Warren, 2000; Azmy et al., 2001; Balter et al., 2011; Sosdian et al., 2012); this is also supported by the stable isotope ($\delta^{18}O$) values that fall within the range of the burial dolomite model (Warren, 2000; Machel, 2004). The $\delta^{13}C$, on the other hand, having 'marine' values, suggests that the original lime mud and/or micritic calcite were derived from seawater (Tucker and Wright, 1990). The likely factor promoting dolomite formation during early burial diagenesis could be the presence of an early, finely-crystalline, less well-ordered dolomite, as is being precipitated in modern tidal flats and

539 microbial mats in Abu Dhabi and Qatar (e.g., Bontognalli et al., 2010; Perri et al., 2018). These
540 early Ca-Mg precipitates could have provided the nuclei and substrates for continued dolomite
541 formation. The near-stoichiometric and relatively well-ordered VF dolomite crystals probably
542 would be the result of dolomite recrystallisation during burial, possibly promoted by an elevated
543 geothermal gradient from crustal thinning and mafic volcanic activity around 2.0 – 1.8 Ga
544 (Anand et al., 2003; Ravikant et al., 2014). Such tectonic-volcanic processes may have
545 diagenetically-modified the then seawater composition and be responsible for the positive Eu
546 anomaly (Eu/Eu* = 89.33-1.03) recorded in VF dolomite.
547
548 **8. CONCLUSIONS**
549 Combined field data and microscopic observations suggest that the Cuddapah Basin
550 carbonate rocks initially precipitated as fine lime mud and/or micritic calcite in tidal–flat and
551 associated shallow-marine environments. These sediments were replaced by dolomicrite during
552 early peritidal dolomitization. Petrographic observations also reveal fabric-retentive dolomite
553 textures, including filaments, in stromatolites, possibly reflecting microbial dolomite
554 precipitation-dolomitisation. During shallow sub-surface burial, fabric destructive dolomitization
555 of undolomitized oolitic grainstone and calcimicrite took place, along with recrystallization of
556 the early-formed peritidal dolomite. The $\delta^{18}O$ and $\delta^{13}C$ values of VF dolomite samples suggest
557 that these dolomites were either precipitated or recrystallised from burial diagenetic fluids that
558 evolved from Eu-enriched seawater. Burial diagenetic precipitation and recrystallisation of
559 dolomite are also supported by depleted Na and Sr contents. Ratios and contents of redox-
560 sensitive metals (Cu, Co, Fe, Mn, Mo, Ni, V, Zn), REE distribution and high Fe_T/Al ratios imply
561 that dolomitizing fluids were anoxic and ferruginous but not euxinic. The positive Eu anomaly
562 could reflect a hydrothermal source and this may have been related to fluids connected to
563 continental rifting and volcanic activity within the CB around 1.9 – 2.0 Ga. The pattern of
564 diagenesis and dolomitisation recorded in the VF is more typical of Phanerozoic platform
565 carbonates than many Precambrian dolomites which show perfect preservation of original
566 textures (such as ooids and fibrous cements) and continued precipitation of dolomite in the burial
567 environment as a dolospar cement.
568
569

Acknowledgments

We thank the Indian Statistical Institute (ISI) for financial support in the form of a DCSW grant to Amlan Banerjee and acknowledge S.N. Das and the late Rajen Oraon for their help in the fieldwork. Marcin D. Syczewski is thanked for helping with work on the SEM. We thank Prof. Bernard Pittet and an anonymous reviewer for their comments and suggestions that improved the quality of the paper. This study was also supported by the Russian Government Programme of Competitive Growth of the Kazan Federal University and by the European Regional Development Fund through the grant Innovative Economy (POIG.02.02.00-00-025/09). This work contributes to the Proterozoic research programme of the ISI.

References

Algeo, T.J., Maynard, J.B., 2004. Trace element behaviour and redox facies in core shales of Upper Pennsylvanian Kansas-type cyclothems. Chemical Geology 206, 289–318.

Anand, M., Gibson, S.A., Subba Rao, K.V., Kelley, S.P., Dickin, A.P., 2003. Early Proterozoic melt generation processes beneath the intra-cratonic Cuddapah Basin, Southern India. Journal of Petrology 44, 2139-2171.

Anderson, T.F., Raiswell, R., 2004. Sources and mechanisms for the enrichment of highly reactive iron in euxinic Black Sea sediments. American Journal of Science 304, 203-233.

Azmy, K., Veizer, J., Misi, A., de Oliveira, T.F., Sanches, A.L., Dardenne, M.A., 2001. Dolomitization and isotope stratigraphy of the Vazante Formation, São Francisco Basin, Brazil. Precambrian Research 112, 303–329.

Balter, V., Lécuyer, C., Barrat, J.A., 2011. Reconstructing seawater Sr/Ca during the last 70 My using fossil fish tooth enamel. Palaeogeography, Palaeoclimatology, Palaeoecology 310, 133–138.

Banner, J.L., 1995. Application of the trace element and isotope geochemistry of strontium to studies of carbonate diagenesis. Sedimentology 42, 805–824.

Barnaby, R.J., Read, J.F., 1992. Dolomitization of a carbonate platform during late burial: Lower to Middle Cambrian Shady Dolomite, Virginia Appalachians. Journal of Sedimentary Petrology 62, 1023–1043.

Bau, M., Koschinsky, A., 2009. Oxidative scavenging of cerium on hydrous Fe oxide: Evidence from the distribution of rare earth elements and yttrium between Fe oxides and Mn oxides in hydrogenetic ferromanganese crusts. Geochemical Journal 43, 37-47.

Bau, M., Möller, P., 1993. Rare earth element systematics of the chemically precipitated component in Early Precambrian iron formations and the evolution of the terrestrial atmosphere-hydrosphere-lithosphere system. Geochimica et Cosmochimica Acta 57, 2239-2249.

Bau, M., 1991. Rare earth element mobility during hydrothermal and metamorphic fluid-rock interaction and the significance of the oxidation state of europium. Chemical Geology 93, 219-230.

Bau, M., 1999. Scavenging of dissolved yttrium and rare earths by precipitating iron oxyhydroxide: Experimental evidence for Ce oxidation, Y-Ho fractionation, and lanthanide tetrad effect. Geochimica et Cosmochimica Acta 63, 67-77.

Bau, M., Dulski, P., 1996. Distribution of Yttrium and Rare-Earth Elements in the Penge and Kuruman Iron Formations, Transvaal Supergroup, South Africa. Precambrian Research 79, 37-55. doi:10.1016/0301-9268(95)00087-9

Bekker, A., Kaufman, A.J., Karhu, J.A., Beukes, N.J., Swart, Q.D., Coetzee, L.L., Eriksson, K.A., 2001. Chemostratigraphy of the Paleoproterozoic Duitschland Formation, South Africa: implications for coupled climate change and carbon cycling. American Journal of Science 301, 261–285.

Bekker, A., Karhu, J.A., Eriksson, K.A., Kaufman, A.J. 2003a. Chemostratigraphy of Paleoproterozoic carbonate successions of the Wyoming Craton: tectonic forcing of biogeochemical change? Precambrian Research 120, 279–325.

Bekker, A., Sial, A.N., Karhu, J.A., Ferreira, V.P., Noce, C.M., Kaufman, A.J., Romano, A.W., Pimentel, M.M., 2003b. Chemostratigraphy of carbonates from the Minas Supergroup, Quadrilátero Ferrífero, Brazil: a stratigraphic record of early Proterozoic atmospheric, biogeochemical and climatic change. American Journal of Science 303, 865–904.

Bellanca, A., Masetti, D., Neri, R., 1997. Rare earth elements in limestone/marlstone couplets from the Albian-Cenomanian Cismon section (Venetian region, northern Italy): assessing REE sensitivity to environmental changes. Chemical Geology 141, 141–152.

Bhaskar Rao, Y.J., Pantulu, G.V.C., Damodar Reddy, V., Gopalan, K. 1995. Time of early sedimentation and volcanism in the Proterozoic Cuddapah basin, South India: evidence from Rb–Sr age of Pulivendla mafic sill. Geological Society of India, Memoir 33, 329–338.

Bolhar, R., Van Kranendonk, M.J., 2007. A non-marine depositional setting for the northern Fortescue Group, Pilbara Craton, inferred from trace element geochemistry of stromatolitic carbonates. Precambrian Research 155, 229–250.

Bontognali, T.R.R., Vasconcelos, C., Warthmann, R.J., Bernasconi, S.M., Dupraz, C., Strohmenger, C.J., McKenzie, J.A., 2010. Dolomite formation within microbial mats in the coastal sabkha of Abu Dhabi (United Arab Emirates). Sedimentology 57, 824–844.

Bots, P., Benning, L.G., Rickaby, R., Shaw, S., 2011. The role of SO_4 in the switch from calcite to aragonite seas. Geology 39, 331-334.

Braithwaite, R., 1991. Dolomites, a review of origins, geometry and textures. Transactions of the Royal Society of Edinburgh: Earth Sciences 82, 99–112.

Breit, G.N., Wanty, R.B., 1991. Vanadium accumulation in carbonaceous rocks: A review of geochemical controls during deposition and diagenesis. Chemical Geology 91, 83- 97.

Budd, D.A., 1997. Cenozoic dolomites of carbonate islands: their attributes and origin. Earth-Science Reviews 42, 1–47.

Burdett, J.W., Grotzinger, J.P., Arthur, M.A., 1990. Did major changes in the stable-isotope composition of Proterozoic seawater occur? Geology 18, 227-230.

Chakrabarti, G., Shome, D., Kumar, S., Armstrong-Altrin, J.S., Sial, A.N., 2011. Carbon and oxygen isotopic variations in stromatolitic dolomites of Palaeoproterozoic Vempalle Formation, Cuddapah Basin, India. Carbonates and Evaporites 26, 181-191.

Chakrabarti, G., Shome, D., Kumar, S., Kah, L., 2014. Carbonate platform development in a Paleoproterozoic extensional basin, Vempalle Formation, Cuddapah Basin, India. Journal of Asian Earth Sciences 91, 263-279.

Collins, A.S. Patranabis-Deb, S. Alexander, E. Bertram, C.N., Falster, G.M., Gore, R.J., Mackintosh, J., Dhang, P.C., Saha, D., Payne, J.L., Jourdan, F., Backe, G., Halverson, G.P., Wade, B.P., 2015. Detrital mineral age, radiogenic isotopic stratigraphy and tectonic significance of the Cuddapah Basin, India. Gondwana Research 28, 1294-1309.

Corsetti, F.A., Kidder, D.L., Marenco, P.J., 2006. Trends in oolite dolomitization across the Neoproterozoic-Cambrian boundary: a case study from Death Valley, California. Sedimentary Geology 191, 135-150.

Crusius, J., Calvert, S., Pedersen, T., Sage, D., 1996. Rhenium and molybdenum enrichments in sediments as indicators of oxic, suboxic and sulfidic conditions of deposition. Earth and Planetary Science Letters 145, 65–78.

Danielson, A., Möller, P., Dulski, P., 1992. The europium anomalies in banded iron formation and the thermal history of the oceanic crust. Chemical Geology 97, 89–100.

Derry, L.A., Jacobsen, S.B., 1990. The chemical evolution of Precambrian seawater: Evidence from REEs in banded iron formations. Geochimica et Cosmochimica Acta 54, 2965-2977.

Derry, L.A., Kaufman, A.J., Jacobsen, S.B., 1992. Sedimentary cycling and environmental change in the Late Proterozoic: evidence from stable and radiogenic isotopes. Geochimica et Cosmochimica Acta 56, 1317–1329.

Derry, L.A., Brasier, M.D., Corfield, R.M., Rozanov, A.Y., Zhuravlev, A.Y., 1994. Sr and C isotopes in Lower Cambrian carbonates from the Siberian craton: A paleoenvironmental record during the 'Cambrian explosion'. Earth and Planetary Science Letters 128, 671–681.

Douville, E., Bienvenu, P., Charlou, J.L., Donval, J.P., Fouquet, Y., Appriou, P., Gamo, T., 1999. Yttrium and rare earth elements in fluids from various deep-sea hydrothermal systems. Geochimica et Cosmochimica Acta 63, 627–643.

Eroglu, S., van Zuilen, M.A., Taubald, H., Drost, K., Wille, M., Swanner, E.D., Beukes, N.J., Schoenberg, R., 2017. Depth-dependent $\delta^{13}C$ trends in platform and slope settings of the Campbellrand-Malmani carbonate platform and possible implications for Early Earth oxygenation. Precambrian Research 302, 122-139.

Fairchild, I.J., Herrington, P.M., 1989. A tempestite-stromatolite-evaporite association (late Vendian, East Greenland): A shoreface-lagoon model. Precambrian Research 43, 101-127.

Ferrill, D.A., Morris, A.P., Evans, M.A., Burkhard, M., Groshong Jr., R.H., Onasch, C.M., 2004. Calcite twin morphology: a low-temperature deformation geothermometer. Journal of Structural Geology 26, 1521-1529.

Font, E., Nédélec, A., Trindade, R.I.F., Macouin, M., Charrière, A., 2006. Chemostratigraphy of the Neoproterozoic Mirassol d'Oeste cap dolostones (Mato Grosso, Brazil): An alternative model for Marinoan cap dolostone formation. Earth and Planetary Science Letters 250, 89-103.

French, J.E., Heaman, L.M., Chacko, T., Srivastava, R.K., 2008. 1891–1883 Ma Southern Bastar–Cuddapah mafic igneous events, India: A newly recognized large igneous province. Precambrian Research 160, 308–322.

German, C.R., Elderfield, H., 1990. Application of the Ce anomaly as a paleoredox indicator: the ground rules. Paleoceanography 5, 823.

German, C.R., Hergt, J., Palmer, M.R., Edmond, J.M., 1999. Geochemistry of a hydrothermal sediment core from the OBS vent-field, 21°N East Pacific Rise. Chemical Geology 155, 65-75.

German, C.R., Higgs, N.C., Thomson, J., Mills, R., Elderfield, H., Blusztajn, J., Fleer, A.P., Bacon, M.P., 1993. A geochemical study of metalliferous sediment from the TAG Hydrothermal Mound, 26°08′N, Mid-Atlantic Ridge. Journal of Geophysical Research 98, 9683-9692.

Gilleaudeau, G.J., Kah, L.C., 2013. Carbon isotope records in a Mesoproterozoic epicratonic sea: Carbon cycling in a low-oxygen world. Precambrian Research 228, 85-101.

Gregg, J.M., Sibley, D.F., 1984. Epigenetic dolomitization and the origin of xenotopic dolomite texture. Journal of Sedimentary Research 54, 908-931.

748 Grotzinger, J.P., 1989. Facies and evolution of Precambrian carbonate depositional systems:
749 emergence of the modern platform archetype. SEPM Special Publication 44, 79-106.

750 Grotzinger, J.P., Read, J.F., 1983. Evidence for primary aragonite precipitation, lower
751 Proterozoic (1.9 Ga) dolomite, Wopmay orogen, northwest Canada. Geology 11, 710-713.

752 Grotzinger, J.P., Kasting, J., 1993. New constraints on Precambrian ocean composition. Journal
753 of Geology 101, 235-243.

754 Haley, B., Klinkhammer, G. P., McManus, J., 2004. Rare earth elements in pore waters of
755 marine sediments. Geochimica et Cosmochimica Acta 68, 1265-1279.
756
757 Hallberg, R.O., 1976. A geochemical method for investigation of palaeoredox conditions in
758 sediments. Ambio Special Report 4, 139-147.
759
760 Hallberg, R.O., 1982. Diagenetic and environmental effects on heavy-metal distribution in
761 sediments: A hypothesis with an illustration from the Baltic Sea. In: Fanning, K.A., Manheim,
762 F.T. (Eds), The dynamic environment of the ocean floor. Lexington Books, Lexington, p. 305-
763 316.
764
765 Hardy, R., Tucker, M.E., 1988. X-ray powder diffraction of sediments. In: Tucker, M.E. (Ed.)
766 Techniques in Sedimentology. Blackwell Scientific Publications, p. 191-228.
767
768 Hatch, J.R., Leventhal, J.S., 1992. Relationship between inferred redox potential of the
769 depositional environment and geochemistry of the Upper Pennsylvanian (Missourian) Stark
770 Shale Member of the Dennis Limestone, Wabaunsee County, Kansas, U.S.A. Chemical
771 Geology 99, 65–82.
772
773 Hird, K., Tucker, M.E., Waters, R.A., 1987. Petrography, geochemistry and origin of Dinantian
774 dolomites from South-East Wales. In: Miller, J., Adams, A.E., and Wright, V.P. (Eds) European
775 Dinantian Environments. Wiley, New York, 359–376.
776
777 Holland, H., Zimmermann, H., 2000. The dolomite problem revisited. International Geology
778 Review 42, 481–490.
779
780 Holland, S.M., Patzkowsky, M.E., 1998. Sequence stratigraphy and relative sea-level history of
781 the Middle and Upper Ordovician of the Nashville Dome, Tennessee. Journal of Sedimentary
782 Research 68, 684-699.
783
784 Hood, A.S., Wallace, M.W., 2018. Neoproterozoic marine carbonates and their
785 paleoceanographic significance. Global and Planetary Change 160, 28-45.
786
787 Hurtgen, M.T., Galen, G.P., Arthur M.A., Hoffman, P.F., 2006. Sulfur cycling in the aftermath of
788 635-Ma snowball glaciation: evidence for a syn-glacial sulfidic deep ocean. Earth and Planetary
789 Science Letters 245, 551–570.
790

Jahn, B.M., Cuvellier, H., 1994. Pb-Pb and U-Pb geochronology of carbonate rocks: an assessment. Chemical Geology 115, 125-151.

Jahn, B.M., Simonson, B.M., 1995. Carbonate Pb-Pb ages of the Wittenoom Formation and Carawine Dolomite, Hamersley Basin, Western Australia (with implications for their correlation with the Transvaal Dolomite of South Africa). Precambrian Research 72, 247-261.

Johannesson, K.H., Zhou, X. 1999. Origin of middle rare earth element enrichments in acid waters of a Canadian High Arctic lake. Geochimica et Cosmochimica Acta 63, 153–165.

Kamber, B.S., Webb, G.E., 2001. The geochemistry of late Archaean microbial carbonate: implications for ocean chemistry and continental erosion history. Geochimica et Cosmochimica Acta 65, 2509-2525.

Kaufman, A.J., Knoll, A.H., 1995. Neoproterozoic variations in the C-isotopic composition of seawater: stratigraphic and biogeochemical implications. Precambrian Research 73, 27-49.

Khelen, A.C., Manikyamba, C., Ganguly, S., Singh, T., Subramanyam, K.S.V., Ahmad, S.M., Reddy, M.R., 2017. Geochemical and stable isotope signatures of Proterozoic stromatolitic carbonates from the Vempalle and Tadpatri Formations, Cuddapah Supergroup, India: Implications on paleoenvironment and depositional conditions. Precambrian Research 298, 365–384.

Knoll, A.H., Kaufman, A.J., Semikhatov, M.A., 1995. The carbon isotopic composition of Proterozoic carbonates of Riphean successions from northwestern Siberia (Anabar Massif, Turukhansk Uplift). American Journal of Science 295, 823–850.

Land, L.S., Hoops, G.K., 1973. Sodium in carbonate sediments and rocks; a possible index to the salinity of diagenetic solutions. Journal of Sedimentary Petrology 43, 614-617.

Lawrence, M.G., Kamber, B.S., 2006. The behaviour of the rare earth elements during estuarine mixing – revisited. Marine Chemistry 100, 147-161.

Lindsay, J.F., Brasier, M.D., 2000. A carbon isotope reference curve for 1700–1575 Ma, McArthur and Mount Isa Basins, Northern Australia. Precambrian Research 99, 271–308.

Lumsden, D.N., 1979. Discrepancy between thin-section and X-ray estimates of dolomite in limestone. Journal of Sedimentary Petrology 49, 429– 435.

Lyons, T.W., Severmann, S., 2006. A critical look at iron paleoredox proxies: New insights from modern euxinic marine basins. Geochimica et Cosmochimica Acta 70, 5698-5722.

Machel, H.G., 2004. Concepts and models of dolomitization: a critical reappraisal. Geological Society, London, Special Publications 235, 7-63.

836 Majumder, T., Patranabis-Deb, S., Nemec, W., 2015. Palaeoproterozoic sedimentation in the
837 Cuddapah Basin of southern India. Abstracts 31st IAS Meeting of Sedimentology, 22-25 June,
838 2015, Kraków, Poland, p. 326.
839
840 Malone, M.J., Baker, P.A., Burns, S.J., 1996. Recrystallization of dolomite: An experimental
841 study from 50–200 ^{o}C. Geochimica et Cosmochimica Acta 60, 2189–2207.
842
843 Melezhik, V.A., Fallick, A.E., Makarikhin, V.V., Lubtsov, V.V., 1997. Links between
844 Palaeoproterozoic palaeogeography and rise and decline of stromatolites: Fennoscandian Shield.
845 Precambrian Research 82, 311–348.
846
847 Michard, A., Albarbde, F., Michard, G., Minster, J.F. and Charlou, J.L., 1983. Rare earth
848 elements and uranium in high-temperature solutions from East Pacific Rise hydrothermal vent
849 field (13 ^{o}N). Nature 303, 795-797.
850
851 Michard, A., 1989. Rare earth element systematics in hydrothermal fluids. Geochimica et
852 Cosmochimica Acta 53, 745–750.
853
854 Montañez, I.P., Banner, J.L., Osleger, D.A., Borg, L.E., Bosserman, P.J., 1996. Integrated Sr
855 isotope variations and sea-level history of Middle to Upper Cambrian platform carbonates:
856 Implications for the evolution of Cambrian seawater $^{87}Sr/^{86}Sr$. Geology 10, 917–920.
857
858 Murray, R.W., Buchholtz Ten Brink, M.R., Gerlach, D.C., Price Russ III, G., Jones, L. D., 1991.
859 Rare earth, major, and trace elements in chert from the Franciscan Complex and Monterey
860 Group, California: Assessing REE sources to fine-grained marine sediments. Geochimica et
861 Cosmochimica Acta 55, 1875-1895.
862
863 Myrow, P.M., 1992. Pot and gutter casts from the Chapel Island Formation, southeast
864 Newfoundland. Journal of Sedimentary Research 62, 992-1007.
865
866 Nagaraja Rao, B.K., Rajurkar, S.T., Ramalingaswamy, G., Ravindra Babu, B., 1987,
867 Stratigraphy, structure and evolution of the Cuddapah Basin. In: Radhakrishna, B.P., (Ed.)
868 Purana Basins of Peninsular India (Middle to Late Proterozoic). Geological Society of India 6,
869 33–86.
870
871 Nédélec, A., Affaton, P., France-Lanord, C., Charrière, A., Alvaro, J., 2007. Sedimentology and
872 chemostratigraphy of the Bwipe Neoproterozoic cap dolostones (Ghana, Volta Basin): A record
873 of microbial activity in a peritidal environment. Comptes Rendus Geoscience 339, 223–239.
874
875 Nordeng, S.H., Sibley, D.E., 1994. Dolomite stoichiometry and Ostwald's step rule. Geochimica
876 et Cosmochimica Acta 58, 191-196.
877
878 Palmer, M.R., 1985. Rare earth elements in foraminifera tests. Earth and Planetary Science
879 Letters 73, 285-298.
880

881 Patranabis-Deb, S., Saha, D., Tripathy, V., 2012. Basin stratigraphy, sea-level fluctuations and
882 their global tectonic connections – evidence from the Proterozoic Cuddapah Basin. Geological
883 Journal 47, 263-283.
884
885 Patranabis-Deb, S., Majumder, T., Khan, S., 2018. Lifestyles of the Palaeoproterozoic
886 stromatolite builders in the Vempalle Sea, Cuddapah Basin, India. Journal of Asian Earth
887 Sciences 157, 360–370.
888
889 Perri, E., Tucker, M.E., Słowakiewicz, M., Whitaker, F., Bowen, L., Perrotta, Ida D., 2018.
890 Carbonate and silicate biomineralization in a hypersaline microbial mat (Mesaieed sabkha,
891 Qatar): Roles of bacteria, extracellular polymeric substances and viruses. Sedimentology 65,
892 1213-1245.
893
894 Petrash, D.A., Bialikb, O.M., Bontognali, T.R.R., Vasconcelos, C., Roberts, J.A., McKenzie,
895 J.A., Konhauser, K.O., 2017. Microbially catalyzed dolomite formation: From near-surface to
896 burial. Earth-Science Reviews 171, 558-582.
897
898 Piper, D.Z., 1974. Rare-earth elements in the sedimentary cycle: a summary. Chemical Geology
899 14, 285-304.
900
901 Pope, M.C., Grotzinger, J.P., 2003. Paleoproterozoic Stark Formation, Athapuscow basin,
902 northwest Canada: Record of cratonic-scale salinity crisis. Journal of Sedimentary Research 73,
903 280-295.
904
905 Rai, A.K., Pandey, U.K., Zakaulla, S., Parihar, P.S., 2015. New 1.9-2.0 Ga, Pb-Pb (PbSL), age of
906 dolomites from Vempalle Formation, Lower Cuddapah Supergroup, Eastern Dharwar Craton,
907 India. Journal of the Geological Society of India 86, 131-136.
908
909 Ravikant V., Hashmi, S., Chatterjee, C., Ji, W-Q., Wu, F-Y., 2014. Initiation of the intra–
910 cratonic Cuddapah basin: evidence from Paleoproterozoic (1995 Ma) anorogenic porphyritic
911 granite in Eastern Dharwar Craton basement. Journal of Asian Earth Sciences 79, 235-245.
912
913 Ravikant, V., 2010. Paleoproterozoic (1.9 Ga) extension and breakup along the eastern margin of
914 the Eastern Dharwar Craton, SE India: New Sm–Nd isochorn age constraints from anorogenic
915 mafic magmatism in the Neoarchean Nellore greenstone belt. Journal of Asian Earth Sciences
916 12, 67-81.
917
918 Sachan, H.K., 1993. Early replacement, dolomitization and deep burial modification and
919 stabilization: A case study from the Zawar area, Rajasthan (India). Carbonates and Evaporites 8,
920 191-198.
921
922 Saha, D., Mazumder, R., 2012. An overview of the Paleoproterozoic geology of peninsular India
923 and key stratigraphic and tectonic issues. Geological Society, London, Special Publications 365,
924 159–182
925

926 Saha, D., Tripathy, V., 2012. Paleoproterozoic sedimentation in the Cuddapah basin, south India
927 and regional tectonics – a review. Geological Society, London, Special Publications 365, 5–28.
928
929 Sass, E., Bein, A., 1988. Dolomites and salinity: a comparative geochemical study. SEPM
930 Special Publications 43, 223–233.
931
932 Sass, E., Katz, A., 1982. The origin of platform dolomites. New evidence. American Journal of
933 Science 282, 1184–1213.
934
935 Saylor, B.Z., Grotzinger, J.P., Germs, J.B., 1995. Sequence stratigraphy and sedimentology of
936 the Neoproterozoic Kuibis and Schwarzrand Subgroups (Nama Group), southwestern Namibia.
937 Precambrian Research 73, 153-171.
938
939 Schier, K., Bau, M., Münker, C., Beukes, N., Viehmann, S., 2018. Trace element and Nd isotope
940 composition of shallow seawater prior to the Great Oxidation Event: Evidence from stromatolitic
941 bioherms in the Paleoproterozoic Rooinekke and Nelani Formations, South Africa. Precambrian
942 Research 315, 92-102.
943
944 Shen, Y.N., Zhang, T.G., Chu, X.L., 2005. C-isotopic stratification in a Neoproterozoic
945 postglacial ocean. Precambrian Research 137, 243–251.
946
947 Sherrell, R.M., Field, M.P., Ravizza, G., 1999. Uptake and fractionation of rare earth elements
948 on hydrothermal plume particles at 9°25′N, East Pacific Rise. Geochimica et Cosmochimica
949 Acta 63, 1709–1722.
950
951 Sibley, D.F., and Gregg, J.M., 1987. Classification of dolomite rock textures. Journal of
952 Sedimentary Petrology 57, 967-975.
953
954 Sosdian, S.M., Lear, C.H., Tao, K., Grossman, E.L., O'Dea, A., Rosenthal, Y., 2012. Cenozoic
955 seawater Sr/Ca evolution. Geochemistry Geophysics Geosystems 13, Q10014.
956
957 Swett, K., Knoll, A.H., 1989. Marine pisolites from Upper Proterozoic carbonates of East
958 Greenland and Spitsbergen. Sedimentology 36, 75–93.
959
960 Tewari, V., Tucker, M.E., 2011. Ediacaran Krol carbonates of the Lesser Himalaya, India:
961 Stromatolitic facies, depositional environment and diagenesis. In: Tewari, V., Seckbach, J.,
962 (eds.), Stromatolites: Interaction of Microbes with Sediments. Springer, 133-156.
963
964 Tribovillard, N., Algeo, T.J., Lyons, T., Riboulleau, A., 2006. Trace metals as paleoredox and
965 paleoproductivity proxies: an update. Chemical Geology 232, 12–32.
966
967 Tripathy, V., Saha, D., 2008. Temporal stress variation around Gani-Kalva and adjoining faults,
968 Cuddaph basin: implications for continental tectonics. In: Biswal, T.K., Pandalai, H.S., Pande,
969 K., Pillai, S.P. (Eds.) Abstract volume, International conference on Tectonics of the Indian
970 Subcontinent, International Association for Gondwana Research Conference Series 5, 209–210.
971

Tucker, M.E., 1982. Precambrian dolomites: Petrographic and isotopic evidence that they differ from Phanerozoic dolomites. Geology 10, 7-12.

Tucker, M.E., 1983. Diagenesis, geochemistry, and origin of a Precambrian dolomite; the Beck Spring Dolomite of eastern California. Journal of Sedimentary Research 53, (4), 1097-1119.

Tucker, M.E., 1984. Calcitic, aragonitic and mixed calcitic-aragonitic ooids from the mid-Proterozoic Belt Supergroup, Montana. Sedimentology 31, 627-644.

Tucker, M.E., 1985. Calcitized aragonite ooids and cements from the Late Precambrian Biri Formation of Southern Norway. Sedimentary Geology 43, 67-84.

Tucker, M.E., Wright, V.R., 1990. Carbonate Sedimentology. Blackwell Scientific, Oxford, 482.

Tucker, M.E., Wright, V.P., Dickson, J.A.D., 2002. Carbonate Sedimentology, Blackwell Science Ltd, 482p.

Turekian, K.K., Wedepohl, K.H., 1961. Distribution of the elements in some major units of the Earth's crust. Geological Society of America Bulletin 72, 175-192.

Vahrenkamp, V.C., Stewart, P.K., 1990. A new distribution coefficient for the incorporation of strontium into dolomite and its implications for the formation of ancient dolomites. Geology 18, 387–391.

Van Smeerdijk Hood, A., Wallace, M.W., 2012. Synsedimentary diagenesis in a Cryogenian reef complex: Ubiquitous marine dolomite precipitation. Sedimentary Geology 255, 56-71.

Veizer, J., Hoefs, J., 1976. The nature of O^{18}/O^{16} and C^{13}/C^{12} secular trends in sedimentary carbonate rocks. Geochimica et Cosmochimica Acta 40, 1387-1395.

Veizer, J., Clayton, R.N., Hinton, R.W., Von Brunn, V., Mason, T.R., Bucks, G., Hoefs, J., 1990. Geochemistry of Precambrian carbonates: 3. Shelf seas and non-marine environments of the Archean. Geochimica et Cosmochimica Acta 54, 2717-2729.

Veizer, J., Clayton, R.N., Hinton, R.W., 1992a. Geochemistry of Precambrian carbonates: VI. Early Paleoproterozoic (2.25 ± 0.25 Ga) seawater. Geochimica et Cosmochimica Acta 56, 875-885.

Veizer, J., Numb, K.A., Clayton, R.N., Hinton R.W., Grotzinger, J.P., 1992b. Geochemistry of Precambrian carbonates: V. Late Paleoproterozoic (1.8 ± 0.2 Ga) seawater. Geochimica et Cosmochimica Acta 56, 2487-2501.

Veizer, J., 1983. Chemical diagenesis of carbonates: theory and application of trace element technique. SEPM Short Course 10, 151.

Wang, W., Bolhar, R., Mei-Fu, Z., Xin-Fu., Z., 2018. Enhanced terrestrial input into Paleoproterozoic to Mesoproterozoic carbonates in the southwestern South China Block during the fragmentation of the Columbia supercontinent. Precambrian Research 313, 1-17.

Wanty, R.B., Goldhaber, M., 1992. Thermodynamics and kinetics of reactions involving vanadium in natural systems: Accumulation of vanadium in sedimentary rocks. Geochimica et Cosmochimica Acta 56, 1471-1483.

Warren, J., 2000. Dolomite: occurrence, evolution and economically important associations. Earth-Science Reviews 52, 1-81.

Wilkinson, B.H., Algeo, T.J., 1989. Sedimentary carbonate record of calcium-magnesium cycling. American Journal of Science 289, 1158-1194.

Yoshioka, H., Asahara, Y., Tojo, B., Kawakami, S., 2003. Systematic variations in C, O, and Sr isotopes and elemental concentrations in Neoproterozoic carbonates in Namibia: implications for a glacial to interglacial transition. Precambrian Research 124, 69-85.

Zachariah, J.K., Bhaskar Rao, Y.J., Srinivasan, R., Gopalon, K., 1999. Pb, Sr, Nd isotope systematics of uranium mineralised stromatolitic dolomites from the Proterozoic Cuddapah Supergroup, south India: constraints on age and provenance. Chemical Geology 162, 49-64.

HIGHLIGHTS

Field study shows that the exposed ~900 m outcrop of Vempalle Formation (VF) of the Cuddapah Basin (CB), India along the south-western margin of the basin is represented by a thick succession of stromatolitic dolomite, dolomitic limestone and limestone (~70%), with minor calcimicrite (~20%), and ~10% siliciclastic sandstone and mudstone. Facies analysis reveals that the succession can be sub-divided into 14 distinct lithofacies which can be grouped into five distinct facies associations, stacked in different orders as part of a major ramp-type carbonate platform.

Petrographic study shows preservation of 10 to 15 % of precursor limestone in the form of remnant patches of calcimicrite and ooids with calcite spar cement. Petrographic analysis suggests that the ooids, preserving primary radial and concentric fabrics and radial fractures, are considered to have been originally precipitated as calcite, which may have been low-Mg. In places the preserved calcite spar, that is partially replaced by fabric destructive dolomite, shows Type I calcite twin lamellae. Petrographic observations suggest that Vempalle Formation dolomite probably formed through very early precipitation, which in stromatolites preserved microbial filaments, as well as through fabric-destructive dolomitization during shallow to moderate burial. Vempalle Formation dolomite is characterized by micritic dolomite crystals that suggest rapid early dolomitization of lime mud and micritic calcite from a supersaturated Mg-Ca-rich solution, probably near-surface or during shallow burial.

Geochemical data suggest that depletion of Na and Sr contents along with negative $\delta^{18}O$ values indicate dolomite recrystallisation during burial and further replacement. Dolomite $\delta^{13}C$ values of -0.5 to 2 ‰ are likely inherited original marine values. Geochemical proxies (trace elements and rare earths) imply that Cuddapah Basin seawater and dolomitizing fluids were anoxic and ferruginous but not euxinic. Geochemical analyses also indicate that the burial diagenetic fluids evolved from Eu-enriched seawater that probably resulted from continental rifting around 1.9 – 2.0 Ga.

In terms of seawater chemistry in the Palaeoproterozoic CB, it is likely that this was a time of calcite precipitation (a “calcite sea”), with anoxic and ferruginous conditions, and an elevated Mg/Ca ratio but not so high that very early fabric-retentive dolomitization of ooids and cements could take place, like those of the Beck Spring Dolomite. The lack of a very high seawater Mg/Ca ratio could be related to the onset of rifting of supercontinent Columbia around 2.0 Ga that coincides with the VF carbonate sedimentation. This tectonic process with a fast rate of sea-floor spreading would draw Mg^{2+} down producing a “calcite ocean”. This ocean chemistry is in contrast to the anoxic, ferruginous and extremely high Mg/Ca conditions that prevailed during Neoproterozoic time.

A Palaeoproterozoic dolomite (Vempalle Formation, Cuddapah Basin, India) showing Phanerozoic-type dolomitisation

Amlan Banerjee[1*], Mirosław Słowakiewicz[2,3], Tuasha Majumder[1], Sayani Khan[1], Sarbani Patranabis-Deb[1], Maurice E. Tucker[4,5], Dilip Saha[1]

[1]Indian Statistical Institute, Geological Studies Unit, Kolkata 700108, India
[2]Faculty of Geology, University of Warsaw, ul. Żwirki i Wigury 93, 02-089 Warszawa, Poland
[3]Kazan Federal University, Kremlovskaya St. 18, 420008 Kazan, Russia
[4]Cabot Institute, University of Bristol, Cantock's Close, Bristol, BS8 1UJ, UK
[5]School of Earth Sciences, University of Bristol, Bristol BS8 1RJ, UK
[*]corresponding author: amlan@isical.ac.in

Abstract: The Palaeoproterozoic Vempalle Formation of the Cuddapah Basin, India, significantly adds to our understanding of the evolution of Precambrian marine carbonate systems and the redox state of the Earth's early oceans. A facies-microfacies-diagenetic-geochemical examination of samples from a 900-m long exposure in a freshly-cut canal section shows that 10 to 15 % of precursor limestone is still preserved in the Vempalle Formation in the form of remnant patches of calcimicrite and ooids with calcite spar cement. The ooids, preserving primary radial and concentric fabrics and radial fractures, are considered to have been originally precipitated as calcite, which may have been low-Mg. In places the preserved calcite spar, that is partially replaced by fabric-destructive dolomite, shows Type I calcite twin lamellae. Petrographic observations demonstrate that Vempalle Formation dolomite formed through very early precipitation, which in stromatolites preserved microbial filaments, as well as through fabric-destructive dolomitization during shallow to moderate burial. Vempalle Formation dolomite is characterized by micritic dolomite crystals which suggest rapid early dolomitization of lime mud and micritic calcite from a supersaturated Mg-Ca-rich solution, probably near-surface or during shallow burial. Depletion of Na and Sr contents of Vempalle Formation dolomite along with negative $\delta^{18}O$ values indicate dolomite recrystallisation during burial and further replacement. Dolomite $\delta^{13}C$ values of -0.5 to 2 ‰ are likely inherited original marine values. Geochemical proxies (trace elements and rare earths) imply that Cuddapah Basin seawater and dolomitizing fluids were anoxic and ferruginous but not euxinic. Geochemical analyses also indicate that the burial diagenetic fluids evolved from Eu-enriched seawater that probably resulted from continental rifting around 1.9 – 2.0 Ga. This probable ocean chemistry is in contrast with the anoxic, ferruginous and extremely high Mg/Ca "dolomite oceans" that prevailed during Proterozoic time. The Vempalle dolomite shows more similarities with dolomitised Phanerozoic platform carbonates than typical Precambrian dolomite with its well-preserved textures and burial dolospar cements.

Keywords: Dolomitization, Proterozoic carbonate rocks, redox, fluid chemistry

1. INTRODUCTION

Carbonate ramps and rimmed platforms are a distinctive feature of Neoarchean to Neoproterozoic deposition and in many cases the dolomite content of these ancient carbonate platforms is high in comparison with those of the Mesozoic and Cenozoic (Saylor et al., 1995; Holland and Zimmermann, 2000; Pope and Grotzinger, 2003). The processes of formation of these ancient dolomites are still the subject of much debate. The Precambrian sedimentary record to about 3.5 Ga includes dolomites and limestones that likely precipitated as primary aragonite and calcite (Grotzinger and Read, 1983; Grotzinger, 1989; Grotzinger and Kasting, 1993). Palaeoproterozoic carbonate sedimentation was marked by less spectacular occurrences of massively-precipitated aragonite and calcite (Grotzinger and Kasting, 1993). Precambrian dolomites may have also formed by precipitation directly from seawater or by dolomitization during very early diagenesis from fluids comparable with seawater (e.g., Veizer and Hoefs, 1976; Tucker, 1982, 1983; Hood and Wallace, 2018). Precambrian dolomites are generally characterised by very well-preserved fabrics of the original carbonate grains and early cements, leading to arguments over primary versus replacement dolomite (Tucker 1982, Hood and Wallace 2018). In addition, many Precambrian dolomites have drusy dolospar cements, precipitated during shallow to moderate burial (e.g. Tucker, 1983; Tewari and Tucker, 2011), a feature rarely seen in Phanerozoic dolomites. In India, several Precambrian sedimentary basins are reported to host dolomite successions several kilometres thick. The Palaeoproterozoic Vempalle Formation (VF), located in the crescent-shaped intracratonic Cuddapah Basin (CB), Eastern Dharwar craton, and a part of the Papaghni Group (Fig. 1), is characterized by the presence of a ~1.9 km-thick stromatolitic dolomite. The VF carbonate platform can be traced for more than 1000 km without any significant physical break from the SE to the NW part of the basin.

Zachariah et al. (1999) obtained a Pb-Pb age of 1756 ± 29 Ma for the VF dolomite. Taking into consideration the age of intruded sills (1817±24 Ma; Bhaskar Rao et al., 1995) within VF carbonate rocks/Pulivendla quartzites and the age of VF dolomite (1756 ± 29 Ma), Zachariah et al. (1999) proposed 1756 ± 29 Ma as the time of dolomitization of the precursor VF limestone. Rai et al. (2015), based on a Pb–Pb (PbSL) age of VF dolomite and of the intruded sills of 1885 Ma (U-Pb and Ar-Ar methods; French et al., 2008; Anand et al., 2003), proposed that

dolomitization of VF limestone might have taken place within 100 My duration of time (from 1900-2000 Ma). This time duration of sedimentation and dolomitization is also reported from the Wittenoom Formation and Carawine Dolomite of the Hamersley Group, Western Australia, where the time between deposition, diagenesis and dolomitization is thought to be within 100-150 My (Jahn and Cuvellier, 1994; Jahn and Simson, 1995). On the other hand, Chakrabarti et al. (2011, 2014), using isotopic ($\delta^{13}C$ and $\delta^{18}O$) and elemental (Mg, Ca, Fe, Mn, Sr and SO_4^{-2}) data, concluded that VF dolomite is primary in nature and precipitated either from ^{18}O depleted marine water or from a geochemically distinct mixed fluid source. Based on collective geochemical signatures, $\delta^{13}C$ and $\delta^{18}O$ isotopic values, flat REE patterns along with Ce, Eu and Gd anomalies, and chondritic to superchondritic Y/Ho ratios, Khelen et al. (2017) have recently proposed that VF dolomite was precipitated from marine water having a hydrothermal signature. These discrepancies in the plumbing mechanism(s) of VF dolomite warrant the need to revisit the question about the origin of VF dolomite and related dolomite-precipitating fluids.

In this project we have used field and petrographic observations and various geochemical proxies to understand the mechanism(s) of formation of the shallow-marine VF dolomite and to assess the redox heterogeneity existing during its time of formation. Geochemical data, integrated with petrology and tectonic history of the CB, help not only to infer the source of Mg-rich fluids but also to contribute to a better understanding of the redox conditions of this Proterozoic shallow-water carbonate. In addition, as will be shown, this Palaeoproterozoic dolomite has more features in common with dolomitised Phanerozoic platform carbonates, than the typical Precambrian dolomite with well-preserved fabrics, likely a reflection of seawater chemistry, redox and microbes.

2. GEOLOGICAL BACKGROUND

The Papaghni Group (~2110 m thick) represents the first sedimentary cycle of the Cuddapah Supergroup (Patranabis-Deb et al., 2012) in the CB. The succession unconformably overlies the basement granite, gneiss and greenstone complex of the Eastern Dharwar craton, which in turn is unconformably overlain by the Chitravati Group (4975 m). The VF (~1900 m) of the Papaghni Group constitutes the lowermost carbonate-dominated unit of the Cuddapah Supergroup and overlies a basal siliciclastic unit, the Gulcheru Quartzite (~210 m), with a

transitional contact (Nagaraja Rao et al., 1987). The Gulcheru Quartzite constitutes a basal conglomerate and immature sandstone unit, deposited in a fan-delta to prodelta setting, which transitionally passes up into a mature quartz arenite unit, deposited in a shallow-shelf environment (Majumder et al., 2015). The VF is represented mostly by thick stromatolitic dolomite and minor limestone (10 to 15%). Near the transition zone to the Gulcheru Quartzite, thin beds of splintery red mudstone alternate with siliciclastic and carbonate beds to form a mixed siliciclastic-carbonate unit (Fig. 2). Tidal and storm currents played a major role in sculpturing the sandstone bodies at this transition.

Tepee structures, desiccation cracks filled with lime mud and sand and halite casts, are common in the lower VF (Fig. 2). The upper part is dominated by bedded dolomite deposited in a range of environments, starting from shallow shelf with intermittent exposure to fairly deep-water conditions below normal wave base. Stromatolite morphologies reflect environments varying from intertidal to subtidal and facies cycles are the result of multiple rhythms of sea-level change (Patranabis-Deb et al., 2018). Demise of the carbonate platform is marked by the deposition of thick brown shale with laterally persistent beds of chert. The common occurrence of sills up to a metre or more thick and thinner dykes of basalt and/or dolerite in the upper part of the VF succession indicates tectonic-magmatic activity (Anand et al., 2003). Conglomerate and pebbly sandstone of the basal Chitravati Group, upon a sharp unconformity, mark the beginning of the second sedimentary cycle. Clasts of chert with stromatolite, oolite, vein quartz, jasper and volcanics, derived from the Papaghni Group, reflect subaerial exposure and erosion during the formation of the unconformity between the two groups.

Rifting of the Eastern Dharwar craton and passive-margin sedimentation deposited the Gulcheru fan-delta succession (Majumder et al., 2015) followed by deposition of the extensive VF carbonate platform (Tripathy and Saha, 2008; Patranabis-Deb et al., 2018). Rai et al. (2015) inferred a minimum age of 2000 Ma for the onset of sedimentation in the Cuddapah Supergroup and this coincides with the onset of rifting of the supercontinent Columbia, as evidenced by widespread emplacement of mafic dykes in and around the CB during this period. The intermittent occurrence of mafic flows, ash-fall tuffs and associated shallow-crustal intrusives in the upper part of the VF (~1.88 Ga; Ravikant, 2010) is related to the second cycle of rifting that

possibly represents the initial phase of fragmentation and separation of the south Indian craton from the North China craton (Ravikant, 2010). With continued passive subsidence, the CB evolved into a large epicontinental sea with a near-complete cessation of coarse clastic influx and deposition of the extensive shale–carbonate succession of the Chitravati Group. Tectonically, the CB is punctuated by multiple unconformities, major tectonic contacts, faults and various basic sills (Saha and Tripathy, 2012; Saha and Mazumder, 2012; Patranabis-Deb et al., 2012; Collins et al., 2015), which affected and shaped its sedimentary succession.

3. METHODS

3.1. *Sample collection for petrological analysis*

Samples were collected at 5-15 m intervals up-section (Table 1) along a freshly cut canal section, nearly 4 km long (hereafter referred as the 'canal section') that exposed the dolomite beds of the VF (~1000 m thick dolomite unit, Fig. 2) near Parnapalle village (N14º32'58.3", E77º58'09.9") in the Cuddapah district, Rayalaseema. Samples collected from the dolomite beds covered eight facies namely F1, F2, F4, F5, F7, F8, F9 and F10 (Table 1; Fig. 2). F3 and F11 are intentionally avoided as they are mostly composed of shale, siltstone and dolomite (Table 2). Thin-sections were made from twenty-nine selected dolomite samples for petrographic analysis. Carbonate components (calcite, dolomite) were determined by staining the thin-sections with Alizarin Red S.

3.2. *X-Ray diffraction*

Twenty-nine selected dolomite samples were powdered for X-ray diffraction analysis on a Panalytical X'Pert Pro diffractometer, equipped with a Cu Kα X-ray source and an X'Celerator detector, operating at the following conditions: 40 kV and 40 mA; range 5 – 80 deg 2θ; step size 0.017 deg 2θ; time per step 50.2 sec; fixed divergence slit, angle 0.5º; sample rotation 1 rev sec^{-1}. The quantities of the mineral phases were determined using the Rietveld method.

3.3. *Major and trace elements*

Forty-two selected dolomite samples were powdered for bulk major, trace and REE analyses, undertaken at the Wadia Institute of Himalayan Geology. The elemental analysis was

performed using an ICP-MS PerkinElmer SCIEX ELAN DRC-e. Concentrations of REE + Y (n = 42) were normalized to the Post-Archaean Australian Shale (PAAS) representing an estimate for the composition of average terrigenous input to the oceanic environment. Specifically, REE fractionation was calculated as Pr_{SN} / Yb_{SN} (SN, shale normalized) to avoid problems in case of anomalous La and Ce concentrations. To avoid any anomalous behaviour of La, Ce, Eu and Gd, the anomalies were calculated using the geometric equations of Lawrence and Kamber (2006) and are given as Ce/Ce^*, Eu/Eu^*, Gd/Gd^* and La/La^*.

3.4. Scanning electron microscopy with energy-dispersive spectroscopy

Thin-sections were examined under a scanning electron microscope (SEM) FE-SIGMA VP (Carl Zeiss Microscopy GmbH) with energy-dispersive (EDS) detector (Quantax XFlash 3|10, Bruker Nano GmbH). Thin-sections were placed on the mount with carbon conductive tape. Then, samples were coated with a 20 nm layer of carbon by vacuum coater (Quorum 150T ES). Furthermore, carbon tape bridges were made for each sample to avoid excessive accumulation of charge. Analyses were done with 120 μm aperture and 15 keV accelerationvoltage. Beam intensity was 2.5 nA and working distance was 7.5 mm.

3.5. *Oxygen and carbon stable isotope analysis*

Thirty-five selected dolomite samples were analysed for bulk carbon and oxygen stable isotopes at the Activation Laboratories Ltd., Canada. Samples were run on a DELTAPlus XL stable isotope ratio mass spectrometer (IRMS) coupled with ConFlo III Interface and EA1110 elemental analyser. Standards NBS-19 ($\delta^{13}C$ = 1.95 ‰ and $\delta^{18}O$ = -2.20 ‰) and NBS-18 ($\delta^{13}C$ = -5.05 ‰ and $\delta^{18}O$ = -23.1 ‰) were used for comparison. The results are expressed relative to the Vienna Peedee Belemnite (VPDB).

4. Sedimentation Pattern and Depositional Environment

The VF is well exposed along the south-western margin of the CB outcrop (Fig. 1a, b and c), represented by a ~1000-m thick succession of stromatolitic dolomite, dolomitic limestone and limestone (~70%), with minor calcimicrite (~20%), and ~10% siliciclastic sandstone and mudstone. Facies analysis reveals that the succession can be sub-divided into 11 distinct lithofacies (Table 1) which may be grouped into inner, mid and outer – ramp associations,

stacked in different orders as part of a major ramp-type carbonate platform (Fig. 3). The platform maintained a shallow depth throughout its life, thus indicating a keep-up mode of deposition, that is where the carbonate succession built up to sea level and kept pace with subsequent sea-level changes, such that a balance was maintained with the generation of accommodation space. Occasional storms and regular tides were important, distributing clastic sediments at particular times, which hampered the growth of the platform in time and space. The depth-controlled growth patterns of the stromatolites give clues to their depositional environment (Patranabis-Deb et al., 2018), which in the canal section reflects a gradient from shallow-water with exposure to shallow to moderate depths.

The VF succession in the canal section (Fig. 2) starts with a basal mixed unit, representing the transition between the basal siliciclastic unit of the Gulcheru Formation and carbonate rocks of the VF. It comprises mixed siliciclastic-dolomite (F1), bedded dolomite with crinkled laminites (F2) and intraformational conglomerate (F9). The mixed siliciclastic-dolomite beds are characterized by flaser bedding and lenticular bedding with preservation of desiccation cracks filled with lime mud and sand and halite casts within shale intervals, tepee structures and fluid-escape structures. The presence of these sedimentary features, suggests intermittent exposure in a supratidal to upper intertidal flat, in an inner ramp setting. Palaeocurrent directions measured from trough cross-stratification from the sandy units indicate east-north-easterly flow.

The mixed siliciclastic unit passes upward to a thick succession of bedded dolomite with crinkled laminites (F2), black dolomite with or without stromatolite (F4), dolomite-micrite rhythmite (F5) and brown shale (F3), without any break. Steel grey to black coloured massive to stromatolitic dolomite beds (F4) with isolated to laterally-linked mutually-aligned stromatolites are observed, alternating with dolomite-micrite rhythmite (F5). Isolated occurrences of stromatolite with low synoptic relief and parallel lamination in black dolomite (F4) indicate a quiescent water environment. The close association of F4 and F5 also suggests their deposition in a low-energy protected environment. Thick occurrences of F2 alternating with F5, with signatures of intermittent exposure at different stratigraphic levels, suggest that they have possibly formed a barrier, which imposed a rimmed-shelf profile to the platform, creating lagoons on the shoreward side with an open shelf to seaward.

The mid-ramp association consists of oolite (F6), with intercalations of dolomite mud rhythmite (F5), columnar stromatolite (F7), conical stromatolite (F8) and thickly – bedded dolomite (F10). The association starts with the occurrence of oolite (F6), as shoaling-up bars. The oolites comprise well-rounded, well-sorted medium- to coarse-grained ooids, usually preserving a concentric fabric with a clastic grain as the nucleus. Medium-to-fine-grained ooids with a radial fabric (with or without a clastic grain in the centre) and superficial ooids are also observed. Oolite beds are generally trough cross-stratified, showing NE and SW palaeocurrent directions with bidirectional pattern. The abundance of siliciclastic grains as nuclei to ooids indicates a ready source of clastics on the landward side. The oolite bank may have further acted as a barrier with the seaward side being cut off from the coastal sediments so that ooids formed without sand nuclei and a radial fabric. F6 is interbedded with small columnar stromatolites (4-14 cm in height). F7 suggests spatial and temporal variations in the intensity and fluctuations of wave action (Swett and Knoll, 1989; Holland and Patzkowsky, 1998) in a lower intertidal to upper subtidal environment. The rhythmite facies (F5) may have been deposited as interbars in a relatively quiet-water protected area between two bars or in a relatively deeper-water environment. Up-section the columns increase in number and size and coalesce to form a continuous biostromal structure (F7), many metres thick, commonly intercalating with parallel-stratified dolomite (F10).

Planar-parallel to wavy-parallel stratified and trough cross-stratified dolomite beds of F10 strongly suggest that this facies was deposited by traction currents. Gutter casts (Fig. 3d) and pillow and ball structures within the dolomite beds suggest storm waves on a shallow shelf. Changes of stromatolite type from shallow intertidal columnar to columnar biostromes, and a conical type, indicate deposition on a low-gradient ramp where the distribution of microbialite facies is distinctly depth-partitioned (Patrabanis-Deb et al., 2018). The gradual change in the shape, size and synoptic relief of stromatolites also suggests balanced sedimentation, deposition and accommodation space generation.

The top part of the VF is mainly characterized by F10 and F11, interpreted to be deposited in an outer ramp environment, below fair-weather wave base. The association comprises a rhythmic occurrence of plane-parallel laminated dolomite (F10) with interbedded

green shale/siltstone and dolomite (F11), commonly interrupted by igneous intrusions. This depozone predominantly involved deposition from background suspension rarely interrupted by strong storm surges. Isolated gutter casts within the dolomite beds are thought to have been produced by storm-generated return flows (Fairchild and Herrington, 1989; Myrow, 1992). Chert and steatite nodules of various shapes and sizes (Fig. 3f) are common with iso-volumetric metasomatic alteration of dolomite to talc observed in the upper part of the VF.

5. RESULTS

5.1. *Petrography*

Petrographic analysis of the VF dolomite led to the identification of four microfacies: i) dolo-micrite with few quartz and feldspar grains, ii) stromatolitic dolomite bindstone, iii) oolitic grainstone (limestone and dolomite), and iv) calcimicrite with local limestone clasts. Micritic dolomite is plane-parallel laminated, where laminae are defined by alternating light (micrite) and dark (clay-rich) layers (Fig. 4a). Dolomicrite is commonly mixed with fine sand or silt-sized grains of well-rounded to sub-rounded quartz and feldspar (Fig. 4b). Dolomicrite shows grain enlargement due to recrystallization (Fig. 4c). Stromatolitic dolomite preserves crinkly to smooth lamination defined by alternating dolomicrite and microbial filaments (Fig. 4d). Preservation of the primary microbial texture suggests that this VF dolomite is either a very early mimetic replacement of $CaCO_3$, preserving the original microbial filaments, or it is a primary microbial dolomite precipitating directly from ancient seawater (Tucker, 1983, Corsetti et al., 2006, van Smeerdijk Hood and Wallace, 2012). Good preservation of microbial structures also indicates little or no recrystallization during diagenesis. The stromatolitic dolomite is characterized by polymodal planar–e and subhedral to anhedral planar–s or non–planar micritic dolomite crystals (see dolomite classification by Sibley and Gregg, 1984, Gregg and Sibley, 1987), with sharp intercrystalline boundaries (Fig. 4e, f). Moreover, the SEM-EDS analysis of thin-sections did not show any relics of calcite crystals.

The coarser carbonate facies include grainstone, mostly with spheroidal ooids, but also eye-shaped ooids. Stages of dolomitization are well-documented and recorded by the ooids (Fig. 5a-f). At one extreme, the ooids are composed entirely of calcite crystals having a radial fabric, such that a continuous sweep of the extinction is seen on stage rotation under crossed polars (Fig.

5a, b). Preserved calcite ooids show well-developed primary concentric, radial and radial–concentric fabrics; some have an outer silicified zone (cf. Tucker, 1984, 1985). Some of the ooids are radially fractured as a result of compaction (Fig. 5a). These radial fractures crudely coincide with the radial fabric which is probably a primary feature. Also the presence of primary radial – concentric fabrics as observed within the unreplaced calcite ooids suggest its growth in a mud-free environment whereas the radial fabric results from ooid growth in a relatively calm environment with the presence of lime mud (Tucker, 1984). The good fabric preservation of the ooids could suggest that they were originally composed of low-Mg calcite since this tends to resist dolomitization; however, they could originally have been high-Mg calcite, with the Mg leached out before dolomitisation (Tucker 1984, 1985). Some calcitic ooids have euhedral rhombic dolomite crystals in the nucleus of the ooid (Fig. 5c). At the other extreme, the ooid cortex is completely replaced by planar–e (euhedral) and subhedral to anhedral planar–s (subhedral) or non–planar micritic dolomite crystals, with sharp but slightly ragged intercrystalline boundaries, completely obliterating the internal fabric but still preserving the shape of the ooids (Fig. 5f). In between there are ooids that show incomplete replacement phenomena where the central part of the ooid is composed of coarse euhedral and mostly planar–e to planar–s dolomite crystals obliterating the internal fabrics, but the outer rim is composed of calcite crystals still preserving the original radial–concentric fabrics (Fig. 5d). The primary radial fabric of the ooid at the peripheral margin is commonly partially destroyed by replacement micritic dolomite (Fig. 5e). Within massive dolomite there are still patches and lenses of limestone that preserve the primary micritic calcite matrix and calcite spar (Fig. 6a); the latter shows Type I calcite twin lamellae and it is partially replaced by dolomicrite destroying the primary fabric (Fig. 6b). Thin-section evidence of fabric-destructive dolomite in VF carbonate rocks indicates a replacement origin (Tucker et al., 2002), and the mimetic to obliterated mosaic texture indicates progressive dolomite replacement (Braithwaite, 1991).

5.2. X-ray diffraction

XRD analysis shows that dolomite is the dominant mineral in the samples analysed, with subordinate quartz and minor K-feldspar (Table 1S, Supplementary section). Barring three samples, calcite is absent in VF dolomite samples analysed. Trace amounts of talc, barite, mica, chlorite and hematite were also detected. Calcium excess of VF dolomites is calculated using the

formula: $CaCO_3$ mol% = 333.33*d_{104} – 911.99 (Lumsden, 1979, where d_{104} is the peak position in angstrom units, Table 2S). VF dolomites have a nearly stoichiometric composition (mole % $CaCO_3$ = 49–51, mean 50) indicating an ideal composition of the dolomite (Mg:Ca = 1). Ordering of VF dolomite crystals ranges from 0.40 to 1.07 (average 0.56), according to the method described by Hardy and Tucker (1988). Only five samples had an ordering ratio <0.5 and >0.4.

5.3. *Geochemistry*

Total iron content of VF dolomite varies from 19,235 ppm to 2170 ppm (average 5240 ppm); Mn ranges from 2040 ppm to 125 ppm (average 320 ppm), whereas Al varies from 19,955 ppm to 160 ppm (average 5475 ppm) (Table 3Sa,b). Average Fe/Mn and Fe/Al ratios are 19.6 and 3.4, respectively. Sodium and Sr concentrations range from 60 ppm to 735 ppm (average 290 ppm) and from 40 ppm to 420 ppm (average 85 ppm), respectively (Table 3Sa,b). Fe and Mn concentrations show a positive correlation (Fig. 7a), whereas the Sr/Ca ratio versus Na_2O shows a poor correlation (Fig. 7b). Mn and Fe concentrations versus the Mg/Ca ratio can be used to explore modification of the carbonate chemistry during burial diagenesis (Gilleaudeau and Kah, 2013). Fe and Mn concentrations of VF dolomites are independent of the Mg/Ca ratio (Fig. 7d, e). The Fe/Sr and Mn/Sr ratios can also be regarded as sensitive indicators of diagenetic alteration as both of the elements Fe and Mn replace Sr during diagenesis (Veizer, 1983; Derry et al., 1992). The Mn/Sr ratio is typically >2 (average 5.1; only five samples have Mn/Sr <2) and the Fe/Sr versus Mn/Sr ratios show positive covariance (Fig. 7c).

V/(V+Ni) ratios vary from 0.6 to 0.9 (average 0.7), whereas the (Cu+Mo)/Zn ratios (Hallberg, 1976; 1982) vary from 5.9 to 0.4 (Table 3Sa). The enrichment factors of redox-sensitive trace elements such as Mo, V and Co ($EF_X = (X_T/Al_T)/(X_{SN}/Al_{SN})$) can be calculated to estimate their relative enrichment or depletion (Tribovillard et al., 2006). VF dolomite is significantly enriched in Mo, V and Co (enrichment factor > 1) relative to PAAS.

The ΣREEs (Table 4S) in dolomite samples range from 0.49 to 11.06 ppm (average 2.4 ppm; standard deviation, SD = 2.5 ppm). Dolomites have mostly homogeneous geochemical features (flat REE + Y patterns, Fig. 8; $(La/Sm)_{SN} \approx 1$, $(Gd/Yb)_{SN} \approx 1$, Fig. 9) with MREE

355 enrichment and a positive Eu anomaly (Eu/Eu* = 82.2 to 1.02, average Eu/Eu* = 8.25, SD =
356 15.6). The dolomite samples display a small negative Gd anomaly (0.8<Gd/Gd*<1.3, average
357 Gd/Gd* = 0.99, SD = 0.09), a positive La anomaly (0.7<La/La*<2.08, average La/La* = 1.08,
358 SD = 0.3) and a slightly positive Ce anomaly (0.7<Ce/Ce*<1.3, average Ce/Ce* = 1.03, SD =
359 0.16). The Y/Ho ratios range between 0.94 and 1.46 (average 1.15, SD = 0.14) and the Pr/Yb
360 ratios range from 0.73 to 3.83 (average 1.32, SD = 0.59), respectively. Marine carbonate
361 sediments in general have a ΣREE range of 0.04 to 14 ppm (Turekian and Wedepohl, 1961). The
362 average ΣREE of typical marine carbonate is 28 ppm (Bellanca et al., 1997). The ΣREE of VF
363 dolomite samples, normalized to PAAS ranges from 11.06 to 0.49 ppm (average 2.4 ppm) and
364 does not show any positive correlation with the major elements (Fe, Mn, Al and Si).
365
366 **5.4.** ***Oxygen and carbon isotopes***
367 The whole–rock $\delta^{18}O$ and $\delta^{13}C$ values of VF dolomite range from −8.1 to −5.2 ‰
368 (average –6.8 ‰) and −0.35 to 2.0 ‰ (average 0.5 ‰), respectively (Table 5S), and they show
369 an inverse correlation (Fig. 10). Most of the $\delta^{13}C$ values are near 0 ‰ (average 0.5 ‰), with six
370 samples showing slightly depleted values (-0.35 ‰ < $\delta^{13}C$ < 0 ‰), and the majority with slightly
371 elevated $\delta^{13}C$, maximizing at 2‰.
372
373 **6. Discussion**
374 **6.1.** ***XRD mineralogy and petrography***
375 The non-ferroan type dolomites ($FeCO_3$ <2 mol%; Tucker and Wright, 1990) are nearly
376 stoichiometric (mol% $CaCO_3$ = 49 to 51, mean 50, Lumsden, 1979) and they are relatively well
377 ordered (degree of order ranging from 0.4 to 1.0, mean 0.6, Hardy and Tucker, 1988). The near
378 stoichiometric and relatively well-ordered nature of the dolomite crystals could reflect slow
379 growth controlled by elevated temperature. This could be the result of dolomitization during
380 burial or burial recrystallization of earlier, near-surface-formed dolomite. Lithospheric stretching
381 and crustal sagging associated with volcanic activity during the interval 1.8 – 2.0 Ga in the CB
382 (Anand et al., 2003; Ravikant et al., 2014) could have provided a higher than normal geothermal
383 gradient during burial.
384

Petrographic analysis of VF dolomite shows patches of remnant calcimicrite (Fig. 6a) and calcite spar still preserving their primary fabrics like calcite twin-lamellae (Fig. 6b). The presence of twin-lamellae in the precursor calcite suggests a minimum temperature of 170^{o}C is required for diagenetic deformation (Ferrill et al., 2004). Since the calcite ooids with original internal fabrics and textures are primary, and there is no evidence of calcitised aragonite (cf. Tucker, 1985), it is likely that the original lime mud (now calcimicrite) would have been calcitic and this was probably the precursor sediment of VF dolomite. Planar-s dolomite crystals (mostly 5-15 μm) show cloudy centres (due to the presence of minute inclusions) and clear rims; this could suggest either replacement of original limestone or recrystallization of an earlier dolomicrite at depth. Petrographic study has shown that VF dolomite is characterized by the presence of micritic dolomite crystals that commonly exhibit crystal enlargement (recrystallization). The widespread occurrence of dolomitic micritic facies in the VF suggests that the dolomite crystals precipitated rapidly from a dolomite-supersaturated fluid with a high Mg/Ca ratio and low SO_4^{-2} concentration, as would be expected in the Proterozoic compared to typical Phanerozoic environments (Tucker, 1982), because of rapid nucleation and crystallization in a supratidal/upper tidal-flat environment. Rapid dolomite precipitation/replacement might also have been facilitated by fine-grained precursor carbonate sediment that had a high reactive surface area to volume ratio and high density of nucleation sites (Sibley and Gregg, 1987). Microbial influences within the sediment inducing suitable conditions for dolomite precipitation may well have been involved as well (e.g. Bontognali et al., 2010; Petrash et al., 2017; Perri et al., 2018).

6.2. *Redox conditions*

MREE enrichment (Haley et al., 2004) (Fig. 8), strong Europium anomalies (Bau, 1991) (Fig. 8) and absence of negative Ce anomalies (Bau and Koschinsky, 2009) (Fig. 11) in VF dolomite are compelling evidence suggesting its formation from anoxic marine-derived waters. High Fe and Mn concentrations (>1000 ppm and >50 ppm, respectively) of dolomites indicate that the fluids responsible for dolomite formation were iron-rich (Fe^{2+}) and reducing in nature (Budd, 1997). The Fe/Mn ratio of VF dolomite, correlated with the Fe/Al ratio, implies insignificant sulphate reduction and pyrite precipitation during dolomite formation (Barnaby and Read, 1992), and this is consistent with the petrographic observations, where little pyrite was

detected. The Fe/Al ratio (Anderson and Raiswell, 2004; Lyons and Severmann, 2006) of VF dolomite also implies that the fluids responsible for dolomite formation were anoxic but not euxinic. Had the palaeo-fluids been euxinic, Fe^{2+} and other metal ions would have preferred to precipitate as sulphides (such as pyrite), and these were not observed. Hatch and Leventhal (1992) suggested a V/(V+Ni) ratio greater than 0.84 for euxinic, 0.54–0.82 for anoxic, and 0.46–0.60 for dysoxic conditions. The V/(V+Ni) values of VF dolomite vary from 0.6 to 0.88 (average 0.7) indicating chiefly anoxic waters of precipitation. The highest V/(V+Ni) ratio likely suggests euxinic depositional conditions. Hallberg (1976, 1982) proposed that the (Cu+Mo)/Zn ratio can also be used as a proxy to infer redox conditions. This ratio increases under reducing conditions and decreases when the environment is oxidising. VF dolomite samples show that the (Cu+Mo)/Zn ratio can be as high as 5.9 or as low as 0.37; this suggests dolomite formation mostly under reducing conditions. The V/(V+Ni) and (Cu+Mo)/Zn ratios also indicate anoxic depositional conditions. Molybdenum and vanadium are enriched in more reducing environments (Crusius et al., 1996; Algeo and Maynard, 2004; Breit and Wanty, 1991; Wanty and Goldhaber, 1992), whereas Co tends to be less soluble under reducing conditions (Algeo and Maynard, 2004). The enrichment factors ($EF_X = (X_T/Al_T)/(X_{SN}/Al_{SN})$; Tribovillard et al., 2006) of redox-sensitive trace elements (Mo, V and Co) show that dolomite samples are significantly enriched in redox-sensitive trace elements relative to PAAS, suggesting reducing conditions during dolomite precipitation.

6.3. *Post-depositional alteration*

The flat REE patterns of VF dolomite could indicate very limited siliciclastic input to the basin during carbonate deposition. The range of PAAS normalized ΣREE values (0.5 ppm-11.0 ppm) and average ΣREE value (2.4 ppm) of VF dolomite suggests that the precursor rock is probably of marine origin (Turekian and Wedepohl, 1961; Bellanca et al., 1997) and the REE contribution from non-carbonate fractions (Fe-Mn oxides and siliciclastic contamination) appears to be minor (Fig. 12, Piper, 1974; Palmer, 1985). In addition, the Mn and Fe concentrations are independent of the Mg/Ca ratio suggesting minimal post-depositional alteration of VF dolomite (Nordeng and Sibley, 1994; Malone et al., 1996; Machel, 2004). However, The Fe/Sr versus Mn/Sr plot (Fig. 7c) shows clustered data with moderate covariance, suggesting that diagenesis could have altered the parent sediment geochemical signal. However,

elevated Mn/Sr ratios of VF dolomite (average 4.9) could be interpreted as a signature of diagenetic alteration (following, for example, Derry et al., 1992, 1994; Kaufman and Knoll, 1995; Montañez et al., 1996), although on the other hand, this may not necessarily always be the case (for an alternative view see Knoll et al., 1995; Lindsay and Brasier, 2000); it could be related to the fluid chemistry (Yoshioka et al., 2003; Shen et al., 2005; Font et al., 2006; Hurtgen et al., 2006; Nédélec et al., 2007). Also, Archean and Palaeoproterozoic dolomites on average contain more Fe and Mn than younger carbonate rocks (Veizer et al., 1990), thus complicating the application of the Mn/Sr ratio as an index of alteration. The low Y/Ho ratio (0.94-1.46; mean 1.15, SD = 0.14) and the Y/Ho and Ce/Ce* cross-plot (Fig. 13) probably indicate a variable degree of contamination of the precursor carbonate by clay material, reflecting the depositional setting in a shoreline or lagoonal environment (Kamber and Webb, 2001).

6.4. *Fluid source*

The PAAS-normalized REE profiles for VF dolomite show no LREE depletion, show MREE enrichment (cf. Haley et al., 2004) and have positive Eu and Y/Ho anomalies with a weakly positive Ce anomaly. These observed REE characteristics are consistent with the chemistry of anoxic marine basins (Bau and Möller, 1993), ferruginous lakes, marine hydrothermal plumes and anoxic diagenetic waters (Johannesson and Zhou 1999; Sherrell et al., 1999; Haley et al., 2004; Wang et al., 2018). The weakly positive Gd anomaly present in VF dolomite may reflect seawater precipitation (Bau, 1999). Eu is also normally enriched in Archean seawater-precipitated carbonate too (Bolhar and Karnendonk, 2007), the source of which can be either hydrothermal solutions derived from mid-ocean ridges and/or back-arc spreading centres, or burial diagenetic fluids (Michard et al., 1983; Michard, 1989; Derry and Jacobsen, 1990; German et al., 1990; Murray et al., 1991; Danielson et al., 1992; German et al., 1993; German et al., 1999; Douville et al., 1999; Kamber and Webb, 2001; Eroglu et al., 2017; Schier et al., 2018). In VF dolomite significant positive correlation is observed between Eu/Eu* and Ba content (Fig. 14) and this clearly indicates the influence of hydrothermal activity on the studied carbonates (Khelen et al., 2017). Extensive volcanic activity in the CB around 1.9 to 2.0 Ga in a continental rift setting (Anand et al., 2003; Ravikant et al., 2014) could be the source for Eu. However, diagenetic alteration of the precursor carbonate sediments is suggested by the

Fe/Sr versus Mn/Sr plot (Fig. 8c), low Y/Ho ratio (0.94-1.46; mean 1.15, SD = 0.14) and the Y/Ho and Ce/Ce* plot (Fig. 13), and this could also have enhanced the Eu anomaly.

Sodium content of dolomites can be used as an indicator of salinity of the fluid from which the dolomites precipitated (Land and Hoops, 1973; Sass and Katz, 1982; Sass and Bein, 1988; Budd, 1997). The low Na concentrations (60-735 ppm, average 290 ppm) of VF dolomite along with the poor correlation of Sr/Ca vs. Na_2O (Fig. 8b) rules out their hypersaline fluid origin and probably suggests a diagenetic fluid source. Depletion in Na, however, can also be a consequence of burial (Sachan, 1993), as successive episodes of dolomitization of limestone and dolomite recrystallisation would reduce the levels of Na (Warren, 2000). Similarly, low strontium concentrations (40–420 ppm, average 85 ppm; average Sr value of lithospheric carbonate rocks is 610 ppm; Turekian and Wedepohl, 1961) of VF dolomite probably reflect a Sr-depleted water-buffered diagenetic system (Budd, 1997; Warren, 2000; Azmy et al., 2001), supporting a burial diagenetic effect (Sachan, 1993; Warren, 2000). Tucker (1983), from studies of the Precambrian Beck Spring Dolomite, suggested that low concentrations of Na and Sr in ancient dolomites excludes precipitation from marine fluids and warrants either fluid–mixing or wet–recrystallization of an initially precipitated poorly-ordered calcian dolomite that drives out Na and Sr.

The $\delta^{13}C$ values (− 0.4 ‰ to 2.0 ‰; average value 0.5 ‰) of dolomite samples probably reflect the carbon isotopic composition of the precursor carbonate precipitated from the Proterozoic seawater. Palaeoproterozoic carbonate successions are characterized by $\delta^{18}O$ values ranging from –6 to –12 ‰ (Tucker, 1982; Burdett et al., 1990; Veizer et al., 1992a; 1992b; Melezhik et al., 1997; Bekker et al., 2001; 2003a, b). The oxygen isotope range (–5.2 to –8.1 ‰) for VF dolomite is within this range and is consistent with precipitation (or recrystallization) during shallow to moderate burial (Sachan, 1993; Warren, 2000).

7. PROBABLE MECHANISM OF DOLOMITIZATION

The field observations and petrographic features of the dolomites within the Palaeoproterozoic VF can be interpreted in terms of early dolomitization of peritidal platform carbonate sediment consisting of lime mud and calcimicrite. Preservation of microbial fabric

508 elements of the stromatolitic dolomite suggests that either VF dolomite associated with
509 microbial-laminites formed as primary precipitates due to microbial activity and minor
510 evaporation (Hird et al., 1987) or that they are very early, replacement mimetic dolomites.
511 During subsequent shallow sub-surface burial and diagenesis, fabric-destructive dolomitization
512 of the undolomitized oolitic grainstones and calcimicrite, along with recrystallization of the
513 early-formed peritidal dolomite happened as suggested by the petrographic textures. In terms of
514 seawater chemistry in the Palaeoproterozoic CB, it is likely that this was a time of calcite
515 precipitation (a "calcite sea"), with anoxic and ferruginous conditions, and an elevated Mg/Ca
516 ratio but not so high that very early fabric-retentive dolomitization of ooids and cements could
517 take place, like those of the Beck Spring Dolomite (Tucker, 1983). The lack of a very high
518 seawater Mg/Ca ratio could be related to the onset of rifting of supercontinent Columbia around
519 2.0 Ga that coincides with the VF carbonate sedimentation. Grotzinger (1989) proposed that
520 Precambrian seawater was oversaturated with respect to calcium carbonate that favoured abiotic
521 carbonate precipitation that gradually decreased the carbonate saturation through the Proterozoic
522 to Phanerozoic levels. This process, coupled with a fast rate of sea-floor spreading, would draw
523 Mg^{2+} down producing a "calcite ocean" (Wilkinson and Algeo, 1989; Bots et al., 2011). This
524 ocean chemistry is in contrast to the anoxic, ferruginous and extremely high Mg/Ca conditions
525 that prevailed during Neoproterozoic time (Hood and Wallace, 2018). In addition, the coarse
526 replacement VF dolomite crystallized from a burial fluid that evolved from the europium-
527 enriched anoxic seawater with a lower SO_4 content (Hood and Wallace, 2018), as marine water
528 or its derivative is the only known infinite source of Mg^{2+} and Ca^{2+}. The PAAS-normalized REE
529 profiles for VF dolomite are consistent with the chemistry of anoxic diagenetic waters. Low Na
530 and Sr concentrations of VF dolomite in and around Parnapalle also suggest their precipitation
531 (or early recrystallisation) during burial diagenesis (Veizer, 1983; Vahrenkamp and Stewart,
532 1990; Tucker and Wright, 1990; Banner, 1995; Budd, 1997; Warren, 2000; Azmy et al., 2001;
533 Balter et al., 2011; Sosdian et al., 2012); this is also supported by the stable isotope ($\delta^{18}O$) values
534 that fall within the range of the burial dolomite model (Warren, 2000; Machel, 2004). The $\delta^{13}C$,
535 on the other hand, having 'marine' values, suggests that the original lime mud and/or micritic
536 calcite were derived from seawater (Tucker and Wright, 1990). The likely factor promoting
537 dolomite formation during early burial diagenesis could be the presence of an early, finely-
538 crystalline, less well-ordered dolomite, as is being precipitated in modern tidal flats and

539 microbial mats in Abu Dhabi and Qatar (e.g., Bontognalli et al., 2010; Perri et al., 2018). These
540 early Ca-Mg precipitates could have provided the nuclei and substrates for continued dolomite
541 formation. The near-stoichiometric and relatively well-ordered VF dolomite crystals probably
542 would be the result of dolomite recrystallisation during burial, possibly promoted by an elevated
543 geothermal gradient from crustal thinning and mafic volcanic activity around 2.0 – 1.8 Ga
544 (Anand et al., 2003; Ravikant et al., 2014). Such tectonic-volcanic processes may have
545 diagenetically-modified the then seawater composition and be responsible for the positive Eu
546 anomaly (Eu/Eu* = 89.33-1.03) recorded in VF dolomite.
547
548 **8. CONCLUSIONS**
549 Combined field data and microscopic observations suggest that the Cuddapah Basin
550 carbonate rocks initially precipitated as fine lime mud and/or micritic calcite in tidal–flat and
551 associated shallow-marine environments. These sediments were replaced by dolomicrite during
552 early peritidal dolomitization. Petrographic observations also reveal fabric-retentive dolomite
553 textures, including filaments, in stromatolites, possibly reflecting microbial dolomite
554 precipitation-dolomitisation. During shallow sub-surface burial, fabric destructive dolomitization
555 of undolomitized oolitic grainstone and calcimicrite took place, along with recrystallization of
556 the early-formed peritidal dolomite. The $\delta^{18}O$ and $\delta^{13}C$ values of VF dolomite samples suggest
557 that these dolomites were either precipitated or recrystallised from burial diagenetic fluids that
558 evolved from Eu-enriched seawater. Burial diagenetic precipitation and recrystallisation of
559 dolomite are also supported by depleted Na and Sr contents. Ratios and contents of redox-
560 sensitive metals (Cu, Co, Fe, Mn, Mo, Ni, V, Zn), REE distribution and high Fe_T/Al ratios imply
561 that dolomitizing fluids were anoxic and ferruginous but not euxinic. The positive Eu anomaly
562 could reflect a hydrothermal source and this may have been related to fluids connected to
563 continental rifting and volcanic activity within the CB around 1.9 – 2.0 Ga. The pattern of
564 diagenesis and dolomitisation recorded in the VF is more typical of Phanerozoic platform
565 carbonates than many Precambrian dolomites which show perfect preservation of original
566 textures (such as ooids and fibrous cements) and continued precipitation of dolomite in the burial
567 environment as a dolospar cement.
568
569

Acknowledgments

We thank the Indian Statistical Institute (ISI) for financial support in the form of a DCSW grant to Amlan Banerjee and acknowledge S.N. Das and the late Rajen Oraon for their help in the fieldwork. Marcin D. Syczewski is thanked for helping with work on the SEM. We thank Prof. Bernard Pittet and an anonymous reviewer for their comments and suggestions that improved the quality of the paper. This study was also supported by the Russian Government Programme of Competitive Growth of the Kazan Federal University and by the European Regional Development Fund through the grant Innovative Economy (POIG.02.02.00-00-025/09). This work contributes to the Proterozoic research programme of the ISI.

References

Algeo, T.J., Maynard, J.B., 2004. Trace element behaviour and redox facies in core shales of Upper Pennsylvanian Kansas-type cyclothems. Chemical Geology 206, 289–318.

Anand, M., Gibson, S.A., Subba Rao, K.V., Kelley, S.P., Dickin, A.P., 2003. Early Proterozoic melt generation processes beneath the intra-cratonic Cuddapah Basin, Southern India. Journal of Petrology 44, 2139-2171.

Anderson, T.F., Raiswell, R., 2004. Sources and mechanisms for the enrichment of highly reactive iron in euxinic Black Sea sediments. American Journal of Science 304, 203-233.

Azmy, K., Veizer, J., Misi, A., de Oliveira, T.F., Sanches, A.L., Dardenne, M.A., 2001. Dolomitization and isotope stratigraphy of the Vazante Formation, São Francisco Basin, Brazil. Precambrian Research 112, 303–329.

Balter, V., Lécuyer, C., Barrat, J.A., 2011. Reconstructing seawater Sr/Ca during the last 70 My using fossil fish tooth enamel. Palaeogeography, Palaeoclimatology, Palaeoecology 310, 133–138.

Banner, J.L., 1995. Application of the trace element and isotope geochemistry of strontium to studies of carbonate diagenesis. Sedimentology 42, 805–824.

Barnaby, R.J., Read, J.F., 1992. Dolomitization of a carbonate platform during late burial: Lower to Middle Cambrian Shady Dolomite, Virginia Appalachians. Journal of Sedimentary Petrology 62, 1023–1043.

Bau, M., Koschinsky, A., 2009. Oxidative scavenging of cerium on hydrous Fe oxide: Evidence from the distribution of rare earth elements and yttrium between Fe oxides and Mn oxides in hydrogenetic ferromanganese crusts. Geochemical Journal 43, 37-47.

Bau, M., Möller, P., 1993. Rare earth element systematics of the chemically precipitated component in Early Precambrian iron formations and the evolution of the terrestrial atmosphere-hydrosphere-lithosphere system. Geochimica et Cosmochimica Acta 57, 2239-2249.

Bau, M., 1991. Rare earth element mobility during hydrothermal and metamorphic fluid-rock interaction and the significance of the oxidation state of europium. Chemical Geology 93, 219-230.

Bau, M., 1999. Scavenging of dissolved yttrium and rare earths by precipitating iron oxyhydroxide: Experimental evidence for Ce oxidation, Y-Ho fractionation, and lanthanide tetrad effect. Geochimica et Cosmochimica Acta 63, 67-77.

Bau, M., Dulski, P., 1996. Distribution of Yttrium and Rare-Earth Elements in the Penge and Kuruman Iron Formations, Transvaal Supergroup, South Africa. Precambrian Research 79, 37-55. doi:10.1016/0301-9268(95)00087-9

Bekker, A., Kaufman, A.J., Karhu, J.A., Beukes, N.J., Swart, Q.D., Coetzee, L.L., Eriksson, K.A., 2001. Chemostratigraphy of the Paleoproterozoic Duitschland Formation, South Africa: implications for coupled climate change and carbon cycling. American Journal of Science 301, 261–285.

Bekker, A., Karhu, J.A., Eriksson, K.A., Kaufman, A.J. 2003a. Chemostratigraphy of Paleoproterozoic carbonate successions of the Wyoming Craton: tectonic forcing of biogeochemical change? Precambrian Research 120, 279–325.

Bekker, A., Sial, A.N., Karhu, J.A., Ferreira, V.P., Noce, C.M., Kaufman, A.J., Romano, A.W., Pimentel, M.M., 2003b. Chemostratigraphy of carbonates from the Minas Supergroup, Quadrilátero Ferrífero, Brazil: a stratigraphic record of early Proterozoic atmospheric, biogeochemical and climatic change. American Journal of Science 303, 865–904.

Bellanca, A., Masetti, D., Neri, R., 1997. Rare earth elements in limestone/marlstone couplets from the Albian-Cenomanian Cismon section (Venetian region, northern Italy): assessing REE sensitivity to environmental changes. Chemical Geology 141, 141–152.

Bhaskar Rao, Y.J., Pantulu, G.V.C., Damodar Reddy, V., Gopalan, K. 1995. Time of early sedimentation and volcanism in the Proterozoic Cuddapah basin, South India: evidence from Rb–Sr age of Pulivendla mafic sill. Geological Society of India, Memoir 33, 329–338.

Bolhar, R., Van Kranendonk, M.J., 2007. A non-marine depositional setting for the northern Fortescue Group, Pilbara Craton, inferred from trace element geochemistry of stromatolitic carbonates. Precambrian Research 155, 229–250.

Bontognali, T.R.R., Vasconcelos, C., Warthmann, R.J., Bernasconi, S.M., Dupraz, C., Strohmenger, C.J., McKenzie, J.A., 2010. Dolomite formation within microbial mats in the coastal sabkha of Abu Dhabi (United Arab Emirates). Sedimentology 57, 824–844.

Bots, P., Benning, L.G., Rickaby, R., Shaw, S., 2011. The role of SO_4 in the switch from calcite to aragonite seas. Geology 39, 331-334.

Braithwaite, R., 1991. Dolomites, a review of origins, geometry and textures. Transactions of the Royal Society of Edinburgh: Earth Sciences 82, 99–112.

Breit, G.N., Wanty, R.B., 1991. Vanadium accumulation in carbonaceous rocks: A review of geochemical controls during deposition and diagenesis. Chemical Geology 91, 83- 97.

Budd, D.A., 1997. Cenozoic dolomites of carbonate islands: their attributes and origin. Earth-Science Reviews 42, 1–47.

Burdett, J.W., Grotzinger, J.P., Arthur, M.A., 1990. Did major changes in the stable-isotope composition of Proterozoic seawater occur? Geology 18, 227-230.

Chakrabarti, G., Shome, D., Kumar, S., Armstrong-Altrin, J.S., Sial, A.N., 2011. Carbon and oxygen isotopic variations in stromatolitic dolomites of Palaeoproterozoic Vempalle Formation, Cuddapah Basin, India. Carbonates and Evaporites 26, 181-191.

Chakrabarti, G., Shome, D., Kumar, S., Kah, L., 2014. Carbonate platform development in a Paleoproterozoic extensional basin, Vempalle Formation, Cuddapah Basin, India. Journal of Asian Earth Sciences 91, 263-279.

Collins, A.S. Patranabis-Deb, S. Alexander, E. Bertram, C.N., Falster, G.M., Gore, R.J., Mackintosh, J., Dhang, P.C., Saha, D., Payne, J.L., Jourdan, F., Backe, G., Halverson, G.P., Wade, B.P., 2015. Detrital mineral age, radiogenic isotopic stratigraphy and tectonic significance of the Cuddapah Basin, India. Gondwana Research 28, 1294-1309.

Corsetti, F.A., Kidder, D.L., Marenco, P.J., 2006. Trends in oolite dolomitization across the Neoproterozoic-Cambrian boundary: a case study from Death Valley, California. Sedimentary Geology 191, 135-150.

Crusius, J., Calvert, S., Pedersen, T., Sage, D., 1996. Rhenium and molybdenum enrichments in sediments as indicators of oxic, suboxic and sulfidic conditions of deposition. Earth and Planetary Science Letters 145, 65–78.

Danielson, A., Möller, P., Dulski, P., 1992. The europium anomalies in banded iron formation and the thermal history of the oceanic crust. Chemical Geology 97, 89–100.

Derry, L.A., Jacobsen, S.B., 1990. The chemical evolution of Precambrian seawater: Evidence from REEs in banded iron formations. Geochimica et Cosmochimica Acta 54, 2965-2977.

Derry, L.A., Kaufman, A.J., Jacobsen, S.B., 1992. Sedimentary cycling and environmental change in the Late Proterozoic: evidence from stable and radiogenic isotopes. Geochimica et Cosmochimica Acta 56, 1317–1329.

Derry, L.A., Brasier, M.D., Corfield, R.M., Rozanov, A.Y., Zhuravlev, A.Y., 1994. Sr and C isotopes in Lower Cambrian carbonates from the Siberian craton: A paleoenvironmental record during the 'Cambrian explosion'. Earth and Planetary Science Letters 128, 671–681.

Douville, E., Bienvenu, P., Charlou, J.L., Donval, J.P., Fouquet, Y., Appriou, P., Gamo, T., 1999. Yttrium and rare earth elements in fluids from various deep-sea hydrothermal systems. Geochimica et Cosmochimica Acta 63, 627–643.

Eroglu, S., van Zuilen, M.A., Taubald, H., Drost, K., Wille, M., Swanner, E.D., Beukes, N.J., Schoenberg, R., 2017. Depth-dependent $\delta^{13}C$ trends in platform and slope settings of the Campbellrand-Malmani carbonate platform and possible implications for Early Earth oxygenation. Precambrian Research 302, 122-139.

Fairchild, I.J., Herrington, P.M., 1989. A tempestite-stromatolite-evaporite association (late Vendian, East Greenland): A shoreface-lagoon model. Precambrian Research 43, 101-127.

Ferrill, D.A., Morris, A.P., Evans, M.A., Burkhard, M., Groshong Jr., R.H., Onasch, C.M., 2004. Calcite twin morphology: a low-temperature deformation geothermometer. Journal of Structural Geology 26, 1521-1529.

Font, E., Nédélec, A., Trindade, R.I.F., Macouin, M., Charrière, A., 2006. Chemostratigraphy of the Neoproterozoic Mirassol d'Oeste cap dolostones (Mato Grosso, Brazil): An alternative model for Marinoan cap dolostone formation. Earth and Planetary Science Letters 250, 89-103.

French, J.E., Heaman, L.M., Chacko, T., Srivastava, R.K., 2008. 1891–1883 Ma Southern Bastar–Cuddapah mafic igneous events, India: A newly recognized large igneous province. Precambrian Research 160, 308–322.

German, C.R., Elderfield, H., 1990. Application of the Ce anomaly as a paleoredox indicator: the ground rules. Paleoceanography 5, 823.

German, C.R., Hergt, J., Palmer, M.R., Edmond, J.M., 1999. Geochemistry of a hydrothermal sediment core from the OBS vent-field, 21°N East Pacific Rise. Chemical Geology 155, 65-75.

German, C.R., Higgs, N.C., Thomson, J., Mills, R., Elderfield, H., Blusztajn, J., Fleer, A.P., Bacon, M.P., 1993. A geochemical study of metalliferous sediment from the TAG Hydrothermal Mound, 26°08′N, Mid-Atlantic Ridge. Journal of Geophysical Research 98, 9683-9692.

Gilleaudeau, G.J., Kah, L.C., 2013. Carbon isotope records in a Mesoproterozoic epicratonic sea: Carbon cycling in a low-oxygen world. Precambrian Research 228, 85-101.

Gregg, J.M., Sibley, D.F., 1984. Epigenetic dolomitization and the origin of xenotopic dolomite texture. Journal of Sedimentary Research 54, 908-931.

748 Grotzinger, J.P., 1989. Facies and evolution of Precambrian carbonate depositional systems:
749 emergence of the modern platform archetype. SEPM Special Publication 44, 79-106.

750 Grotzinger, J.P., Read, J.F., 1983. Evidence for primary aragonite precipitation, lower
751 Proterozoic (1.9 Ga) dolomite, Wopmay orogen, northwest Canada. Geology 11, 710-713.

752 Grotzinger, J.P., Kasting, J., 1993. New constraints on Precambrian ocean composition. Journal
753 of Geology 101, 235-243.

754 Haley, B., Klinkhammer, G. P., McManus, J., 2004. Rare earth elements in pore waters of
755 marine sediments. Geochimica et Cosmochimica Acta 68, 1265-1279.
756
757 Hallberg, R.O., 1976. A geochemical method for investigation of palaeoredox conditions in
758 sediments. Ambio Special Report 4, 139-147.
759
760 Hallberg, R.O., 1982. Diagenetic and environmental effects on heavy-metal distribution in
761 sediments: A hypothesis with an illustration from the Baltic Sea. In: Fanning, K.A., Manheim,
762 F.T. (Eds), The dynamic environment of the ocean floor. Lexington Books, Lexington, p. 305-
763 316.
764
765 Hardy, R., Tucker, M.E., 1988. X-ray powder diffraction of sediments. In: Tucker, M.E. (Ed.)
766 Techniques in Sedimentology. Blackwell Scientific Publications, p. 191-228.
767
768 Hatch, J.R., Leventhal, J.S., 1992. Relationship between inferred redox potential of the
769 depositional environment and geochemistry of the Upper Pennsylvanian (Missourian) Stark
770 Shale Member of the Dennis Limestone, Wabaunsee County, Kansas, U.S.A. Chemical
771 Geology 99, 65–82.
772
773 Hird, K., Tucker, M.E., Waters, R.A., 1987. Petrography, geochemistry and origin of Dinantian
774 dolomites from South-East Wales. In: Miller, J., Adams, A.E., and Wright, V.P. (Eds) European
775 Dinantian Environments. Wiley, New York, 359–376.
776
777 Holland, H., Zimmermann, H., 2000. The dolomite problem revisited. International Geology
778 Review 42, 481–490.
779
780 Holland, S.M., Patzkowsky, M.E., 1998. Sequence stratigraphy and relative sea-level history of
781 the Middle and Upper Ordovician of the Nashville Dome, Tennessee. Journal of Sedimentary
782 Research 68, 684-699.
783
784 Hood, A.S., Wallace, M.W., 2018. Neoproterozoic marine carbonates and their
785 paleoceanographic significance. Global and Planetary Change 160, 28-45.
786
787 Hurtgen, M.T., Galen, G.P., Arthur M.A., Hoffman, P.F., 2006. Sulfur cycling in the aftermath of
788 635-Ma snowball glaciation: evidence for a syn-glacial sulfidic deep ocean. Earth and Planetary
789 Science Letters 245, 551–570.
790

Jahn, B.M., Cuvellier, H., 1994. Pb-Pb and U-Pb geochronology of carbonate rocks: an assessment. Chemical Geology 115, 125-151.

Jahn, B.M., Simonson, B.M., 1995. Carbonate Pb-Pb ages of the Wittenoom Formation and Carawine Dolomite, Hamersley Basin, Western Australia (with implications for their correlation with the Transvaal Dolomite of South Africa). Precambrian Research 72, 247-261.

Johannesson, K.H., Zhou, X. 1999. Origin of middle rare earth element enrichments in acid waters of a Canadian High Arctic lake. Geochimica et Cosmochimica Acta 63, 153–165.

Kamber, B.S., Webb, G.E., 2001. The geochemistry of late Archaean microbial carbonate: implications for ocean chemistry and continental erosion history. Geochimica et Cosmochimica Acta 65, 2509-2525.

Kaufman, A.J., Knoll, A.H., 1995. Neoproterozoic variations in the C-isotopic composition of seawater: stratigraphic and biogeochemical implications. Precambrian Research 73, 27-49.

Khelen, A.C., Manikyamba, C., Ganguly, S., Singh, T., Subramanyam, K.S.V., Ahmad, S.M., Reddy, M.R., 2017. Geochemical and stable isotope signatures of Proterozoic stromatolitic carbonates from the Vempalle and Tadpatri Formations, Cuddapah Supergroup, India: Implications on paleoenvironment and depositional conditions. Precambrian Research 298, 365–384.

Knoll, A.H., Kaufman, A.J., Semikhatov, M.A., 1995. The carbon isotopic composition of Proterozoic carbonates of Riphean successions from northwestern Siberia (Anabar Massif, Turukhansk Uplift). American Journal of Science 295, 823–850.

Land, L.S., Hoops, G.K., 1973. Sodium in carbonate sediments and rocks; a possible index to the salinity of diagenetic solutions. Journal of Sedimentary Petrology 43, 614-617.

Lawrence, M.G., Kamber, B.S., 2006. The behaviour of the rare earth elements during estuarine mixing – revisited. Marine Chemistry 100, 147-161.

Lindsay, J.F., Brasier, M.D., 2000. A carbon isotope reference curve for 1700–1575 Ma, McArthur and Mount Isa Basins, Northern Australia. Precambrian Research 99, 271–308.

Lumsden, D.N., 1979. Discrepancy between thin-section and X-ray estimates of dolomite in limestone. Journal of Sedimentary Petrology 49, 429– 435.

Lyons, T.W., Severmann, S., 2006. A critical look at iron paleoredox proxies: New insights from modern euxinic marine basins. Geochimica et Cosmochimica Acta 70, 5698-5722.

Machel, H.G., 2004. Concepts and models of dolomitization: a critical reappraisal. Geological Society, London, Special Publications 235, 7-63.

836 Majumder, T., Patranabis-Deb, S., Nemec, W., 2015. Palaeoproterozoic sedimentation in the
837 Cuddapah Basin of southern India. Abstracts 31st IAS Meeting of Sedimentology, 22-25 June,
838 2015, Kraków, Poland, p. 326.
839
840 Malone, M.J., Baker, P.A., Burns, S.J., 1996. Recrystallization of dolomite: An experimental
841 study from 50–200 ^{o}C. Geochimica et Cosmochimica Acta 60, 2189–2207.
842
843 Melezhik, V.A., Fallick, A.E., Makarikhin, V.V., Lubtsov, V.V., 1997. Links between
844 Palaeoproterozoic palaeogeography and rise and decline of stromatolites: Fennoscandian Shield.
845 Precambrian Research 82, 311–348.
846
847 Michard, A., Albarbde, F., Michard, G., Minster, J.F. and Charlou, J.L., 1983. Rare earth
848 elements and uranium in high-temperature solutions from East Pacific Rise hydrothermal vent
849 field (13 ^{o}N). Nature 303, 795-797.
850
851 Michard, A., 1989. Rare earth element systematics in hydrothermal fluids. Geochimica et
852 Cosmochimica Acta 53, 745–750.
853
854 Montañez, I.P., Banner, J.L., Osleger, D.A., Borg, L.E., Bosserman, P.J., 1996. Integrated Sr
855 isotope variations and sea-level history of Middle to Upper Cambrian platform carbonates:
856 Implications for the evolution of Cambrian seawater $^{87}Sr/^{86}Sr$. Geology 10, 917–920.
857
858 Murray, R.W., Buchholtz Ten Brink, M.R., Gerlach, D.C., Price Russ III, G., Jones, L. D., 1991.
859 Rare earth, major, and trace elements in chert from the Franciscan Complex and Monterey
860 Group, California: Assessing REE sources to fine-grained marine sediments. Geochimica et
861 Cosmochimica Acta 55, 1875-1895.
862
863 Myrow, P.M., 1992. Pot and gutter casts from the Chapel Island Formation, southeast
864 Newfoundland. Journal of Sedimentary Research 62, 992-1007.
865
866 Nagaraja Rao, B.K., Rajurkar, S.T., Ramalingaswamy, G., Ravindra Babu, B., 1987,
867 Stratigraphy, structure and evolution of the Cuddapah Basin. In: Radhakrishna, B.P., (Ed.)
868 Purana Basins of Peninsular India (Middle to Late Proterozoic). Geological Society of India 6,
869 33–86.
870
871 Nédélec, A., Affaton, P., France-Lanord, C., Charrière, A., Alvaro, J., 2007. Sedimentology and
872 chemostratigraphy of the Bwipe Neoproterozoic cap dolostones (Ghana, Volta Basin): A record
873 of microbial activity in a peritidal environment. Comptes Rendus Geoscience 339, 223–239.
874
875 Nordeng, S.H., Sibley, D.E., 1994. Dolomite stoichiometry and Ostwald's step rule. Geochimica
876 et Cosmochimica Acta 58, 191-196.
877
878 Palmer, M.R., 1985. Rare earth elements in foraminifera tests. Earth and Planetary Science
879 Letters 73, 285-298.
880

881 Patranabis-Deb, S., Saha, D., Tripathy, V., 2012. Basin stratigraphy, sea-level fluctuations and
882 their global tectonic connections – evidence from the Proterozoic Cuddapah Basin. Geological
883 Journal 47, 263-283.
884
885 Patranabis-Deb, S., Majumder, T., Khan, S., 2018. Lifestyles of the Palaeoproterozoic
886 stromatolite builders in the Vempalle Sea, Cuddapah Basin, India. Journal of Asian Earth
887 Sciences 157, 360–370.
888
889 Perri, E., Tucker, M.E., Słowakiewicz, M., Whitaker, F., Bowen, L., Perrotta, Ida D., 2018.
890 Carbonate and silicate biomineralization in a hypersaline microbial mat (Mesaieed sabkha,
891 Qatar): Roles of bacteria, extracellular polymeric substances and viruses. Sedimentology 65,
892 1213-1245.
893
894 Petrash, D.A., Bialikb, O.M., Bontognali, T.R.R., Vasconcelos, C., Roberts, J.A., McKenzie,
895 J.A., Konhauser, K.O., 2017. Microbially catalyzed dolomite formation: From near-surface to
896 burial. Earth-Science Reviews 171, 558-582.
897
898 Piper, D.Z., 1974. Rare-earth elements in the sedimentary cycle: a summary. Chemical Geology
899 14, 285-304.
900
901 Pope, M.C., Grotzinger, J.P., 2003. Paleoproterozoic Stark Formation, Athapuscow basin,
902 northwest Canada: Record of cratonic-scale salinity crisis. Journal of Sedimentary Research 73,
903 280-295.
904
905 Rai, A.K., Pandey, U.K., Zakaulla, S., Parihar, P.S., 2015. New 1.9-2.0 Ga, Pb-Pb (PbSL), age of
906 dolomites from Vempalle Formation, Lower Cuddapah Supergroup, Eastern Dharwar Craton,
907 India. Journal of the Geological Society of India 86, 131-136.
908
909 Ravikant V., Hashmi, S., Chatterjee, C., Ji, W-Q., Wu, F-Y., 2014. Initiation of the intra–
910 cratonic Cuddapah basin: evidence from Paleoproterozoic (1995 Ma) anorogenic porphyritic
911 granite in Eastern Dharwar Craton basement. Journal of Asian Earth Sciences 79, 235-245.
912
913 Ravikant, V., 2010. Paleoproterozoic (1.9 Ga) extension and breakup along the eastern margin of
914 the Eastern Dharwar Craton, SE India: New Sm–Nd isochorn age constraints from anorogenic
915 mafic magmatism in the Neoarchean Nellore greenstone belt. Journal of Asian Earth Sciences
916 12, 67-81.
917
918 Sachan, H.K., 1993. Early replacement, dolomitization and deep burial modification and
919 stabilization: A case study from the Zawar area, Rajasthan (India). Carbonates and Evaporites 8,
920 191-198.
921
922 Saha, D., Mazumder, R., 2012. An overview of the Paleoproterozoic geology of peninsular India
923 and key stratigraphic and tectonic issues. Geological Society, London, Special Publications 365,
924 159–182
925

926 Saha, D., Tripathy, V., 2012. Paleoproterozoic sedimentation in the Cuddapah basin, south India
927 and regional tectonics – a review. Geological Society, London, Special Publications 365, 5–28.
928
929 Sass, E., Bein, A., 1988. Dolomites and salinity: a comparative geochemical study. SEPM
930 Special Publications 43, 223–233.
931
932 Sass, E., Katz, A., 1982. The origin of platform dolomites. New evidence. American Journal of
933 Science 282, 1184–1213.
934
935 Saylor, B.Z., Grotzinger, J.P., Germs, J.B., 1995. Sequence stratigraphy and sedimentology of
936 the Neoproterozoic Kuibis and Schwarzrand Subgroups (Nama Group), southwestern Namibia.
937 Precambrian Research 73, 153-171.
938
939 Schier, K., Bau, M., Münker, C., Beukes, N., Viehmann, S., 2018. Trace element and Nd isotope
940 composition of shallow seawater prior to the Great Oxidation Event: Evidence from stromatolitic
941 bioherms in the Paleoproterozoic Rooinekke and Nelani Formations, South Africa. Precambrian
942 Research 315, 92-102.
943
944 Shen, Y.N., Zhang, T.G., Chu, X.L., 2005. C-isotopic stratification in a Neoproterozoic
945 postglacial ocean. Precambrian Research 137, 243–251.
946
947 Sherrell, R.M., Field, M.P., Ravizza, G., 1999. Uptake and fractionation of rare earth elements
948 on hydrothermal plume particles at 9°25′N, East Pacific Rise. Geochimica et Cosmochimica
949 Acta 63, 1709–1722.
950
951 Sibley, D.F., and Gregg, J.M., 1987. Classification of dolomite rock textures. Journal of
952 Sedimentary Petrology 57, 967-975.
953
954 Sosdian, S.M., Lear, C.H., Tao, K., Grossman, E.L., O'Dea, A., Rosenthal, Y., 2012. Cenozoic
955 seawater Sr/Ca evolution. Geochemistry Geophysics Geosystems 13, Q10014.
956
957 Swett, K., Knoll, A.H., 1989. Marine pisolites from Upper Proterozoic carbonates of East
958 Greenland and Spitsbergen. Sedimentology 36, 75–93.
959
960 Tewari, V., Tucker, M.E., 2011. Ediacaran Krol carbonates of the Lesser Himalaya, India:
961 Stromatolitic facies, depositional environment and diagenesis. In: Tewari, V., Seckbach, J.,
962 (eds.), Stromatolites: Interaction of Microbes with Sediments. Springer, 133-156.
963
964 Tribovillard, N., Algeo, T.J., Lyons, T., Riboulleau, A., 2006. Trace metals as paleoredox and
965 paleoproductivity proxies: an update. Chemical Geology 232, 12–32.
966
967 Tripathy, V., Saha, D., 2008. Temporal stress variation around Gani-Kalva and adjoining faults,
968 Cuddaph basin: implications for continental tectonics. In: Biswal, T.K., Pandalai, H.S., Pande,
969 K., Pillai, S.P. (Eds.) Abstract volume, International conference on Tectonics of the Indian
970 Subcontinent, International Association for Gondwana Research Conference Series 5, 209–210.
971

Tucker, M.E., 1982. Precambrian dolomites: Petrographic and isotopic evidence that they differ from Phanerozoic dolomites. Geology 10, 7-12.

Tucker, M.E., 1983. Diagenesis, geochemistry, and origin of a Precambrian dolomite; the Beck Spring Dolomite of eastern California. Journal of Sedimentary Research 53, (4), 1097-1119.

Tucker, M.E., 1984. Calcitic, aragonitic and mixed calcitic-aragonitic ooids from the mid-Proterozoic Belt Supergroup, Montana. Sedimentology 31, 627-644.

Tucker, M.E., 1985. Calcitized aragonite ooids and cements from the Late Precambrian Biri Formation of Southern Norway. Sedimentary Geology 43, 67-84.

Tucker, M.E., Wright, V.R., 1990. Carbonate Sedimentology. Blackwell Scientific, Oxford, 482.

Tucker, M.E., Wright, V.P., Dickson, J.A.D., 2002. Carbonate Sedimentology, Blackwell Science Ltd, 482p.

Turekian, K.K., Wedepohl, K.H., 1961. Distribution of the elements in some major units of the Earth's crust. Geological Society of America Bulletin 72, 175-192.

Vahrenkamp, V.C., Stewart, P.K., 1990. A new distribution coefficient for the incorporation of strontium into dolomite and its implications for the formation of ancient dolomites. Geology 18, 387–391.

Van Smeerdijk Hood, A., Wallace, M.W., 2012. Synsedimentary diagenesis in a Cryogenian reef complex: Ubiquitous marine dolomite precipitation. Sedimentary Geology 255, 56-71.

Veizer, J., Hoefs, J., 1976. The nature of O^{18}/O^{16} and C^{13}/C^{12} secular trends in sedimentary carbonate rocks. Geochimica et Cosmochimica Acta 40, 1387-1395.

Veizer, J., Clayton, R.N., Hinton, R.W., Von Brunn, V., Mason, T.R., Bucks, G., Hoefs, J., 1990. Geochemistry of Precambrian carbonates: 3. Shelf seas and non-marine environments of the Archean. Geochimica et Cosmochimica Acta 54, 2717-2729.

Veizer, J., Clayton, R.N., Hinton, R.W., 1992a. Geochemistry of Precambrian carbonates: VI. Early Paleoproterozoic (2.25 ± 0.25 Ga) seawater. Geochimica et Cosmochimica Acta 56, 875-885.

Veizer, J., Numb, K.A., Clayton, R.N., Hinton R.W., Grotzinger, J.P., 1992b. Geochemistry of Precambrian carbonates: V. Late Paleoproterozoic (1.8 ± 0.2 Ga) seawater. Geochimica et Cosmochimica Acta 56, 2487-2501.

Veizer, J., 1983. Chemical diagenesis of carbonates: theory and application of trace element technique. SEPM Short Course 10, 151.

Wang, W., Bolhar, R., Mei-Fu, Z., Xin-Fu., Z., 2018. Enhanced terrestrial input into Paleoproterozoic to Mesoproterozoic carbonates in the southwestern South China Block during the fragmentation of the Columbia supercontinent. Precambrian Research 313, 1-17.

Wanty, R.B., Goldhaber, M., 1992. Thermodynamics and kinetics of reactions involving vanadium in natural systems: Accumulation of vanadium in sedimentary rocks. Geochimica et Cosmochimica Acta 56, 1471-1483.

Warren, J., 2000. Dolomite: occurrence, evolution and economically important associations. Earth-Science Reviews 52, 1-81.

Wilkinson, B.H., Algeo, T.J., 1989. Sedimentary carbonate record of calcium-magnesium cycling. American Journal of Science 289, 1158-1194.

Yoshioka, H., Asahara, Y., Tojo, B., Kawakami, S., 2003. Systematic variations in C, O, and Sr isotopes and elemental concentrations in Neoproterozoic carbonates in Namibia: implications for a glacial to interglacial transition. Precambrian Research 124, 69-85.

Zachariah, J.K., Bhaskar Rao, Y.J., Srinivasan, R., Gopalon, K., 1999. Pb, Sr, Nd isotope systematics of uranium mineralised stromatolitic dolomites from the Proterozoic Cuddapah Supergroup, south India: constraints on age and provenance. Chemical Geology 162, 49-64.

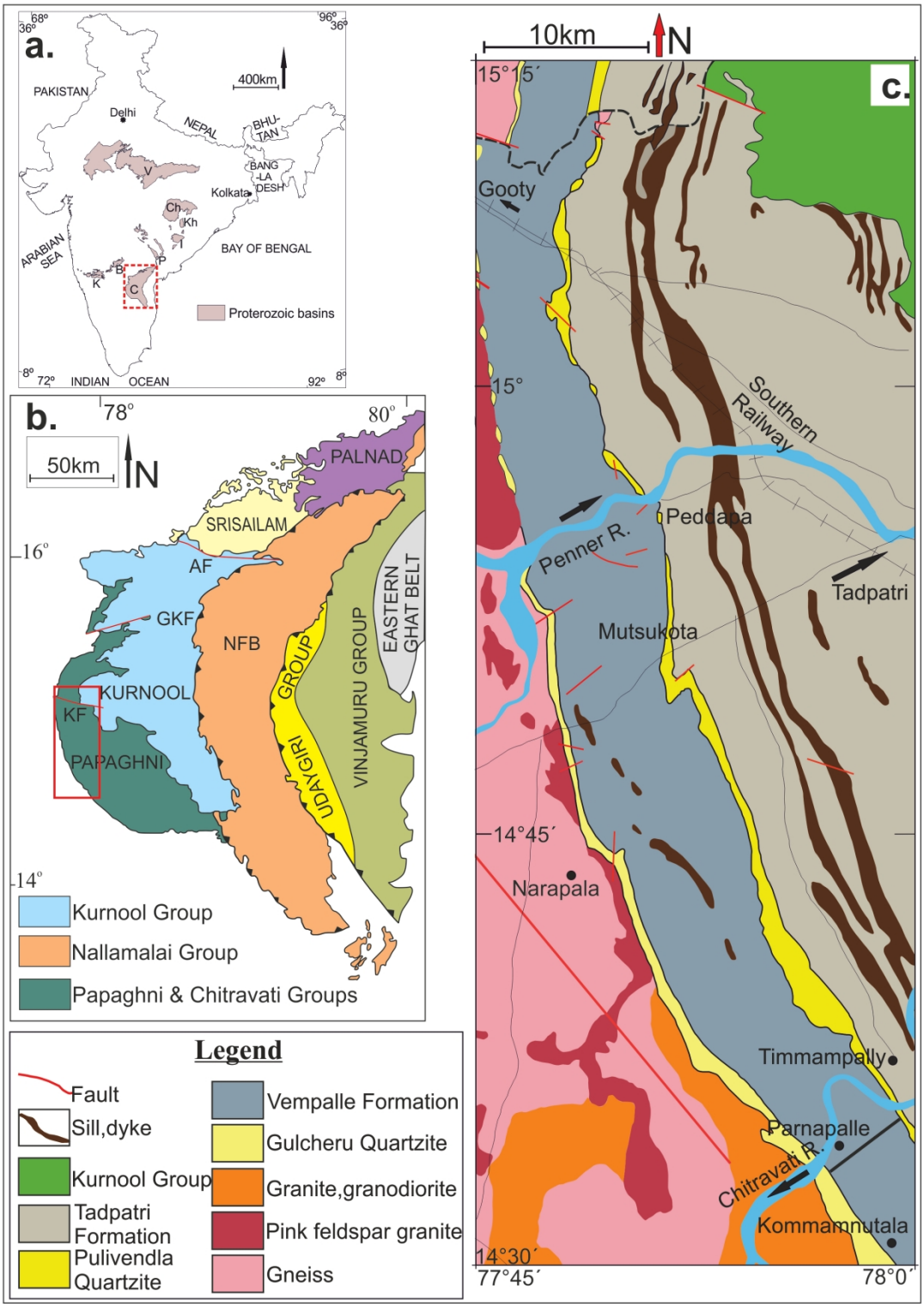

Fig. 1. (a) Distribution of the major Proterozoic basins in India. The red, dashed, outlined rectangle demarcates the Cuddapah Basin; (b) Outline sketch of the Cuddapah Basin showing four sub-basins (after Ramam and Murty, 1997). The red, outlined rectangle demarcates the study area in the Papaghni sub-basin, Cuddapah Basin; (c) General geological map of the south-western part of the Papaghni sub-basin showing the different lithostratigraphic units of formation status. The study area is located near Parnapalle village (N14º32'58.3", E77º58'09.9").

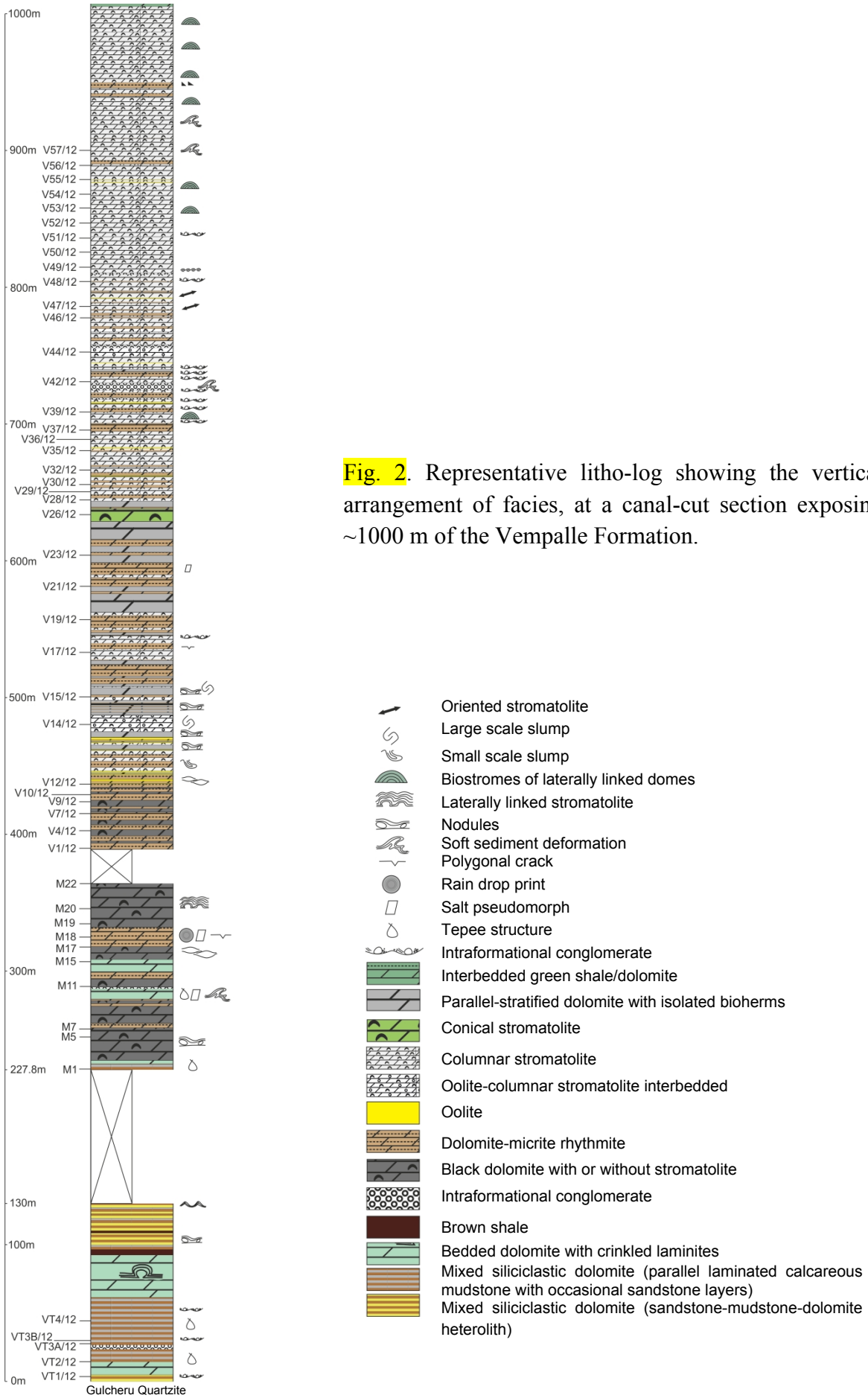

Fig. 2. Representative litho-log showing the vertical arrangement of facies, at a canal-cut section exposing ~1000 m of the Vempalle Formation.


3a


3b


3c


3d

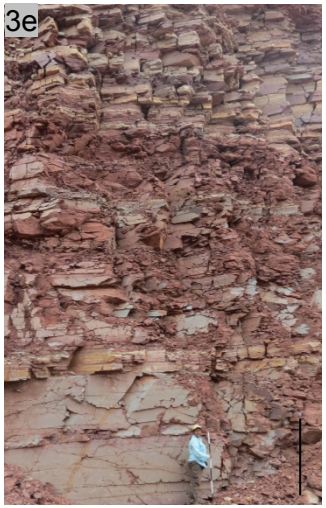
3e

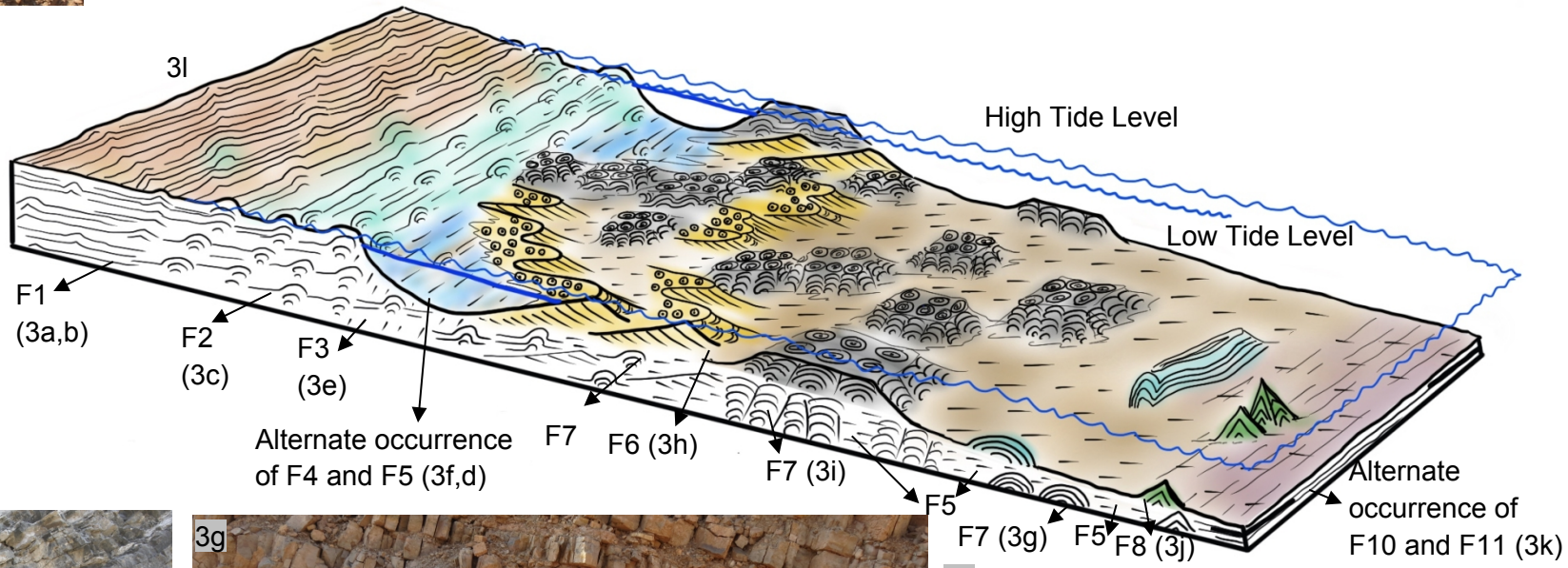
3l
High Tide Level
Low Tide Level
F1
(3a,b)
F2
(3c)
F3
(3e)
Alternate occurrence
of F4 and F5 (3f,d)
F7
F6 (3h)
F7 (3i)
F5
F7 (3g)
F5
F8 (3j)
Alternate
occurrence of
F10 and F11 (3k)


3f


3g


3h


3i


3j


3k

Fig. 3. Field photographs showing different features of the Vempalle Formation, referred in the interpretative block diagram showing the VF depositional environment. a) Mixed siliciclastic dolomite (sandstone-mudstone heterolith, F1); b) Mixed siliciclastic dolomite (laminated calcareous mudstone with siliciclastic input, F1); c) Bedded dolomite with crinkled laminites (F2) characterized by flat or wavy lamination; d) Dolomite-micrite rhythmite (F5) characterized by buff-coloured dolomite alternating with green or brown shale; e) Thick occurrence of brown shale (F3), where the bed-sets (~1.5 m) laterally persist more than 10 m; f) Black dolomite with chert nodules (F4); g) Tabular biostromes of laterally-linked domes of stromatolite (F7); h) Planar- and trough-stratified oolitic grainstone beds (F6); i) Tabular biostromes of columnar stromatolites; j) Tabular biostromes of conical stromatolites (F9); k) Tabular beds of parallel stratified dolomite (F10) alternating with buff-coloured marl and green shale (F11) with steatite (talc) interbeds; l) Schematic representation of the palaeogeography of the VF. The hammer in photograph a, c is 32.5 cm in length. The hammer in photograph b is 28.5 cm and the scale in photograph j is 15 cm. The bar scale in other photographs (marked by black coloured line) is 1.6 m long.

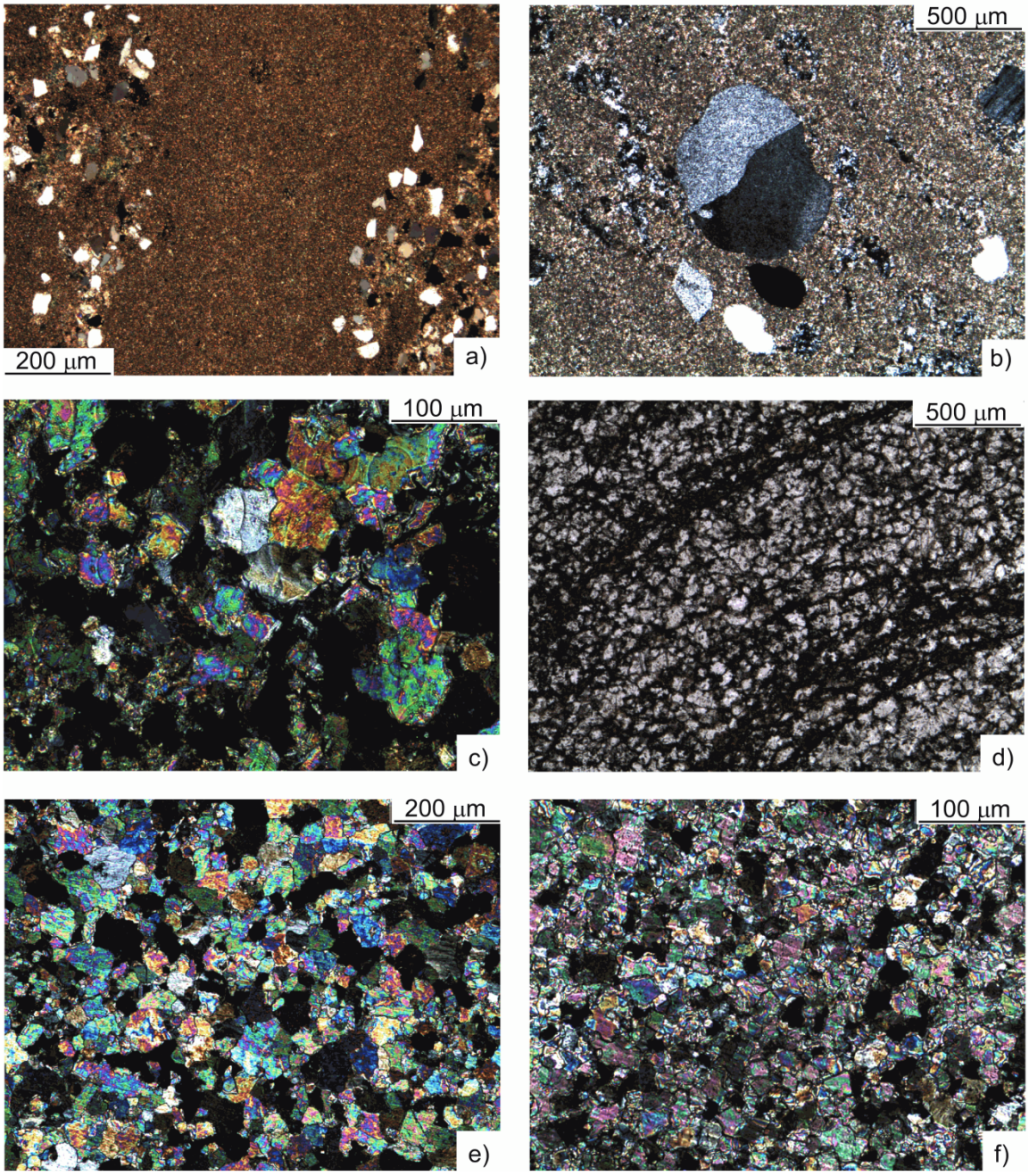

Fig. 4. a) Mixed siliciclastic-carbonate with >10% of terrigenous material characterized mostly by sub-rounded to well-rounded quartz with minor feldspar (XPL). b) Lithic fragments of quartz (centre) and feldspar (upper right). c) Non-planar polymodal relatively coarse-crystalline dolomite completely replaced the calcimicrite matrix. Note the curved crystal faces and undulose extinction of the non-planar dolomite (XPL). d) Stromatolitic dolomite showing alternate occurrence of fine- and coarse- crystalline dolomite and microbial laminae (PPL). e) Polymodal non-planar dolomite crystals from the coarse-crystalline layers of the stromatolitic dolomite. Note the preservation of crystal-face junctions in the non-planar dolomite compared to the planar-s dolomite (XPL). f) Fine-crystalline polymodal planar-s to non-planar dolomite crystals from the dolomite layers of the stromatolitic dolomite (XPL).

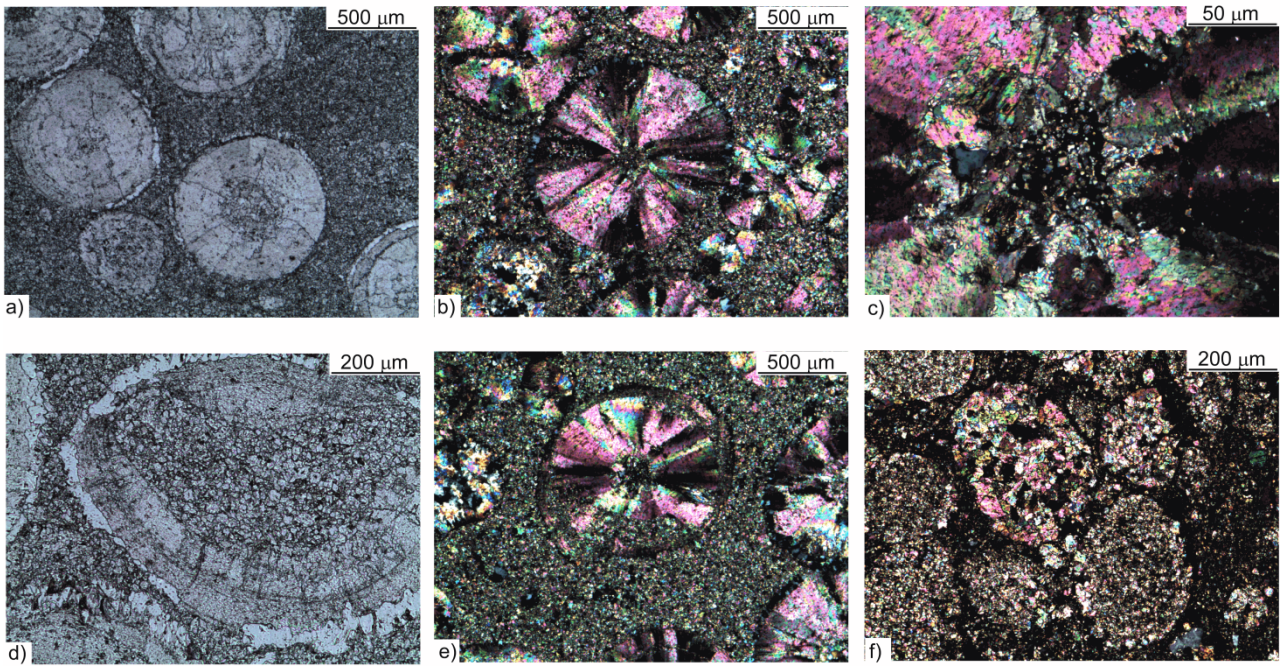

Fig. 5. a) Ooids of different sizes showing concentric rims and radial cracks (PPL); b) Ooids composed of calcite crystals, showing radial fabric (XPL) c) Presence of euhedral rhombic dolomite crystals at the nucleus of the ooid. Radial fabric is clearly visible showing sweeping extinction (XPL); d) Partially replaced ooid grain preserving concentric rims and radial fabric at the outer margin. Dolomite replacement at the inner part of the ooid completely destroyed the primary fabric. Also note presence of silica rim at the margin of the ooid (PPL); e) Partial destruction of the primary radial fabric of the ooid at the peripheral margin by micritic dolomite crystals during replacement (XPL); f) ooid cortex is completely replaced by planar-e, planar - s and non-planar micritic dolomite crystals completely obliterating the internal fabric but still preserving the shape of the ooids.

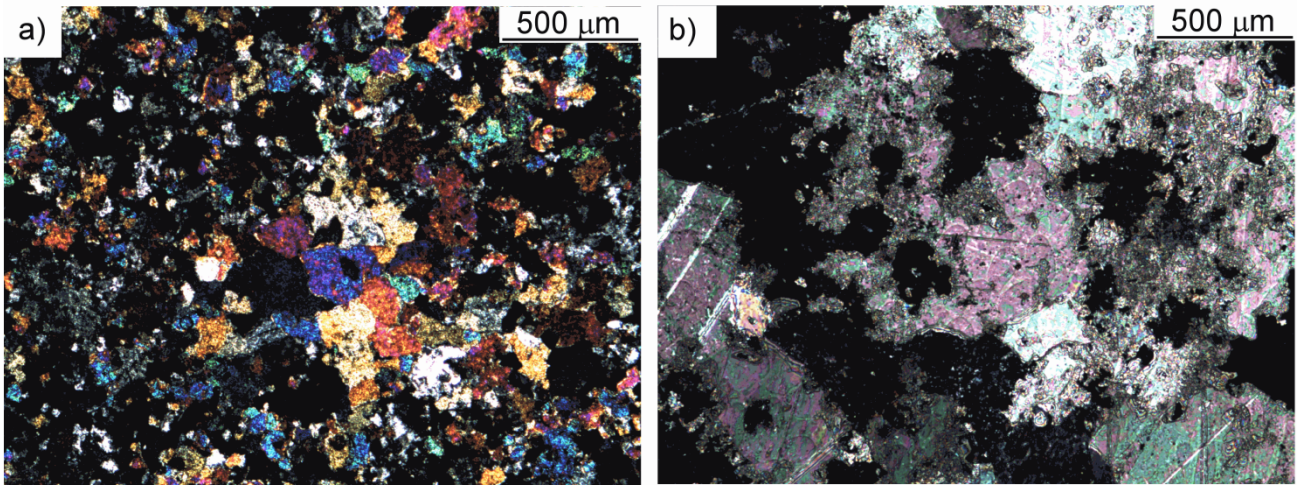

Fig. 6. Photomicrograph of massive VF dolomite from the upper part of the formation. a) Still preserved unreplaced calcimicrite with medium-grained, polymodal calcite microspar (XPL). b) Calcite spar showing lamellae engulfing dolomite crystals (XPL).

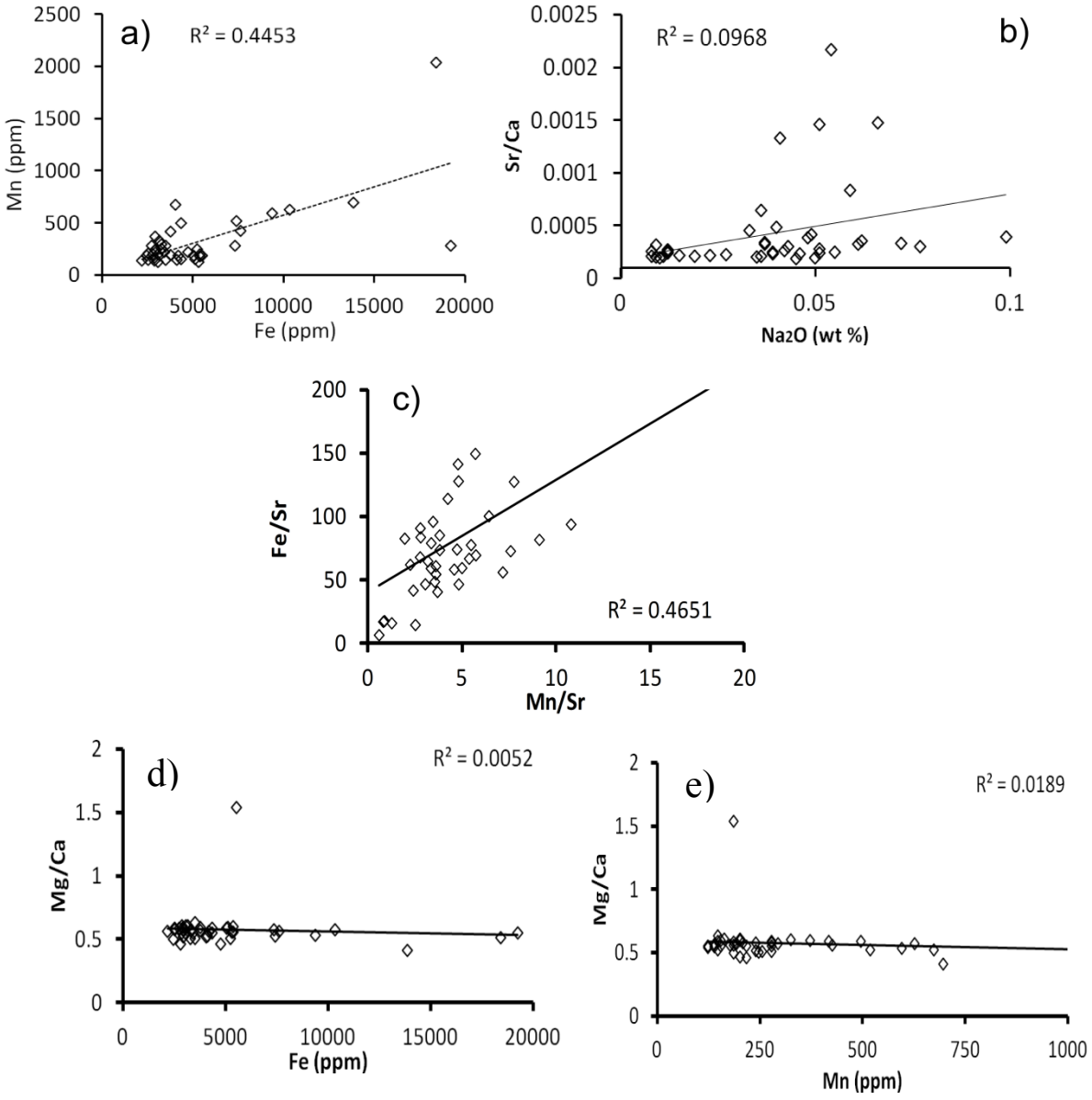

Fig. 7. Cross-plots of a) Mn vs Fe, b) Sr/Ca vs Na_2O, and c) Fe/Sr vs Mn/Sr d) Mg/Ca vs Fe and e) Mg/Ca vs Mn from VF dolomite samples (oxide percent is converted in to ppm: oxide percent x conversion factor x 10000).

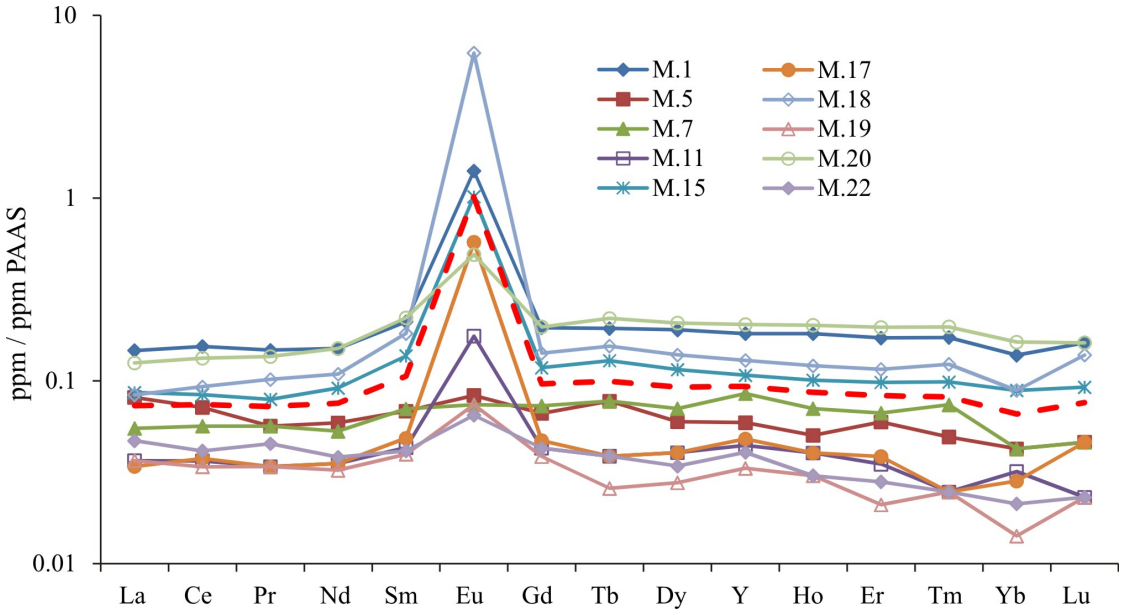

Fig. 8. Example of the typical PAAS-normalized REE patterns of Vempalle Formation dolomite samples. A red dashed-line represents an average of a chosen data-set and shows a pronounced positive Eu anomaly.

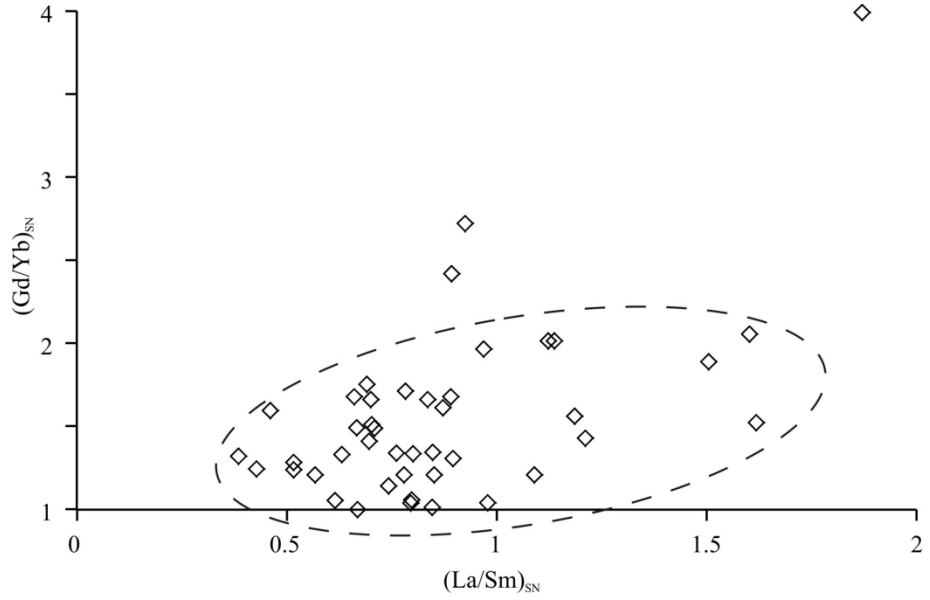

Fig. 9. Distribution of PAAS-normalised $(Gd/Yb)_{SN}$ vs $(La/Sm)_{SN}$ of Vempalle Formation dolomite samples.

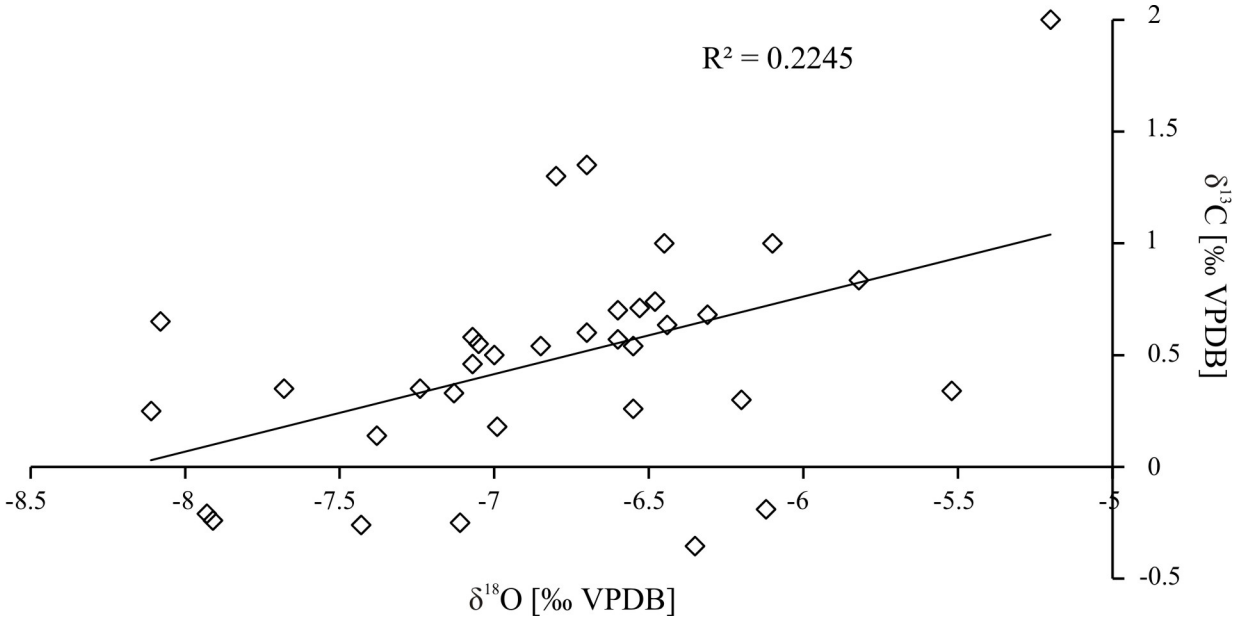

Fig. 10. Cross-plot of oxygen vs carbon isotope values obtained from the Vempalle Formation dolomites showing an inverse correlation.

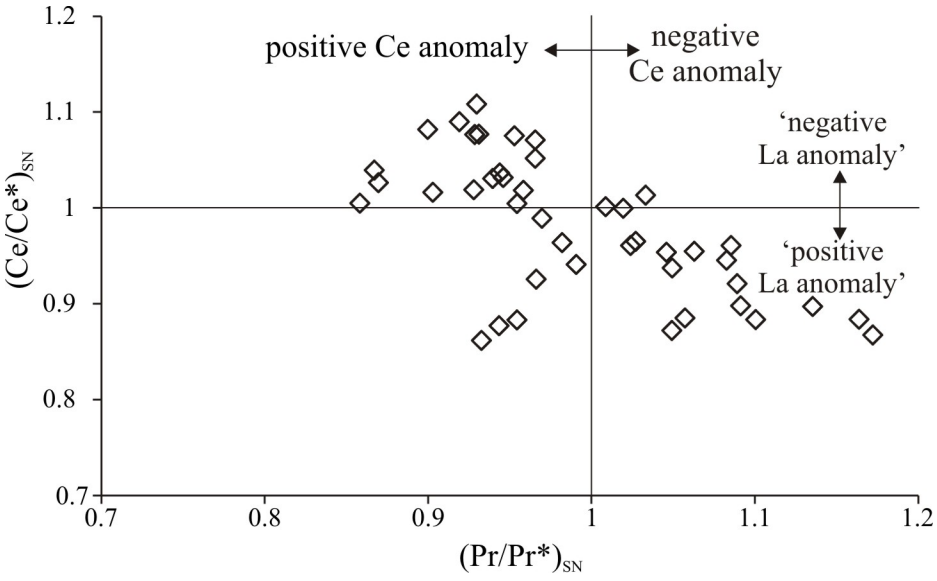

Fig. 11. Plot of Ce_{SN} and Pr_{SN} anomalies for the Vempalle Formation dolomites shows a wide range of anomalies from large positive Ce anomalies to moderately negative anomalies. Fields after Bau and Dulski (1996).

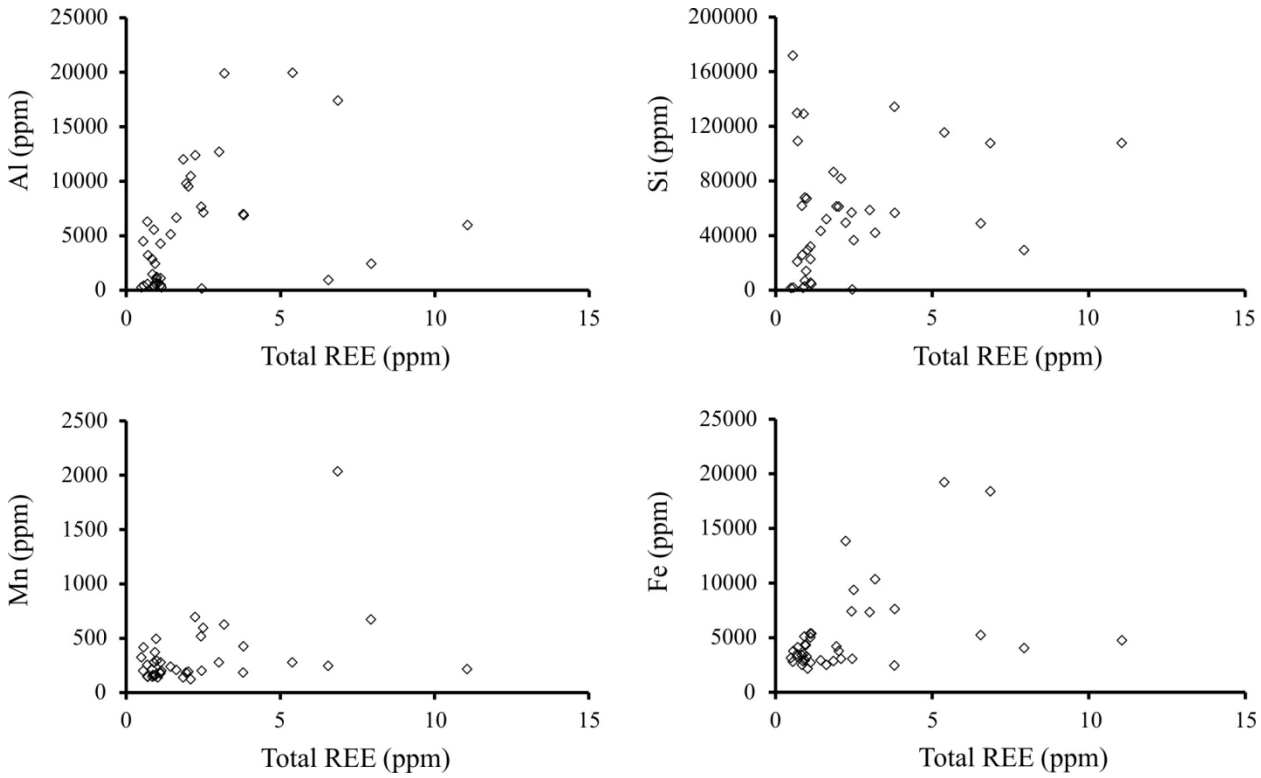

Fig. 12. The PAAS-normalized low ΣREE of the Vempalle Formation dolomites suggests that the precursor rock is probably of marine origin and the REE contribution from non-carbonate fractions (Fe-Mn oxides and siliciclastic contamination) appears to be minor.

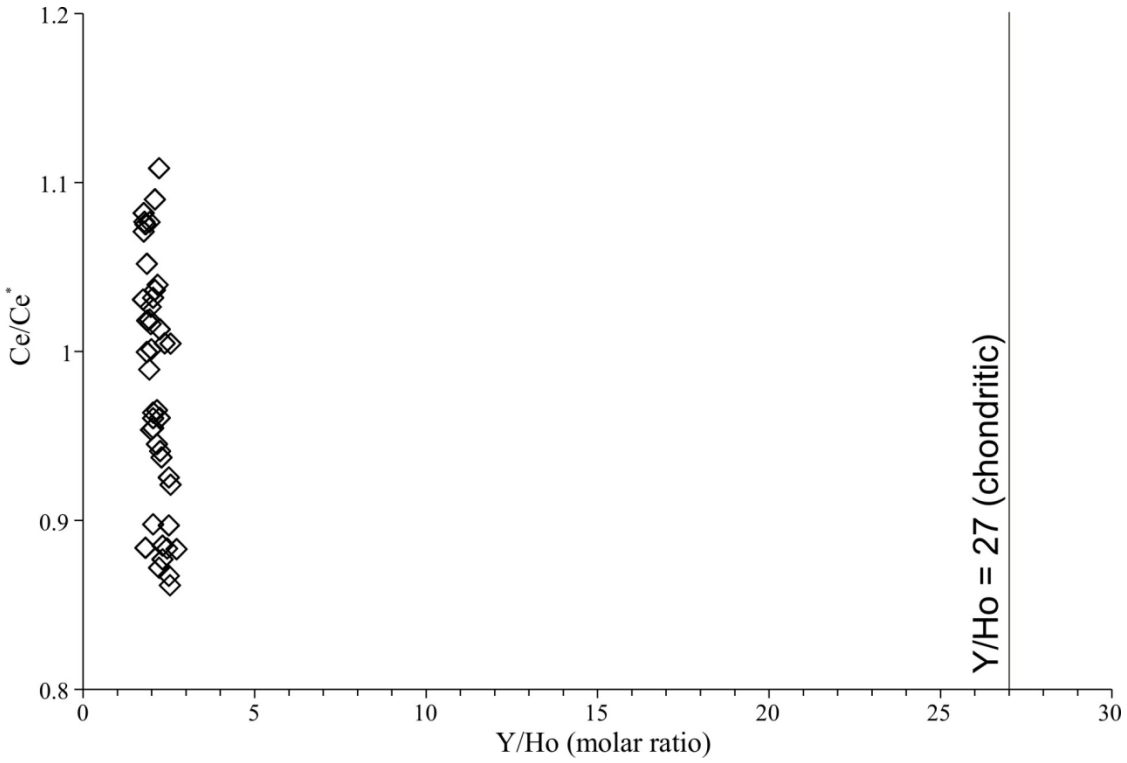

Fig. 13. Correlation between Y/Ho versus Ce/Ce* of the Vempalle Formation dolomites suggests variable contamination of the precursor carbonate sediments.

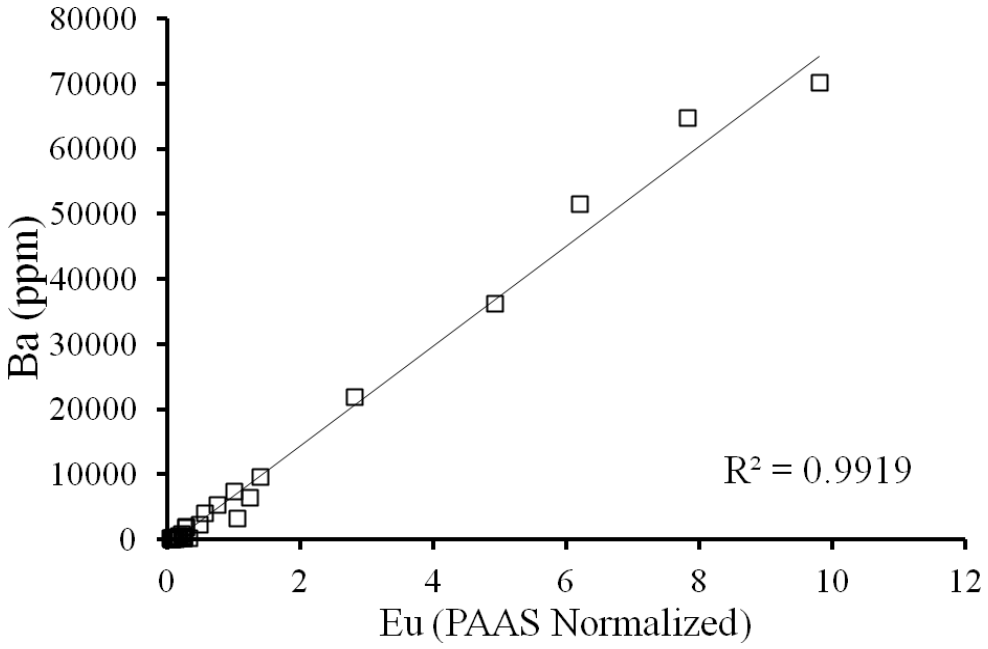

Fig. 14. Strong correlation between Ba (ppm) versus PAAS normalized Eu of the VF dolomites clearly indicates the signature of hydrothermal activity.

TABLES

Table 1. Sample list of Vempalle Formation rocks from the Papaghni Group. ✔ - Sample analyzed; -- - sample not analyzed

Sample No.	Color of Rock Sample	Lithology	Facies	Height	Major oxide	Trace element	REE	XRD	Isotope
V_T1/12	Light Grey, 5Y 6/1	Locally algal laminated fine grained dolomicrite	F1	3.56m	✔	-	--	✔	--
V_T2/12	Grayish pink (5R 8/2) with elongated patches of grayish purple	Laminated Fine grained dolomicrite	F1	14.4m	✔	✔	✔	✔	--
V_T3A/12	Grayish pink (5R 8/2) with banding of grayish purple	Fine grained dolomicrite	F1	26.72m	✔	✔	✔	✔	--
V_T3B/12	Very light gray (N8) colored clast in a Grayish pink (5R 8/2) colored cement	Intraformational Conglomerate (Large, elongated limestone clasts in dolomite cement)	F1	29.92m	✔	✔	✔	✔	--
V_T4/12	Grayish Pink, 5R 8/2	Algal laminated Fine grained dolomicrite	F1	44.3m	✔	✔	✔	✔	--
	97.85m Unexposed								
M1	Medium gray, N5	Fine grained dolomicrite	F1	228.35m	✔	✔	✔	✔	✔
M5	Dark gray, N3	Fine grained black dolomite	F4	251.85m	✔	✔	✔	--	--
M7	Medium dark gray, N4	Fine grained black dolomite	F4	257.65m	✔	✔	✔	✔	--
M11	Very light gray, N8	Fine grained black dolomite	F4	287.7m	✔	✔	✔	--	--
M15	Light Gray, N7	Algal laminated bedded dolomite	F2	306.88m	✔	✔	✔	✔	--
M17	Medium gray, N5	Fine grained black dolomite	F4	317.63m	✔	✔	✔	--	--
M18	Medium light gray, N6	Fine grained dolomite	F5	324.92m	--	✔	--	✔	--
M19	Grayish black, N2	Medium grained black dolomite	F4	334.62m	✔	✔	✔	--	--
M20	Pale brown, 5YR 5/2	Algal laminated fine-grained bedded dolomite	F2	345.69m	✔	✔	✔	✔	--
M22	Grayish black, N2	Medium grained black dolomite with stromatolite	F4	364.14m	✔	✔	✔	✔	--
	25m unexposed								
V1/12	Light Gray, N7	Fine grained dolomite	F5	389.83m	--	✔	✔	✔	--

V4/12	Grayish black, N2	Fine grained black dolomite	F4.	402.69m	--	-	--	--	✔
V7/12	Light Gray, N7	Fine grained dolomite	F5	415.2m	--	-	--	--	✔
V9/12	Grayish black, N2	Fine grained black dolomite	F4.	423.82m	--	-	--	--	✔
V10/12	White, N9	Fine grained dolomite	F5	428.25m	✔	✔	✔	✔	--
V12/12	Grayish black, N2	Fine grained dolomite	F5	436.73m	--	-	--	--	✔
V14/12	Medium gray, N5	Stromatolitic black dolomite	F7	480.33m	--	-	--	--	✔
V15/12	Medium light gray, N6	Fine grained dolomite	F5	501.66m	✔	✔	✔	✔	--
V17/12	Light Gray, N7	Stromatolitic dolomite	F7	533.04m	✔	✔	✔	✔	✔
V19/12	Medium light gray, N6	Fine grained dolomicrite	F10	557.03m	✔	✔	✔	--	✔
V21/12	Medium light gray, N6	Fine grained dolomite	F5	580.83m	✔	✔	✔	✔	✔
V23/12	Pale yellowish brown, 10YR 6/2	Very fine-grained dolomite	F5	604.02m	✔	-	--	--	--
V26/12	Medium dark gray, N4	Stromatolitic dolomite	F8	633.75m	✔	✔	✔	✔	✔
V28/12	Medium dark gray, N4	Stromatolitic dolomite	F7	644.53m	✔	✔	✔	--	--
V29/12	Light Gray, N7	Stromatolitic dolomite	F7	650.54m	--	✔	✔	--	--
V30/12	Light Gray, N7	Stromatolitic dolomite	F7	655.74m	✔	✔	✔	✔	--
V32/12	Light Gray, (N7) with medium dark gray (N4) colored banding	Stromatolitic dolomite	F7	666.4m	✔	✔	✔	--	--
V35/12	Very light gray, N8	Fine grained dolomite	F5	682.2m	✔	✔	✔	✔	✔
V36/12	Medium light gray, N6	Fine grained dolomite	F5	687.65m	✔	✔	✔	--	--
V37/12	Grayish red purple (5RP 4/2) with dark reddish brown (10R 3/4) laminites in between	Dolomicrite	F5	695.67m	✔	✔	✔	✔	--
V39/12	Pale yellowish brown, 10YR 6/2	Fine grained dolomite	F5	706.8m	✔	✔	✔	✔	--

V42/12	Grayish pink, 5R 8/2	Stromatolitic dolomite	F7	730.93m	✔	✔	✔	✔	✔
V44/12	Medium gray, N5	Stromatolitic dolomite	F7	752.63m	✔	✔	✔	✔	--
V44/12	Cream/white	oolite	F8	752.81m	✔	-	✔	--	--
V46/12	Medium light gray, N6	Fine grained dolomite	F5	775.16m	✔	✔	✔	--	--
V47/12	Grayish black, N2	Stromatolitic black dolomite	F7	786.01m	--	-	--	--	✔
V48/12	Pale yellowish brown (10YR 6/2) colored large clasts in black (N1) colored cement	Intraformational Conglomerate (Large, elongated limestone clasts in dolomicrite)	F9	804.32m	✔	✔	✔	✔	--
V49/12	Alternate layering of medium gray (N5) and grayish black (N2) color	Stromatolitic dolomite	F7	814.72m	--	-	--	✔	--
V50/12	Grayish black, N2	Stromatolitic dolomite	F7	825.72m	✔	✔	✔	✔	✔
V51/12	Medium gray, N5	Stromatolitic dolomite	F7	835.92m	✔	✔	✔	--	--
V52/12	Pale brown, 5YR 5/2	Stromatolitic dolomite	F7	846.92m	✔	✔	✔	--	--
V53/12	Pale yellowish brown, 10YR 6/2	Stromatolitic dolomite	F7	857.92m	✔	✔	✔	✔	--
V54/12	Medium dark gray, N4	Stromatolitic dolomite	F7	868.07m	✔	✔	✔	--	--
V55/12	Medium dark gray, N4	Stromatolitic dolomite	F7	878.79m	✔	✔	✔	✔	✔
V56/12	Medium dark gray, N4	Stromatolitic dolomite	F7	889.09m	✔	✔	✔	✔	--
V57/12	Alternate layering of light gray (N7) and black (N1) color	Stromatolitic dolomite	F7	900.09m	✔	✔	✔	✔	--

Table 2. Facies descriptions of Vempalle Formation rocks from the Papaghni Group.

Facies	Description	Interpretation
F1: Mixed siliciclastic-dolomite	Dolomite-sandstone-mudstone heterolithic beds, occupying ~100 m of the lowermost part of the succession Planar to wavy-parallel laminated or trough cross stratified 2-14 cm thick medium to fine-grained sandstone alternating with either reddish brown or local green mudstone or 5-25 cm, massive or planar parallel laminated tabular dolomite beds. Locally sandstones amalgamate to form 20-30 cm thick beds with ripple drift lamination, flaser bedding and graded bedding. Birds-eye structure (fenestral fabric, now filled with silica), locally developed breccias, tepee antiform structures, buckled margins of saucer-like megapolygons and chert nodules are common in the dolomites. Well-rounded, very coarse to coarse sand inter-layers or intraclastic conglomerate with sand matrix are also common.	The heterolith with flaser bedding, syneresis cracks strongly support a supratidal to upper intertidal zone of deposition for the sediments. Tepee structures, fluid-escape structures along with breccias indicate subaerial exposure in a tropical to subtropical climate; and back-beach or back-barrier deposition. Flat parallel laminae of the dolomites suggest supratidal to intertidal deposition with gentle waves.
F2: Bedded dolomite with crinkled laminites (bindstone)	Laterally-persistent, 50-80 cm thick, tabular beds (amalgamated up to 1.5 m) of grey fine-grained dolomite characterized by flat or wavy beds, 2-5 cm thick, light colored dolomite, separated by brown colored mm thin laminae. Crinkled lamination with sharp angular kinks (relict ripple marks), and mud drapes. Randomly distributed, irregularly-shaped fenestrae, parallel to bedding and soft-sediment deformation with microfaults.	Crinkle lamination and fenestrae suggesting tidal flat.
F3: Brown shale/ mudstone	Thin-bedded (0.5-2 cm), reddish brown, plane-parallel to wavy-parallel laminated mudstone. Individual beds laterally pinch out within a meter, but bed-sets, ~1.5 m thick, can be traced laterally up to 10 m. Wrinkle marks (adhesion ripples) and dolomite-filled polygonal cracks common on top surfaces of beds.	Thin-bedded parallel-laminated mudrock reflects low-energy sedimentation. The brown colour suggests well-drained, relatively oxidizing conditions.
F4: Black dolomite with or without stromatolite (wackestone)	Characterized by tabular, laterally persistent 40-60 cm thick (maximum 1.2 m) steel grey to black colored stromatolitic dolomite beds within brown, green or grey stripped shale. Stromatolite bed boundaries sharp with convex-up upper surface forming isolated bioherms or laterally-linked mutually-aligned biostromes with 3-15 cm high columns. Internal laminae of stromatolites closely packed, smooth convex up with low synoptic relief. Cm-scale slump structures and dolomite or silica filled irregularly shaped laminoid fenestrae. Chert nodules restricted to dolomite beds. Some dolomite beds massive in nature, either microbialites reworked or not developed.	Laterally-persistent stromatolitic dolomite beds within variegated colored shale indicates quiet conditions with fluctuating sea level and/or sediment supply. Small slumps and broken stromatolites suggest occasional storms. Transitional zone between subtidal to intertidal is suggested, where high sedimentation rate favored massive carbonate and a lower rate permitted stromatolite growth.
F5: Dolomite-micrite rhythmite (wackestone-mudstone)	Alternating grey to buff colored massive, normally graded to plane-parallel laminated fine-grained dolomite (2-25 cm bed thickness) and green to brown colored plane to wavy parallel-laminated calcareous mudstone (1-5 cm beds). Symmetrical ripples on bed upper surfaces. Dolomite-filled polygonal cracks, salt pseudomorphs, rain-drop prints at several horizons.	Fine grain-size and plane-parallel lamination suggests low energy in a shallow shelf/lagoon. Normal grading, rip-up clasts and symmetrical ripples point to occasional storms. Polygonal cracks, salt pseudomorphs, rain-drop prints indicate emergence in intertidal area of the shallow coast. Predominance

		of mud indicates restricted environment, possibly lagoon.
F6: Cross-stratified oolite (grainstone)	Oolite of well-rounded, well-sorted medium to coarse ooids as linear positive relief bodies, mostly forming shoaling-up bars and banks. Successive 10-70 cm thick wavy lenticular or pinch and swale beds separated by 1-2 cm thin mud layers constitute a shoreline barrier structure. Beds generally trough cross- stratified with subordinate planar cross-stratification, with a NE or SE palaeocurrent direction and a small component towards the SW. Local herringbone cross-stratification. Bed tops show symmetrical ripples with NE-SW ripple axis, straight, rounded crests and tuning-fork bifurcation. Ooids generally preserve a concentric fabric with clastic grains in the core. Medium to fine-grained ooids with a radial fabric and some superficial ooids.	Oolite beds with planar or trough cross-stratification deposited by migrating 2D and 3D subaqueous dunes in high-energy subtidal to intertidal shoals. Presence of herringbone cross-stratification and bidirectional palaeocurrents suggests a tidal influence in association with wave action. Oolite deposition with concentric fabric and clastic core points to an environment with high salinity and wave-agitated shoreline. Sand free ooids with radial fabric may be deposited in relatively quiet water.
F7: Columnar stromatolite (bindstone)	Laterally persistent biostromes and bioherms of columnar stromatolite. 2 types: (a) Tabular biostromes (0.7-2 m height), with erect, locally inclined, cylindrical columns, convex up, closely-spaced, linked smooth to wavy internal laminae with low synoptic relief. (b) Biostromes of laterally-linked domes (1.5-2 m width and 25-80 cm height) with crinkly to smooth laminae parallel to the dome surface. Intraformational conglomerates at the head part of stromatolites locally present.	Smooth lamination indicates quiet water. Large sizes suggest growth in deep water. Intraformational conglomerates reflect frequent storm events.
F8: Conical stromatolite (bindstone)	Biostromes and bioherms of conical stromatolites, embedded within calcareous mudstone. Individual stromatolites isolated to partially linked with open spacing ranging between 5-30 cm and sharp apical angle varying between 20^0-40^0 with moderate to high synoptic relief, closely packed, smooth internal laminae. Biostromes laterally persistent and vary in height from 15-55 cm, bounded by sharp upper and lower surfaces.	Conical shape with high apical angle suggests deep water below wave base, where microbes need to grow fast with maximum apex reaching the light in a deep subtidal environment.
F9: Intraformational conglomerate (grainstone/packstone)	2 types of conglomerate, occurring concurrently in the succession. (a) 3.2-30.8 cm thick, planar tabular beds of matrix-supported, massive ungraded to inversely-graded beds of intraformational conglomerate.. Poorly-sorted, sub-rounded clasts of stromatolite, lime mud and oolite with various shapes (lensoid, elongated, spherical, sinusoidal) and sizes (0.5-17 cm) embedded in a calcareous matrix.. Conglomerates alternate with beds of same lithology as the clasts. Small-scale slumps and fluid-escape structures common. Large (30-41 cm) cabbage-shaped oncoids present. Laterally-persistent, 0.4-1.5 m thick, grey to buff colored, planar, tabular, normally-graded beds of intraformational conglomerate. Conglomerates occur as thin layers (14-32 cm thick) mainly in the lower parts of beds, upon a sharp erosional surface, and grade upward to grey colored fine-grained dolomite. Conglomerates comprise clasts (0.6-9 cm) of lime mud and/or shale, in a micritic matrix.	Conglomerates are event beds from mass flow and/or break-up of stromatolites either by local earthquakes or strong storms. Laterally-persistent graded beds suggest deposition by strong storm events. Presence of oncoids indicates wave reworking during storms.

F10: Parallel-stratified dolomite with isolated bioherms (packstone)	5-40 cm thick (amalgamated up to 1.2 m), planar, tabular dark grey colored dolomite beds with sharp to slightly uneven lower and upper bounding surfaces. Internally, plane-parallel to wavy-parallel laminated. Trough cross-stratification, pillow and ball structure and gutter casts common. Isolated bioherms with domal morphology (width 45 cm, height 26 cm) and interspaces filled with muddy carbonate in some restricted dolomite beds. Abundant chert and steatite nodules of various shapes (kidney-bean shaped, lensoid, spherical) and sizes (long axis of 3-26 cm and short axis of 2.5-14 cm). Dolomite beds commonly alternating with mm to 6 cm thick calcareous mudstone.	Plane-parallel stratification attributed to tractional deposition by waves with high near-bottom orbital velocities. Trough cross-stratification suggests 3D dune migration. Gutter casts from storm events. Isolated bioherms indicate quiet conditions, without regular wave and current activity. Chert and steatite nodules from later diagenetic event/s.
F11: Interbedded green shale/siltstone and dolomite (wackestone-mudstone)	1-2 cm thin laterally pinching out, plane-parallel laminated green to dark green colored shale /siltstone alternating with laterally persistent, 1-5 cm thick, plane to wavy-parallel or ripple cross- laminated buff to light grey colored very fine-grained dolomite.	Plane-parallel laminated shale deposited by suspension fall-out below storm wave base. Green colour from reducing environment.

TABLES

Table 1S. Modal percentage of mineral phases identified in Vempalle Formation dolomites using the bulk XRD method.

ID	Dolomite	Calcite	Quartz	K-feldspar	Mica	Talc	Chlorite	Barite	Hematite	Total
VT1/12	80.4	0	9.3	4.2	6.1	0	0	0	0	100
VT2/12	90.4	0	4.7	4.9	0	0	0	0	0	100
VT3A/12	93.2	0	6	0.8	0	0	0	0	0	100
VT4/12	83.9	0	9.1	7	0	0	0	0	0	100
M1	83.3	0	15.7	1	0	0	0	0	0	100
M7	97.1	0	2.9	0	0	0	0	0	0	100
M15	99.6	0	0.4	0	0	0	0	0	0	100
M20	88.7	0	8.6	2.7	0	0	0	0	0	100
M18	87.9	1.1	7.4	0	0	0	0	3.6	0	100
M22	100	0	0	0	0	0	0	0	0	100
V1/12	86	0	9.3	0	0	0	0	4.7	0	100
V10/12	40.9	0	20.4	0	0	38.7	0	0	0	100
V15/12	82.5	4.3	11.8	0	0	1.3	0	0	0	99.9
V17/12	82.6	4.4	11.7	0	0	1.3	0	0	0	100
V21/12	99.8	0	0.2	0	0	0	0	0	0	100
V26/12	100	0	0	0	0	0	0	0	0	100
V30/12	96.1	0	3.9	0	0	0	0	0	0	100
V35/12	84.8	0	12.5	0	0	0	0	2.7	0	100
V37/12	83.3	0	7.1	7.7	0	0	1	0	0.8	99.9
V39/12	85.9	0	8.1	0.5	0	0	0	5.4	0	99.9
V42/12	95.1	0	3.4	1.5	0	0	0	0	0	100
V44/12	83.4	0	16.6	0	0	0	0	0	0	100
V48/12	86	0	12.9	1.1	0	0	0	0	0	100
V49/12	71.5	0	28.5	0	0	0	0	0	0	100
V50/12	93.8	0	3.7	2.5	0	0	0	0	0	100
V53/12	87.3	0	10	2.7	0	0	0	0	0	100
V55/12	82.7	0	16.1	1.2	0	0	0	0	0	100
V56/12	71	0	28.1	0.9	0	0	0	0	0	100
V57/12	90.5	0	8.3	1.1	0	0	0	0	0	99.9

Table 2S. Calculated calcium (Ca) excess (Lumsden, 1979) and ordering of Vempalle Formation dolomite crystals (Tucker 1995).

ID	mole % $MgCO_3$	mole % $CaCO_3$	Order
VT 1/12	44	50	0.4
VT 2/12	44	50	0.57
VT 3A/12	44	50	0.57
VT 4/12	43	50	0.51
M1	43	50	0.46
M7	45	49	1.07
M15	44	50	0.55
M20	44	50	0.57
M18	44	50	0.46
M22	44	50	0.57
V1/12	44	50	0.47
V10/12	44	50	0.58
V15/12	44	50	0.57
V17/12	44	50	0.57
V21/12	43	50	0.47
V26/12	44	49	0.56
V30/12	44	50	0.56
V35/12	44	50	0.56
V37/12	43	51	0.58
V39/12	44	50	0.56
V42/12	44	50	0.56
V44/12	43	50	0.56
V48/12	43	50	0.56
V49/12	44	49	0.56
V50/12	44	49	0.56
V53/12	43	50	0.56
V55/12	44	50	0.56
V56/12	44	49	0.56
V57/12	44	50	0.56

Table 3Sa. Major and trace element concentrations (n = 42) from Vempalle Formation dolomites. The major element concentrations are in wt% whereas Sr concentration is in ppm.

ID	Na_2O	MgO	Al_2O_3	SiO_2	P_2O_5	K_2O	CaO	TiO_2	MnO	Fe_2O_3	SUM	LOI	Sr
VT1/12	0.054	16.55	1.10	10	0.04	0.28	26.95	0.058	0.031	0.42	55.48	36.41	418
VT2/12	0.049	18.55	3.76	9.01	0.43	2.43	27.36	0.113	0.081	1.48	63.26	39.00	81
VT3A/12	0.033	18.02	1.35	7.84	0.31	2.33	28.49	0.079	0.077	1.34	59.87	38.06	93
VT3B/12	0.045	18.06	2.34	10.57	0.06	1.54	36.95	0.100	0.090	1.98	71.735	39.39	50
VT4/12	0.040	17.15	1.45	12.16	0.21	2.07	27.60	0.103	0.067	1.06	61.91	37.29	95
M1	0.036	18.40	1.30	12.13	0.02	0.12	27.66	0.031	0.055	1.09	60.85	38.46	128
M5	0.012	21.25	0.12	1.50	0.01	0.04	30.09	0.005	0.048	0.42	53.49	42.27	52
M7	0.015	20.75	0.20	3.01	0.01	0.14	29.71	0.012	0.064	0.62	54.53	41.61	46
M11	0.043	15.78	1.19	27.75	0.02	0.02	26.30	0.011	0.033	0.47	71.61	31.58	56
M15	0.008	21.73	0.03	0.12	0.00	0.01	30.19	0.003	0.026	0.44	52.56	42.69	56
M17	0.012	21.07	0.09	1.18	0.00	0.03	30.14	0.007	0.036	0.39	52.96	42.24	58
M18	0.041	17.48	0.46	6.29	0.01	0.05	28.34	0.027	0.087	0.58	53.37	39.99	269
M19	0.009	21.60	0.05	0.36	0.00	0.05	30.20	0.006	0.042	0.45	52.77	41.76	43
M20	0.055	18.62	2.40	12.56	0.03	0.22	27.34	0.082	0.036	1.05	62.39	39.56	49
M22	0.011	21.24	0.08	0.40	0.00	0.01	30.25	0.005	0.054	0.54	52.59	44.16	46
V10/12	0.048	25.68	0.45	51.47	0.01	0.01	14.07	0.001	0.024	0.79	92.55	20.89	39
V15/12	0.099	19.21	0.23	14.36	0.01	0.01	28.36	0.001	0.038	0.47	62.78	36.73	80
V17/12	0.059	14.73	1.32	*28.73*	0.02	0.01	24.97	0.022	0.024	0.35	70.23	30.21	149
V19/12	0.009	21.72	0.07	0.39	0.00	0.01	30.13	0.005	0.021	0.41	52.77	41.94	68
V21/12	0.008	22.29	0.11	4.48	0.00	0.04	29.67	0.005	0.019	0.50	57.12	41.34	44
V23/12	0.037	17.97	1.78	15.80	0.01	0.14	27.30	0.046	0.016	0.76	63.86	38.51	64
V26/12	0.012	21.33	0.07	0.56	0.00	0.01	30.19	0.005	0.020	0.73	52.93	44.38	56
V28/12	0.037	17.04	0.61	23.37	0.01	0.04	27.50	0.007	0.019	0.59	69.22	37.04	66
V30/12	0.077	19.49	0.81	6.85	0.01	0.03	29.53	0.016	0.023	0.77	57.60	41.51	64
V32/12	0.010	21.34	0.05	0.97	0.00	0.07	30.07	0.005	0.026	0.77	53.31	41.92	42
V35/12	0.051	16.54	0.18	10.47	0.01	0.01	27.71	0.022	0.032	0.75	55.77	38.41	289
V36/12	0.072	15.75	3.29	23.02	0.37	1.50	26.08	0.202	0.263	2.63	73.18	34.66	62
V37/12	0.062	16.56	3.77	24.71	0.06	1.38	25.36	0.226	0.036	2.75	74.91	34.81	64
V39/12	0.066	14.07	1.13	23.07	0.03	0.16	25.69	0.054	0.028	0.68	64.98	32.87	271
V42/12	0.019	20.38	0.21	4.87	0.01	0.44	29.35	0.038	0.024	0.72	56.06	43.85	44
V44/12Grey	0.061	13.65	0.85	36.76	0.01	0.01	24.87	0.005	0.026	0.40	76.64	23.27	57
V44/12Cream	0.027	18.60	0.46	14.51	0.00	0.07	28.43	0.010	0.020	0.62	62.75	24.89	45
V46/12	0.051	15.83	1.05	27.62	0.01	0.01	26.37	0.012	0.036	0.50	71.49	30.34	52
V48/12	0.042	18.39	1.80	13.09	0.02	0.39	27.27	0.071	0.025	0.54	61.64	39.47	51
V50/12	0.023	19.56	0.12	6.31	0.01	0.60	29.27	0.045	0.018	0.31	56.26	39.50	46
V51/12	0.046	17.30	2.27	18.53	0.01	0.07	26.68	0.057	0.018	0.41	65.39	36.73	44
V52/12	0.039	18.24	0.54	13.24	0.00	0.02	27.84	0.008	0.028	0.49	60.45	35.09	46
V53/12	0.039	18.13	1.85	13.12	0.02	0.23	27.31	0.053	0.024	0.60	61.37	37.66	49
V54/12	0.050	20.42	0.28	5.52	0.01	0.27	29.32	0.020	0.019	0.36	56.26	38.29	41
V55/12	0.051	17.03	1.98	17.49	0.01	0.01	26.55	0.031	0.016	0.44	63.61	34.49	45
V56/12	0.036	19.08	1.26	11.15	0.01	0.17	28.01	0.033	0.027	0.36	60.13	36.43	42
V57/12	0.035	19.51	0.97	9.28	0.01	0.26	28.51	0.037	0.031	0.42	59.06	38.53	42

Table 3Sb. The trace element concentrations (n = 43, in ppm) obtained from Vempalle Formation dolomites.

ID	Ni	Cu	Co	Zn	Pb	Li	Cd	Mo	Ga	Sb	V	Rb	Ba
VT 2/12	16	7	12.9	20	10.8	13	0.082	0.4	4.4	0.34	33	28	170
VT 3B/12	12	7	15.9	17	6.8	9	0.074	0.4	7.5	0.22	26	22	464
VT 4/12	9	101	19.8	17	6.5	6	0.068	0.4	3.9	0.24	47	22	141
VT 34/12	12	8	13.4	17	6.2	8	0.09	0.4	4.4	0.24	35	18	216
M.1	8	7	9.7	12	8.4	20	0.069	0.3	70.8	0.19	17	6	9550
M.5	4	24	6.1	12	4.5	18	0.109	0.4	1.8	0.33	16	2	86
M.7	5	9	9.9	9	8.2	11	0.067	1.2	0.7	0.12	13	2	30
M.11	4	8	8.8	10	2.6	12	0.004	0.2	7.1	0.12	11	2	520
M.15	6	11	7.8	10	7.1	33	0.053	0.3	56	0.12	23	11	7389
M.17	5	10	7.8	18	6.7	5	0.03	0.4	30.5	0.1	14	1	4044
M.18	6	9	17.8	15	6.7	11	0.028	0.4	366	0.2	21	2	51515
M.19	4	19	12.5	9	5.6	3	0.023	1.3	2	0.12	11	1	146
M.20	10	74	15.9	15	9.7	28	0.17	0.5	17.6	0.24	26	15	2218
M.22	3	6	35.6	10	7.2	5	0.072	0.3	1.8	0.09	14	2	81
V 1/12	5	10	13.3	12	6	14	0.032	0.6	465	0.1	17	7	64776
V.10/12	5	8	5.4	12	6.3	27	0.026	0.4	3.1	0.12	13	1	189
V 15/12	4	6	15.1	10	6.1	10	0.021	0.2	2.4	0.16	9	0.3	169
V.17/12	4	20	14.7	15	5.5	35	0.19	0.2	170	0.17	15	5	21793
V 19/12	4	7	4.8	11	6.2	8	0.027	0.2	11.7	0.1	18	1	857
V.21/12	5	8	5.8	11	11.5	4	0.115	0.4	1.2	0.12	12	1	71
V 26/12	5	5	4.1	8	4.8	4	0.03	0.6	13	0.08	11	1	1786
V 28/12	6	14	11.8	15	5.2	10	0.135	0.5	14.8	0.17	9	2	1903
V 29/12	4	12	5.1	11	9.5	5	0.09	0.3	2	0.15	11	5	123
V.32/12	8	8	10.3	12	10	4	0.049	2.9	2.1	0.16	13	4	130
V 35/12	6	6	12	9	4.5	5	0.013	0.2	264	0.09	14	1	36249
V 36/12	20	38	19.4	22	5.5	16	0.06	0.7	28	0.29	45	49	3183
V.37/12	19	17	15.6	24	5.6	99	0.145	0.5	49	0.36	38	42	6312
V 39/12	5	25	12.4	14	6	6	0.152	0.6	501	0.16	11	4	70163
V 42/12	6	16	8.1	13	4.6	4	0.105	0.2	2.5	0.19	17	7	151
V 46/12	4	6	25.5	9	4.7	4	0.013	0.3	0.7	0.07	8	1	41
V 48/12	6	24	8.3	21	8.7	53	0.044	0.5	4.9	0.2	18	17	280
V 51/12	4	7	10	12	8	25	0.09	0.3	3.6	0.14	21	13	154
V 52/12	5	21	17	12	6.6	4	0.129	0.2	1.4	0.16	15	2	67
V 53/12	8	10	7.8	15	8.9	17	0.036	0.3	5.9	0.16	16	12	385
V 55/12	6	19	18.7	17	8.3	25	0.168	0.4	2.4	0.23	11	10	116
V 56/12	4	8	11	13	7.5	17	0.038	0.2	1.5	0.12	12	9	57
V 57/12	5	16	11.4	19	9.7	22	0.199	0.3	2.2	0.18	13	9	100
V.44/12	4	9	37.2	10	3.6	5	0.014	0.2	2.7	0.12	30	2	86
V.44/12	4	13	9.1	7	2.9	20	0.008	0.4	1.9	0.12	14	4	94
V.54/12	3	11	4.8	9	4.1	5	0.016	0.2	1.8	0.13	10	5	114
V.30/12	4	7	6.3	7	2.4	3	0.003	0.2	38.4	0.11	11	1	5220
VT.3A/12	10	9	12.3	13	3.7	7	0.052	0.3	4	0.23	30	17	209
V.50/12	3	13	8.4	16	5.1	18	0.018	0.1	2.8	0.18	17	10	126

Table 4S. The PAAS-normalized REE concentrations (ppm) of samples from Vempalle Formation dolomites.

Element	M.1	M.5	M.7	M.11	M.15	M.17	M.18	M.19	M.20	M.22	VT 2/12
La	0.147	0.081	0.055	0.037	0.086	0.034	0.084	0.037	0.126	0.047	0.183
Ce	0.155	0.072	0.057	0.036	0.084	0.038	0.093	0.034	0.133	0.041	0.202
Pr	0.147	0.057	0.057	0.034	0.079	0.034	0.102	0.034	0.136	0.045	0.193
Nd	0.150	0.059	0.053	0.035	0.091	0.035	0.109	0.032	0.150	0.038	0.212
Sm	0.211	0.068	0.070	0.043	0.137	0.049	0.182	0.040	0.222	0.041	0.261
Eu	1.407	0.083	0.074	0.176	1.019	0.574	6.213	0.074	0.491	0.065	0.333
Gd	0.195	0.067	0.073	0.043	0.118	0.047	0.142	0.039	0.197	0.043	0.247
Tb	0.194	0.078	0.078	0.039	0.129	0.039	0.155	0.026	0.220	0.039	0.233
Dy	0.190	0.060	0.071	0.041	0.115	0.041	0.139	0.028	0.207	0.034	0.212
Y	0.181	0.059	0.085	0.044	0.107	0.048	0.130	0.033	0.204	0.041	0.211
Ho	0.182	0.050	0.071	0.040	0.101	0.040	0.121	0.030	0.202	0.030	0.202
Er	0.172	0.060	0.067	0.035	0.098	0.039	0.116	0.021	0.196	0.028	0.189
Tm	0.173	0.049	0.074	0.025	0.099	0.025	0.123	0.025	0.198	0.025	0.173
Yb	0.138	0.043	0.043	0.032	0.089	0.028	0.089	0.014	0.163	0.021	0.163
Lu	0.162	0.046	0.046	0.023	0.092	0.046	0.139	0.023	0.162	0.023	0.162
∑REE	3.804	0.932	0.972	0.683	2.446	1.117	7.935	0.490	3.006	0.562	3.176

Element	VT3B/12	VT 4/12	VT 34/12	V 1/12	V.10/12	V 15/12	V.17/12	V 19/12	V.21/12	V 26/12	V 28/12	V 29/12
La	0.120	0.120	0.141	0.092	0.246	0.113	0.063	0.076	0.050	0.039	0.031	0.065
Ce	0.126	0.132	0.155	0.097	0.165	0.079	0.062	0.058	0.048	0.039	0.029	0.054
Pr	0.113	0.125	0.147	0.102	0.136	0.068	0.057	0.057	0.045	0.045	0.034	0.057
Nd	0.112	0.136	0.150	0.103	0.127	0.065	0.059	0.050	0.047	0.044	0.029	0.053
Sm	0.142	0.180	0.177	0.214	0.132	0.070	0.085	0.050	0.056	0.059	0.036	0.054
Eu	0.259	0.241	0.259	7.824	0.167	0.111	2.824	0.231	0.074	0.287	0.287	0.093
Gd	0.144	0.163	0.180	0.155	0.142	0.073	0.073	0.054	0.054	0.054	0.034	0.056
Tb	0.155	0.168	0.181	0.168	0.116	0.065	0.065	0.052	0.052	0.052	0.039	0.052
Dy	0.145	0.177	0.167	0.162	0.088	0.053	0.068	0.041	0.047	0.051	0.028	0.051
Y	0.148	0.156	0.163	0.152	0.096	0.063	0.067	0.048	0.056	0.056	0.030	0.063
Ho	0.151	0.161	0.172	0.151	0.071	0.050	0.071	0.040	0.040	0.040	0.030	0.050
Er	0.144	0.168	0.158	0.140	0.067	0.049	0.070	0.039	0.039	0.046	0.028	0.053
Tm	0.173	0.198	0.173	0.148	0.049	0.049	0.074	0.025	0.025	0.049	0.025	0.049
Yb	0.142	0.163	0.135	0.124	0.035	0.035	0.064	0.028	0.032	0.032	0.021	0.039
Lu	0.162	0.139	0.139	0.185	0.046	0.046	0.092	0.023	0.023	0.023	0.023	0.046
∑REE	2.237	2.427	2.496	9.817	1.682	0.990	3.792	0.872	0.686	0.917	0.705	0.835

Table 4S. contd.

Element	V.32/12	V 35/12	V 36/12	V.37/12	V 39/12	V 42/12	V 46/12	V 48/12	V 51/12	V 52/12	V 53/12
La	0.092	0.060	0.270	0.243	0.071	0.058	0.060	0.139	0.086	0.050	0.115
Ce	0.088	0.067	0.299	0.234	0.065	0.060	0.058	0.127	0.092	0.048	0.114
Pr	0.091	0.079	0.283	0.215	0.057	0.068	0.057	0.125	0.091	0.057	0.125
Nd	0.088	0.083	0.330	0.230	0.065	0.065	0.059	0.127	0.100	0.056	0.124
Sm	0.103	0.157	0.523	0.306	0.137	0.086	0.072	0.155	0.141	0.072	0.151
Eu	0.102	4.926	1.065	1.250	9.806	0.139	0.083	0.194	0.176	0.083	0.241
Gd	0.094	0.127	0.487	0.303	0.088	0.079	0.071	0.144	0.131	0.062	0.133
Tb	0.090	0.155	0.530	0.336	0.090	0.078	0.065	0.142	0.129	0.065	0.129
Dy	0.071	0.143	0.491	0.323	0.085	0.075	0.058	0.137	0.135	0.060	0.120
Y	0.070	0.144	0.441	0.337	0.096	0.085	0.063	0.133	0.148	0.056	0.119
Ho	0.061	0.131	0.464	0.323	0.091	0.071	0.061	0.121	0.131	0.050	0.111
Er	0.056	0.119	0.456	0.326	0.098	0.074	0.053	0.123	0.123	0.046	0.123
Tm	0.049	0.123	0.469	0.346	0.099	0.074	0.049	0.123	0.123	0.049	0.123
Yb	0.039	0.096	0.379	0.291	0.071	0.053	0.043	0.110	0.124	0.035	0.099
Lu	0.046	0.139	0.370	0.323	0.139	0.046	0.046	0.115	0.115	0.046	0.115
∑REE	1.140	6.549	6.857	5.386	11.058	1.111	0.896	2.015	1.845	0.835	1.943

Element	V 55/12	V 56/12	V 57/12	V.44/12	V.44/12	V.54/12	V.30/12	VT.3A/12	V.50/12
La	0.230	0.089	0.092	0.045	0.052	0.063	0.031	0.136	0.063
Ce	0.190	0.084	0.080	0.039	0.052	0.053	0.024	0.148	0.055
Pr	0.147	0.091	0.079	0.045	0.057	0.057	0.023	0.136	0.057
Nd	0.153	0.088	0.080	0.038	0.053	0.050	0.024	0.147	0.062
Sm	0.142	0.112	0.094	0.040	0.074	0.058	0.032	0.175	0.074
Eu	0.167	0.130	0.120	0.056	0.102	0.083	0.769	0.259	0.093
Gd	0.146	0.105	0.092	0.043	0.069	0.056	0.028	0.167	0.073
Tb	0.129	0.116	0.103	0.039	0.078	0.065	0.026	0.168	0.065
Dy	0.115	0.109	0.096	0.036	0.068	0.053	0.019	0.160	0.066
Y	0.130	0.137	0.122	0.041	0.070	0.067	0.030	0.170	0.081
Ho	0.101	0.111	0.101	0.030	0.061	0.050	0.020	0.151	0.061
Er	0.126	0.112	0.098	0.028	0.056	0.049	0.021	0.154	0.070
Tm	0.123	0.123	0.099	0.025	0.049	0.049	0.025	0.173	0.074
Yb	0.096	0.099	0.089	0.021	0.046	0.046	0.014	0.138	0.060
Lu	0.092	0.115	0.092	0.023	0.046	0.046	0.023	0.139	0.069
∑REE	2.089	1.623	1.438	0.548	0.933	0.845	1.108	2.423	1.023

Table 5S. The $\delta^{18}O$ and $\delta^{13}C$ values of Vempalle Formation dolomites.

ID	$\delta^{13}C$ (‰ PDB)	$\delta^{18}O$ (‰ PDB)
R1	0.71	-6.53
R2	0.635	-6.44
R3	0.57	-6.6
R4	0.74	-6.48
R5	0.58	-7.07
R6	0.54	-6.55
R7	0.65	-8.08
R8	0.5	-7
R9	0.33	-7.13
R10	0.35	-7.68
R11	0.14	-7.38
M1	0.835	-5.82
M15	2	-5.2
M20	0.55	-7.05
V1/12	1.3	-6.8
V4/12	0.25	-8.11
V7/12	-0.24	-7.91
V9/12	-0.21	-7.93
V12/12	0.18	-6.99
V14/12	0.46	-7.07
V17/12	0.68	-6.31
V19/12	-0.26	-7.43
V21/12	-0.25	-7.11
V23/12	0.6	-6.7
V26/12	0.54	-6.85
V30/12	1.35	-6.7
V35/12	0.35	-7.24
V39/12	0.7	-6.6
V42/12	-0.19	-6.12
V44/12	0.3	-6.2
V47/12	-0.355	-6.35
V50/12	0.26	-6.55
V53/12	1	-6.45
V55/12	0.34	-5.52
V57/12	1	-6.1